AN EXPERIMENTAL STUDY OF LOW PRESSURE PARALLEL PLATE RADIO FREQUENCY DISCHARGES

A thesis for the degree of

PHILOSOPHIAE DOCTOR

Presented to

DUBLIN CITY UNIVERSITY

By

RUTH ANN DOYLE B Sc

School of Physical Sciences

DUBLIN CITY UNIVERSITY

Research Supervisor Dr Michael B Hopkins

External Examiner Professor K Wiesemann

December 1994

Acknowledgements

I would like to thank all those who have helped during the duration of this work with special thanks to my supervisor Dr Mike Hopkins for all his support and encouragement during the last few years Also thanks to Dr Bill Graham, Dr Will M^{c} Coll, Prof Larry Overzets and Enda M^{c}Glynn for all the helpful discussions To fellow post graduates past and present, thank you for all the fun

To my family who have been a help and support throughout my time in college and finally to Conor, for keeping things together, thankyou

Declaration

I hereby certify that this material, which I now submit for assessment on the programme of study leading to the award of Philosophiae Doctor is entirely my own work and has not been taken from the works of others save and to the extent that such work has been cited and acknowledged within the text of my work

Signed _____

Ruth A Doyle

Date _____

Contents

Table of Figures

Abstract.

Radio frequency generated plasmas are used extensively in commercial manufacturing systems for a range of different applications including reactive ion etching, thin film deposition and surface modification To optimise such processes a thorough understanding of the physical processes within the plasma is essential

In this thesis low pressure radio frequency argon plasmas are investigated in order to understand further the physics of their behaviour under certain conditions Tuned Langmuir probes and microwave interferometry are used as diagnostics methods to measure different plasma parameters as a function of gas pressure, current density and applied voltage The spatial variations of these parameters are examined within the bulk plasma In particular the electron distribution function was obtained from the Langmuir probe to observe transitions between heating modes which occur under certain conditions of the plasma To further understand this transition a small variable transverse magnetic field was applied to the plasma to confine the electrons and modify their trajectories Mathematical models devised and compared to the experimental results showed an excellent agreement Finally the tuned probe was installed on other research systems in Ireland and abroad to characterise the plasma produced by different gases, with other methods of power coupling and in various chamber geometries

Chapter 1 : Introduction to Plasma Physics.

1.1 Introduction.

The rapid development of plasma physics in the fifties and sixties was stimulated by research directed towards achieving controlled thermonuclear fusion as a solution to the energy crisis [1] This brought about research into high energy ion and neutral beams and magnetic confinement of hot dense plasmas With the advent of the laser in the sixties, so too came the field of laser plasma physics, with applications in both materials and surface processing [2]

More recently though, the area of low pressure plasma physics has become quite important due to its uses in primarily the semiconductor industry Initially dc glow discharges were considered however their spatial inhomogeneity, the low discharge current densities and the dependence on the surface of the electrodes, because of secondary electron emission, has made them quite unsuitable for etching [3] Radio frequency generated plasmas are the principal type used in industry for materials processing, etching and sputtering applications [4-7], because they do not suffer the disadvantages of the dc system They can also be operated at much lower pressures and can be used to process insulating materials

A lot of research has been carried out to investigate topics such as, power input to the etch rates [8,9], energy transfer to the wafers [10,11] and the positive and negative ions which are formed [12] As a result, different system configurations have been developed to optimise the process performance Most recently have been the moves towards using inductively rather than capacitively coupled plasma, as surface mounted technology expands and the need for smaller dimensions in the etch profiles becomes important [13]

This thesis examines capacitively coupled rf plasmas using tuned Langmuir probes and microwave interferometry in an attempt to gain a fuller understanding of the operation of the plasma Comparisons between experimental data obtained here and computer simulations are also made to relate directly the plasma theory with experimental measurements The intension of this chapter is to introduce the concept of a plasma Some terms used to define and compare plasmas are also presented Finally several different diagnostic techniques are reviewed Although these were not

the main analysis methods used for the work presented here they are mentioned throughout this thesis with a view to future work to be performed and collaborative work that is currently being undertaken with other research groups

1.2 Definition of a plasma.

Although a large percentage of the universe, quoted by some to be ~99% [14,15], is said to be in a plasma state, the Earth is quite different with naturally occurring plasmas being very rare indeed The reason for this is explained by the Saha equation which predicts the amount of ionisation to expect in a gas in thermal equilibrium as,

$$\frac{n_i}{n_n} = 2.4\text{x}10^{21}\ \frac{T^{\frac{3}{2}}}{n_i}\ e^{\frac{U_i}{kT}} \quad , \qquad \textbf{Eqn: 1.1}$$

where n_n is the gas density, U_i is the ionisation potential of the gas, T the temperature and k the Boltzmann constant As an example, air at room temperature has the ratio n_i/n_n is 10^{-122} Obviously then any gas is not by definition a plasma since most gases will have some small degree of ionisation even at room temperature A plasma is thus defined specifically as, a quasineutral gas of charged and neutral particles which exhibits collective behaviour Quasineutral implies that the density of positive particles is approximately equal to the density of negative particles Since long range coulombic forces exist between particles within the plasma, elements of force exerted on a particle will affect other particles not only in the immediate area but also much further afield This is the condition of collective behaviour, where motions depend not only on the local region but also on remote regions A plasma can also be defined mathematically in terms of the Debye length which will be shown later see Section 1 4

1.3 Temperature.

Within a plasma there exists a range of particles with different velocities and consequently different energies The most probable distribution of these velocities is known as a Maxwellian distribution which in one dimension is given as,

$$f(\mathrm{v}) = A \exp\left[\frac{-\frac{1}{2} m \mathrm{v}^2}{kT}\right] , \qquad \textbf{Eqn: 1.2}$$

where $f\,d$v is the number of particles per m^3 with velocities between v and v + dv. The density of the particles is given as a sum over all the available velocities,

$$n = \int_{-\infty}^{\infty} f(\mathrm{v})\,dv \quad . \qquad \textbf{Eqn: 1.3}$$

The constant A in equation (1.2) is related to the density and found to be,

$$A = n\left(\frac{m}{2\pi kT}\right)^{\frac{1}{2}} \quad . \qquad \textbf{Eqn: 1.4}$$

The temperature, is a term used to characterise the energy of the particles in a Maxwellian distribution. In one dimension the average kinetic energy of the particles in the plasma can be computed from Equations (1.2) and (1.3).

$$E_{av} = \frac{\int_{-\infty}^{\infty} \frac{1}{2} m \mathrm{v}^2 f(\mathrm{v})\,dv}{\int_{-\infty}^{\infty} f(\mathrm{v})\,dv} \qquad \textbf{Eqn: 1.5}$$

Evaluation of the integral results in a average energy, E_{av} equal to ½kT. This can be extended to 3 dimensions showing E_{av} = 3/2kT or ½kT per degree of freedom. The temperature and average energy are closely related so the temperature in plasmas is most commonly measured in units of electron-volts.

It must also be noted that within the plasma itself there may be several different temperatures. The ions and electrons often have different temperatures because collision rates among ions or among electrons may not be the same as the rate of collisions between an ion and an electron. If a magnetic field is present one type of particle may have separate temperatures perpendicular or parallel to the field. It will be shown later, Section 4.3, how electrons in the plasma under certain conditions are split into two different temperature groups each having a different

effect on the plasma

1.4 Debye Shielding.

In defining a plasma the term collective behaviour was used This refers to the way in which a plasma will act to shield any disturbance from the bulk of the plasma If a charged body is placed within the plasma, particles of the opposite charge will be attracted to it, masking its effect on the rest of the plasma, as shown in Figure 1 1 For the case of the plasma at zero Kelvin, the charge body will be completely shielded so that neutrality is maintained in the bulk of the plasma, outside of the charge cloud If however the temperature is raised above this value, the particles will have some random thermal energy which increases the shielding distance A quantity called the Debye length is the measure of the thickness or shielding distance of the cloud To compute the size of this region some definitions are necessary It is first assumed that the charged body has a potential ϕ m the x = 0 plane and that it is infinitely thin The mass ratio of ions to electron is taken to be infinite this just assumes that the electrons, due to their greater mobility do all of the shielding regardless of the polarity of the body, by either providing a surplus or a deficit of charge to perform the shielding Poisson's equation in one dimension is given as

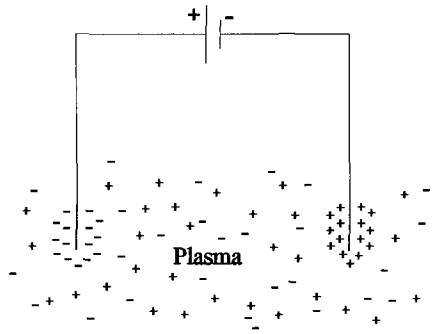

Figure 1 1 Debye shielding

$$\epsilon_o \frac{d^2\phi}{dx^2} = -e(n_i - n_e) \quad . \qquad \textbf{Eqn: 1.6}$$

The variation of the electron density n_e, over the region of the disturbance is given as function of the total electron density, the potential and the temperature

$$n_e(x) = n_\infty \exp\left(\frac{e\,\phi(x)}{kT_e}\right) \quad . \qquad \textbf{Eqn: 1.7}$$

Substitution of equation (1 7) into (1 6) and expansion of the resulting exponential using the Taylor series results in

$$\epsilon_0 \frac{d^2\phi}{dx^2} = \frac{e^2 n_\infty}{kT_e}\phi \quad . \qquad \textbf{Eqn: 1.8}$$

The quantity λ_d , known as the Debye length, can now be defined as,

$$\lambda_d = \left(\frac{\epsilon_0 kT_e}{e^2 n_\infty}\right)^{\frac{1}{2}} \quad . \qquad \textbf{Eqn: 1.9}$$

This term can be used to mathematically characterise a plasma For the plasma to be quasineutral, the dimensions of the plasma must be greater than the Debye length and the number of particles in a Debye sphere must be much greater than one, or

$$\begin{aligned} \lambda_d &\ll L \\ N_d &\gg 1 \end{aligned} \quad , \qquad \textbf{Eqn: 1.10}$$

where N_d is the number of particles within a sphere of radius λ_d The quantity λ_d is of great importance when working with probes in plasma and is fundamental to the calculation of various plasma parameters

1.5 Plasma parameters.

In order to characterise a plasma several parameters have been defined by which plasmas can be compared These include the temperature, as mentioned previously, the density of charged species, the plasma or space potential, the floating potential and the electron energy distribution function (eedf) These are all discussed in detail in Section 3 2 3 and 3 2 4 with a view to their calculation from the tuned probe data However a brief definition of each is given here for the benefit of understanding the diagnostic techniques employed to measure these parameters, which shall be reviewed in Section 1 7

Temperature. This parameter describes the energy of particles in a maxwellian distribution The greater the temperature of the plasma the greater the energies of the electrons

Electron or ion density This is simply the number of electrons or ions in a unit volume In the present work the density varies from 10^{9}-$10^{11}cm^{-3}$, while in general in laboratory plasmas the density can range from 10^{8}-$10^{20}cm^{-3}$

Plasma/space potential If a body is placed within a plasma and biased to remove the sheath formed around itself, ie no electric fields are present, electrons and ions will migrate to the body due only to their thermal velocities The potential of the body at this point is known as the plasma or space potential

Floating potential This is the potential that an unbiased conducting body placed within a plasma will attain Equal fluxes of electrons and ions must impinge upon the body since no net current can be collected

Electron energy distribution function This parameter shows how the energy is distributed among the electrons ie the density of electrons within each energy interval The eedf, $f(\epsilon)$, is normally represented in units of eV^{-1} In this text however we refer to $\epsilon^{-1/2}$ $f(\epsilon)$ as the eedf This is not strictly an eedf but is acceptable for the analysis of the results presented here

1.6 Radio frequency plasmas.

Plasmas can be produced by applying an ac voltage at radio frequency to appropriate gases at low pressures The theory associated with these plasmas is reviewed in detail in Chapter 2 Rf generated plasmas are preferred in industry as they can be operated at much lower pressures, they are more efficient at promoting ionisation and sustaining the discharge than dc plasmas meaning more current can be driven through the discharge for a given voltage [7,16] since the impedance of the plasma which is often capacitive will decrease with increasing frequency

This manner of producing a plasma while much better for sputtering and

deposition work in industrial applications has major implications for any diagnostic techniques employed Although the ions and neutrals are in general unable to follow the applied rf signal, the electrons can and do add a time varying factor to all the plasma parameters This time varying element causes many problems particularly for probes placed within plasmas For this reason diagnostic techniques have had to be re-examined and in some cases redesigned for operation in rf plasmas Besides their direct affect on diagnostic systems, rf plasmas are also responsible for leakages to the ground lines and loading of impedances which can cause erroneous measurements to be taken

1.7 Methods of plasma diagnostics.

There are several methods of analysing rf plasma behaviour, each one with its own particular advantages and disadvantages Each technique operates at its optimum in certain types of plasmas A few of these techniques are mentioned below with a summary of how they function

1.7.1 Electrostatic Probes.

There are quite a number of different probe techniques employed for plasma diagnostics These include emissive, capacitive and collecting probes Some of them can operate in single, double or triple mode though only single mode operation is covered here Details of the latter two techniques may be found in references [17-20]

(i) An emissive probe is primarily used to measure the plasma potential It consists of a hot wire which is immersed in the plasma The probe is heated to allow thermionic emission of the electrons, and is biased with respect to the plasma potential, see Figure 1 2 taken from Kemp et al [21]. When the bias of the probe is more negative than the plasma potential the electrons can leave the probe and be collected by the plasma however when the probe is more positive than the space potential the electrons

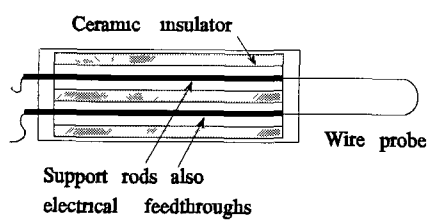

Figure 1 2 A typical emissive probe

can not leave the probe but electrons are collected by the probe By identifying the transition from current collection to emission it is then possible to determine the plasma potential In fact the probe floats at the plasma potential where emission and collection are balanced Emissive probes are best used for measurement within the sheath regions of plasmas or in magnetised or turbulent plasmas since disturbance by the probe is minimised as no net current is collected from the plasma [22,23]

(ii) Capacitive probes with a high impedance to ground have been used to measure time varying plasma potentials in rf discharges However a numerical simulation of the convoluting effect of the rf potential on the probe characteristic must be used to estimate the actual characteristic and derive the correct plasma parameters [24] The numerical simulations used require the plasma to be maxwellian which is not always the case [25] These probes can be more suitable than emissive or collector probes in certain plasma, eg high frequency measurements in strong B fields In this case once the impedance of the probe is high compared to the source impedance at all the frequencies present and providing sheath effect may be neglected, the probe can successfully track the potential without significantly loading the plasma [26] A capacitive probe designed for measuring the rf fundamental and harmonic amplitudes within the plasma and sheaths is shown [27] Additions can be made to the probe tip to increase the area depending on the density of the plasma

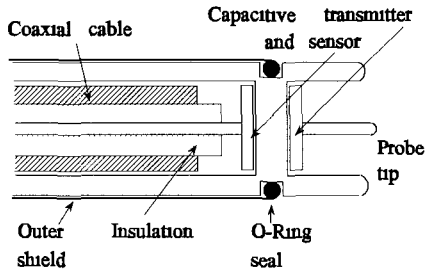

Figure 1 3 Capacitive probe for rf potential measurements

(iii) Collecting probes are the most commonly used in plasma diagnostics of all the probe techniques available They are discussed at further length in Section 3 2 with particular attention paid to the tuned Langmuir probe

1.7.2 Thomson scattering.

Thomson scattering as a diagnostic technique is generally confined to high

temperature, highly ionised plasmas where the output light signal is quite large A photon of light with angular frequency ω and wave vector k impinges on an electron at rest After the collision the photon frequency and wave vector are changed to ω' and k′ respectively while the electron recoils with momentum P_e [28] A schematic diagram of a typical system setup is shown in Figure 1 4 Photomultiplier tubes are generally used as detectors The angle at which they are placed with respect to the light out, decides which plasma parameters can be measured In theory this is quite easy although in practise many light baffles are required to reduce spurious reflections from the optics of the systems, that only changing the scattering angle θ by a few degrees would be possible The different values of scattering angle produce quite different spectra The relationship between the signal output, the system setup and the plasma parameters is defined by the scattering parameter α where,

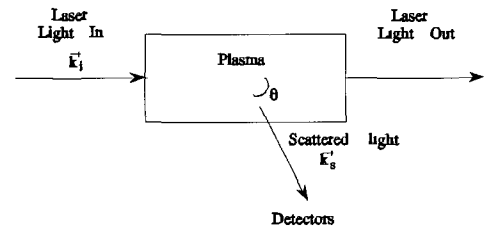

Figure 1 4 Typical schematic setup for Thomson scattering experiments

$$\alpha \approx \frac{\lambda_i}{4\pi \sin\frac{\theta}{2}} \sqrt{\frac{e^2 n_e}{\epsilon_0 k T_e}} \quad , \qquad \textbf{Eqn: 1.11}$$

and λ_i is the wavelength of the incident light When $\alpha \ll 1$, kT_e can easily be found and when $\alpha \gg 1$, n_e can be measured [29]

The output spectrum is also related to the electron velocity distribution function f(v) [30] There are quite a few problems inherent with the use of Thomson scattering as a diagnostic technique Firstly the Thomson scatter signal must be determined from the Rayleigh scattering signal given by the neutrals in the plasma The signal must also be distinguished from Raman scattering and laser induced florescence which occur due to impurities within the gas Calibration of the Thomson scattering signal can be seriously hindered by these effects which can be completely unpredictable [31]. In low pressure plasmas, bremstrahlung arising from electron

neutral elastic collisions is also observed, and finally, the optics necessary to operate the system can cause reflections which complicate analysis of the results [32]

1.7.3 Photodetachment.

Like the preceding diagnostic technique, photodetachment also requires the use of laser light This type of plasma analysis is used mainly to measure the negative ion density in electronegative plasmas such as CF_4 and hydrogen plasmas [33,34] A photon of light with sufficient energy to detach an electron from a negative ion causes an increase in the localised electron density This increase can then be measured using an electrostatic probe or microwave mterferometry depending on the geometry of the system Care must be taken when deciding the type of laser to use for this purpose as the photon energy must be large enough to overcome the electron affinity for the ion but no so large as to cause photo-ionisation or photo-emission [35] If the laser intensity is sufficient to cause saturation, that is detach all the negative ions in the laser path, the density of the negative ions will be proportional to the increase in electron density

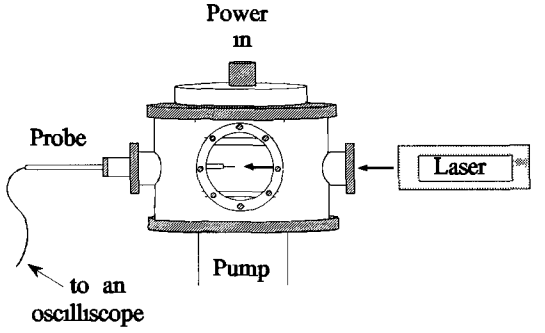

Figure 1 5 Schematic representation of a typical photodetachment setup

1.7.4 Optical emission spectroscopy.

Optical emission spectroscopy is a major diagnostic tool for reactive and sometimes corrosive plasmas, because it is a non-invasive technique Emissions of interest originate from the fraction of plasma species electronically excited to higher states This fraction is determined by the electron energy distribution function (eedf) of the plasma The emission intensities are therefore related to the density of the species involved and the eedf [36] However since most changes to the plasma parameters affect both the density and eedf, emission spectroscopy cannot be used as a monitor for the density of the plasma species To overcome this difficulty the

method of actinometry has been introduced Here the ratio of emission from the reactive atom to a gas atom has been used to measure the reactive atoms' concentration There are still problems associated with this technique, mainly that the excitation be by single step electron impact excitation of the ground state atom [37]

An addition to passive emission spectroscopy has been plasma induced emission spectroscopy (PIE) in which the excited species are probed without any perturbation to the plasma The excellent time and space resolution achievable with this technique has lead to investigations into the sheath regions of γ mode plasmas to observe the behaviour of fast secondary electrons [38], and the discovery of time dependant excitation of atomic levels within silane[39]

1.8 Modelling rf plasmas.

Computer models have become a major part of plasma physics Many different types of models have been formed to analyse the different aspects that are of interest within the plasma Equivalent circuit models too are an ideal way of examining certain parameters of the plasma This section reviews both of these techniques as means of gaining a fuller understanding of the workings of a plasma

1.8.1 Computer modelling.

Computer modelling is a fast and relatively inexpensive means of scrutinising all the different regions of the plasmas For rf plasma modelling several different techniques are available to examine the electric fields within the plasma, the sheath behaviour, the electron energy distribution functions, etc The principle techniques are shown

(i) Fluid (continuum) models have been used to model the axial variations [40] in the entire discharge and have been successful in computing the external discharge parameters such as Langmuir probe characteristics, power densities and also the mechanisms for transfer of energy to the bulk electrons in the sheath region The local field approximation which assumes that the electrons are in equilibrium with the local electric field, is only valid for charged particles if the space and time variations in the electric field are small relative to the distance and time between collisions [41]

For this reason fluid models are not valid for electrons within the sheath regions This type of model is best suited to high pressure dense plasmas [42]where the behaviour of the individual particles is ignored However it has been employed to model low pressure rf inductive[43,44] and capacitively [45,46] coupled plasmas in two dimensions quite successfully

(ii) Monte Carlo/ Particle-in-cell models are used more frequently for low pressure gas discharge modelling as the response of the individual particles are examined For this reason the sheath regions [47-52], which are of fundamental importance for heating in rf plasmas, can be examined in great detail The electron energy

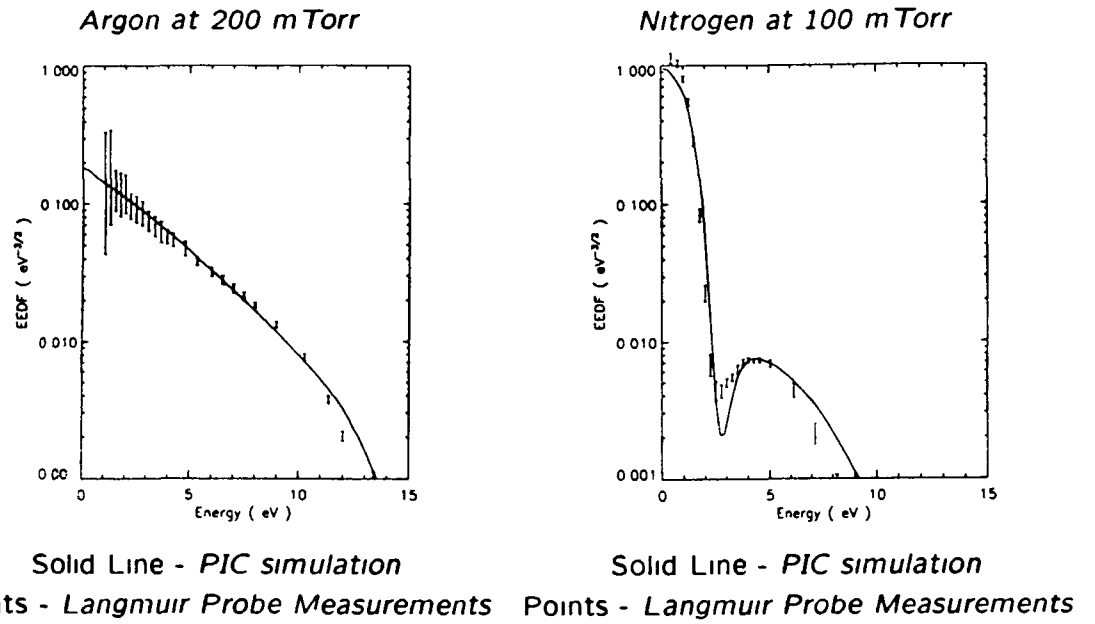

Figure 1 6 Comparison between PIC simulations and experimental results for (a) argon and (b) nitrogen taken from Turner et al [53, 54]

distribution function can also be simulated and compared with experimental measurements [43] In the particle-in-cell (pic) method, the trajectories of many electrons and ions are integrated forward in time and macroscopic quantities such as

currents and charge densities are constructed by summing the individual particle contributions. The Monte Carlo method is used to include collisions between charged and neutral particles [55-57]. The main advantages of this technique include knowing exactly where a particle is, so that a very thin beam of particles can be resolved accurately, in the sheath region, for example. Another advantage is that they scale better as more dimensions are added [58]. PIC/MCC codes were used for the modelling work presented here and compare very well with the experimental data as shown. The deviations between the two are due to using a one dimensional model and neglecting wall losses.

1.8.2 Equivalent circuit models.

Equivalent circuit models have been developed over the years to aid in the understanding of the different types of plasmas. For radio frequency plasmas alone there have been numerous models developed, at various levels of simplification, to describe parallel plate capacitively coupled plasmas [59], sputtering system [60] and etching systems [61] etc. The function of these models is to provide immediate accurate information regarding the behaviour of the plasma. Most models are concentrated towards the sheath regions or are used to estimate the power deposited within each region of the plasma [16]. For the work presented here the most accurate model to use would be that shown below, taken from Köhler et al [62], which describes an asymmetric planar electrode rf plasma. The sheaths which are mainly capacitive are represented by a capacitor with a resistor in parallel. The resistance reflects the power dissipated within the sheaths while the high electron mobility, which produces a non-linear current to the electrodes, is represented by the diodes. The bulk plasma is represented by a resistor, though some models use both a resistor and an inductor to account for the resistance due to electron collisions with the gas atoms in the bulk and the plasma

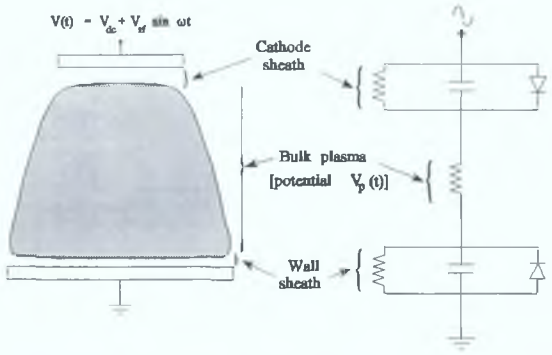

Figure 1.7: Equivalent circuit of an rf plasma system, taken from Köhler et al, ref [62].

inductance due to electron inertia in the rf field [63] Electrical models of this type are used in conjunction with experimental systems to examine the influence of different gases on the plasma impedance [64] and examine how the power deposited within the plasma can be linked to driving frequency and current etc [16]

1.9 Outline of proposed research.

Although our knowledge of rf plasmas has greatly increased in the last few years, this has come about primarily through computational rather than experimental means The reason for this has been the advances in computing power while experimental progress has been hampered by the lack of suitable reliable diagnostic equipment The purpose of this thesis to present an experimental study of low pressure rf plasma using specifically designed diagnostic methods and from the results obtained, examined the plasma parameters and heating regimes of the plasma

Tuned Langmuir probes and microwave interferometry were the main analysis methods used, however a current and voltage probe is also incorporated into the system to measure accurately both current an voltage waveforms and allow consistent plasmas to be produced

Probe analysis of plasmas is still a very popular technique since it has proved to be quite a reliable diagnostic method when properly used However a parameter termed here as the sheath resistance, has until now been neglected even though its affect on the plasma can be quite serious A means by which this parameter can be measured along with some explanation of its occurrence is presented in Chapter 4 [64] Initial measurements of its value in the system used here are also shown

The heating regimes of low pressure plasmas are reviewed with an emphasis placed on the transition from stochastic to bulk heating This work was performed primarily on argon plasmas to observe how the Ramsauer effect enhanced the transition Comparisons between the computationally predicted pressure at which this transition should occur and the actual pressure value are also made

In order to further our understanding of these heating regimes a small variable transverse magnetic field was applied to the plasma while in the stochastic heating mode Theoretically the magnetic field will reduce the fast electron mobility perpendicular to the applied electric field and cause a heating regime transition The

eedfs along with some results obtained from computational models are shown in Chapter 6

Spatial measurements throughout the plasma, using the tuned probe, as a function of pressure were taken to examine the electron temperature and bulk fields variations within the plasma Comparison with the work of others is shown in Chapter 5 [65] Using the diffusion equation a theoretical prediction of the electron density profile throughout the plasma was formulated, the results of which are compared to the actual experimental findings

Collaborative work performed on other systems is reviewed in Chapter 7 The intension of this work was to take experimental measurements using the tuned probe and compare them to other diagnostic techniques already employed on theses systems All of this work is still continuing however initial results are presented and again comparisons with theoretical predictions presented

Finally some conclusion from the work presented along with suggestions for further work to be carried out are shown in Chapter 8

References.

[1] M N Rosenbluth and R Z Sagdeev, *Basic Plasma Physics I*, North Holland Publishers, 1983

[2] M W Blades, P Banks, C Gill, D Huang, C Le Blanc and D Liang, IEEE Trans Plasma Sci 19(6),1991, 1090-1113

[3] J V Scanlan, PhD Thesis, Dublin City University, 1990

[4] J W Coburn, IEEE Trans Plasma Sci 19(6), 1991, 1048-1062

[5] J L Shohet, IEEE Trans Plasma Sci 19(5), 1991, 725-733

[6] D B Graves, IEEE Trans Plasma Sci 22(1),1994, 31-42

[7] B Chapman, Glow Discharge Process, Wiley New York, 1980

[8] S J Pearton and W S Hobson, J Appl Phys 66 (10), 1989, 5009-5017

[9] W G M van den Hoek, C A M de Vries and M G J Heijman, J Vac Sci Technol B % (3), 1987, 647-651

[10] S J Pearton and W S Hobson, J Appl Phys 66 (10), 1989, 5018-5025

[11] H Kersten, R J M M Smjkers, J Schulze, G M W Kroesen, H Deutsch and F J de Hoog, Appl Phys Lett 64 (12), 1994, 1496-1498

[12] Y Lin and L J Overzet, Appl Phys Lett 62 (7), 1993, 675-677

[13] R Patrick, P Schoenborn and H Toda, J Vac Sci Technol A 11 (4), 1993, 1296-2000

[14] F F Chen, *Introduction to plasma physics and controlled fusion, Volume 1 Plasma Physics*, Second edition, Plenum Press, NewYork, 1990

[15] Y Elizer and S Elizer, *The Fourth State of Matter*, IOP publishing, England 1989

[16] C Beneking, J Appl Phys 68 (9), 1990,4461-4473

[17] D M Manos, J Vac Sci Technol A , 3(3), 1985, 1059-1065

[18] E O Johnson and L Malter, Phys Rev 80(1), 1950, 58-68

[19] A.M Pointu, Appl Phys Lett 48(12), 1986, 762-763

[20] F F Chen, Rev Sci Instrum , 35(9), 1964, 1208-1212

[21] R F Kemp and J M Sellen, Jr , Rev Sci Instrum 37 (4), 1966, 455-461

[22] N Hershkowitz, IEEE Trans Plasma Sci , 22 (1), 1994, 11-21

[23] J T Tang, C Kim, R Stenzel and L L Higgins, Rev Sci Instrum 50 (11), 1979, 1458-1460

[24] N Hershkowitz, M H Cho, C H Nam and T Intrantor, Plasma Chem and Plasma Process 8 (1), 1988, 35-52

[25] J V Scanlan, PhD Thesis, Dublin City University, 1991

[26] N Benjamin, Rev Sci Instrum 53 (10), 1982, 1541-1543

[27] S E Savas and K G Donohoe, Rev Sci Instrum 60 (11), 1989, 3391-3395

[28] A I M Rae, *Quantum Mechanics*, IOP Publishing, England, 1986

[29] A W DeSilva and G C Goldenbaum, *Methods of Experimental Physics Plasma Physics Vol 9A* edited by H R Griem and R H Lovberg, Academic Press, New York, 1976

[30] T S Brown and D J Rose, J Appl Phys 37 (7), 1966, 2907-2714

[31] M Bassan, L Giugicotti and R Pasqualotto, Appl Optics, 32 (27), 1993, 5313-5323

[32] Personal correspondence with W Kahnert, Ruhr Universitat, Bochum, 1994

[33] J L Jauberteau, G J Meeusen, M Haverlag, G M W Kroesen and F J de Hoog, Appl Phys Lett., 55 (25), 1989, 2597-2599

[34] M Bacal and G,W, Hamilton, Phys Rev, Lett , 42 (23), 1979, 1538-1540

[35] K N Mellon, PhD Thesis, Dublin City University, 1993

[36] J W Coburn and M Chen, J Appl Phys 51(6) 1980, 3134-3137

[37] L F Dimauro, R A Gottscho and T A Miller, J Appl Phys 56 (7), 1984, 2007-2011

[38] R Flohr and A Piel, Phys Rev Lett , 70 (8), 1993, 1108-1111

[39] G de Rosny, E R Mosburg Jr , J R Abelson, G Devaud and R C Kerns, J Appl Phys 54 (5), 1983, 2272-2275

[40] F.F. Young and C-H. Wu. Appl. Phys. Lett 62 (5) 1993, 473-475

[41] G G Lister, J Phys D 25, 1992, 1649-1680

[42] Ph Belenguer and J P Boeuf Phys Rev A 41, (8), 1990, 4447-4459

[43] G DiPeso, V Vahedi, D W Hewett and T D Rognlien, J Vac Sci Technol A 12 (4), 1994, 1387-1396

[44] A J Paranjpe, J Vac Sci Technol A 12(4), 1994, 1221-1228

[45] P M Meijer, J D P Passchier, W J Goedheer, J Bezemer and W G J H.M van Sark, Appl Phys Lett 64 (14), 1994,1780-1782

[46] D P Lymberopoulous and D J Economou, J Vac Sci Technol A 12 (4), 1994, 1229-1236

[47] D Vender and R W Boswell, J Vac Sci A 10 (4), 1992, 1331-1338

[48] R W Boswell and I J Morey, Appl Phys Lett 52 (1), 1988, 21-23

[49] P W May, D F Kemperer and D Field, J Appl Phys 73 (4), 1993, 1634-1643

[50] R W Boswell, A J Lichtenberg and D Vender, IEEE Trans Plasma Sci 20 (2), 1992, 62-64

[51] M Surendra and D Vender, Appl Phys Lett 65 (2) 1994, 153-155

[52] M Surendra and D Vender, Phys Rev Lett 66 (11), 1991, 1469-1472

[53] M M Turner, R A Doyle and M B Hopkins, Appl Phys Lett 62 (25), 1993, 3247-3249

[54] M M Turner and M B Hopkins, Phys Rev Lett , 69(24), 1992, 3511-3514

[55] C K Birdsall, IEEE Trans Plasma Sci 19 (2), 1991, 65-85

[56] M Surendra and D B Graves, IEEE Trans Plasma Sci 19 (2), 1991, 144-157

[57] D Vender and R W Boswell, IEEE, Trans Plasma Sci 19 (2), 1991, 725-732

[58] W N G Hitchon, G J Parker and J E Lawler, IEEE Trans Plasma Sci 19 (2), 1991, 228-237

[59] J Forster, Appl Phys Lett 62 (26), 1993, 3249-3431

[60] H R Koenig and L I Maissel, IBM J Res Develop, 1970, 168-171.

[61] A J van Roosmalen, W G M van den Hoek and H Kalter, J Appl Phys 58 (2), 1985, 653-658

[62] K Kohler, J W Coburn, D E Horne and E Kay, J Appl Phys 57 (1), 1985, 59-66

[63] V A Godyak, R.B Piejak and B M Alexandrovich, IEEE Trans Plasma Sci 19 (4), 1991, 660 - 676

[64] P Beltzinger, J Appl Phys 67 (1), 1990, 130-138

[64] V A Godyak, R B Piejak and B M Alexandrovich, Plasma Sci Sources and Technol 1, 1992, 36-58

[65] V A Godyak and R B Piejak, Appl Phys Lett 63(23), 1993, 3137-3139

Chapter 2 : Theory of rf Plasmas.

2.1 Introduction.

Plasmas generated using radio frequencies, 13 56MHz, behave in quite a different manner to those generated using a dc bias The main reason for this being the ability of electrons to follow the applied electric field while the heavier ions, like the backround neutrals, remain unperturbed The effect of this behaviour changes the mechanisms by which the plasma is sustained and heated, particularly at low pressures

Plasma are used frequently in industry for etching or deposition purposes [1,2] In general the need arises to cover substrates in electrically insulating materials If the material is placed within a dc discharge however, it will quickly attain the floating voltage potential This results in equal fluxes of electrons and ions to its surface regardless of the applied voltage to the driving electrode, its behaviour being analogous to a capacitor within a dc circuit The use of ac discharges means that the substrate continuously charges and discharges and so the flux of charged particles to its surface can be changed by varying the driving frequency and the applied potential

As well as the ability to bombard insulating surfaces, it also transpires that rf discharges are more efficient at promoting ionisation, can be operated at much lower gas pressures and have decreasing impedances with increasing driving frequencies such that more current can be driven through the plasma for a given voltage [3] The purpose of this section is to examine why and how the plasma behaves as it does and how different system configurations and power coupling techniques alter the measured plasma parameters

2.2 System Configurations.

The symmetry of the system, ie the ratio of the area of the driving electrode to the grounded electrode, greatly alters the way in which a substrate may be etched or covered with a thin film The manner in which power is coupled to the plasma, whether it be capacitive, dc or inductively coupled, also plays an important role [4] The following section reviews some of theses configurations.

2.2.1 System Symmetry.

Commercial plasma processing systems are generally capacitively coupled parallel plate devices with one electrode driven and the other at ground potential. If the electrodes are of uneven area the system is termed asymmetric, as opposed to two electrodes of equal area, which defines a symmetric system [5]. In many cases the size of the electrodes are the same while the walls of the chamber are also grounded, which also gives rise to an asymmetric setup as shown in Figure 2.1. Most processing systems tend to favour the use of asymmetric systems as ions are accelerated toward the driven electrode. This is due to the establishment of a negative dc bias necessary to maintain electronic current continuity.

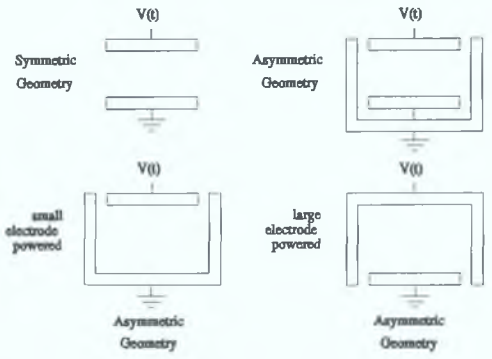

Figure 2.1: Different system geometries.

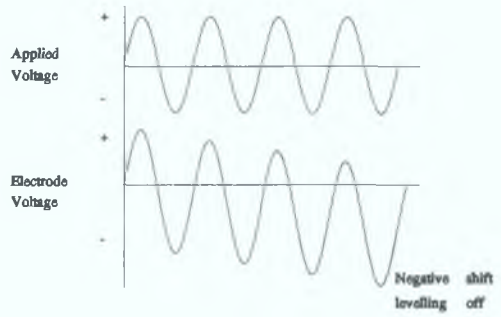

Figure 2.2: Development of the dc bias.

The electrons, due to their greater mobility respond faster, than the ions, to a disturbance to the plasma. During the positive half of the rf cycle many electrons are attracted to the electrode, while during the negative half, the ions, which are much slower in responding, cannot reach the electrode as fast. This leads to the formation of a negative dc bias on the driving electrode to reduce the number of electrons collected, as well as increase and accelerate the ions collected [6].

2.2.2 Power Coupling.

There are several means by which power is coupled from the rf generator into the plasma itself, each different technique having its own particular advantages and uses. As the demand for etching of smaller features increases in industry, a great deal of interest is presently being shown in the use of inductively coupled (transformer

coupled) plasmas [7] At present capacitively coupled plasmas are used for the etching of wafers and in the manufacture of thin films such as diamond like carbon for materials processing

Inductively Coupled Plasmas

It has been found using inductively coupled plasma, such as the Lam Research 9400 shown in Figure 2 3 [8], that ion densities of the order of 10^{11} cm^{-3} at ~5mTorr can be achieved These higher densities result in much faster etch rates The planar inductive plasma source consists of a flat spiral coil mounted above an upper ceramic plate with rf power supplied through a matching network The plasma is excited by the induced rf electric field There is no electrical displacement current driven through the sheath in front of the wafer Conditions are therefore similar to the sheath in a dc plasma, which is characterised by sheath voltages of the order of the mean energies of the electrons The wafer is mechanically clamped to a helium cooled lower electrode and a second power generator allows for independent wafer biasing [9] This type of setup produces a more uniform ion density near the surface of the substrate which in turn produces a more homogenous etch of the wafer [10]

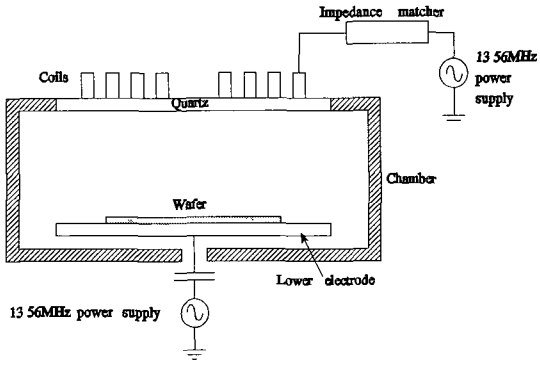

Figure 2 3 Lam Research 9400 inductively coupled etcher

Other uses of inductively coupled plasmas are in plasma torches, where the plasma is formed when energy is transferred to the gas by means of an induction coil The torch consists of concentric tubes generally composed of quartz The plasma forms above the inner tube and within the outer tube, its location determined largely by the position of the coil which is coupled to the rf generator [11] Although not fully understood yet these plasma have found applications in welding, chemical synthesis and spray coating [12].

Capacitively Coupled Plasmas.

At present parallel plate capacitively coupled plasma are used in industry for plasma etching and thin film deposition. For this technique, power is supplied from the rf generator, through a matching network and blocking capacitor, to the plasma. Matching units are necessary to ensure that maximum power is deposited within the plasma and minimum power reflected back towards the generator: matching units merely match the output impedance of the generator with the input impedance of the plasma [13]. Since the impedance of the plasma changes with pressure and other factors the components of the matching unit are generally variable so that optimum power transfer can be obtained for all conditions. The blocking capacitor ensures that no dc current can flow through the plasma. This has the effect of maintaining the negative offset in asymmetric configurations, and so allows ion bombardment of the substrate. Neglecting this capacitor removes the negative dc bias as current can flow out of the system. The matching network used in the work presented here is shown in Figure 2.4. Systems which are dc coupled to the rf generator employ the same type of matching unit shown except with the blocking capacitor removed. This results in very high plasma potentials as the dc bias disappears [5].

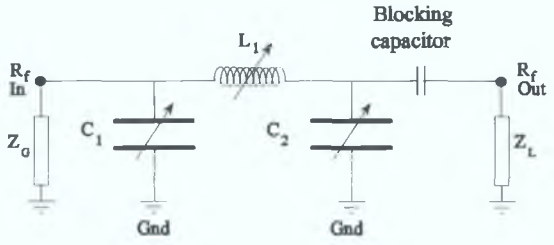

Figure 2.4: Schematic diagram of the matching unit.

2.3 Processes within the Plasma.

When the plasma has been formed by whatever means, it then must sustain itself until the power is removed. However since the plasma is composed of many particles some charged and some neutral, collisions between them will occur, many will get lost to the walls and some will recombine. The frequency at which all of these events occurs is quite important as this determines the type of plasma formed.

2.3.1 Collisions.

Just as there is a distribution of particle velocities, so too is there a distribution

of free path lengths ie statistically the distance a particle goes before colliding This distance is called the mean free path and given as

$$\lambda_m = \sum_n \frac{1}{N_n \sigma_n} \quad , \qquad \textbf{Eqn: 2.1}$$

where N_n is the number of particles of species n per m^3 and σ_n is the cross sectional area for collisions between electrons and particles of species n The mean time between collisions for a particle travelling at velocity v is then

$$\tau = \frac{\lambda_m}{v} \quad . \qquad \textbf{Eqn: 2.2}$$

The frequency of collisions ν, is therefore the inverse of τ If a maxwellian velocity distribution is assumed to govern the electrons, then the total collision frequency must be summed over all the velocities and so is given as

$$v = N_n \overline{\sigma v} \quad . \qquad \textbf{Eqn: 2.3}$$

Having established that there exists a frequency with which collisions occur, it must be noted that there are several different types of collisions, both elastic and inelastic, which the particles may undergo, with each of these processes having a different frequency of occurrence and effect on the plasma These types include electron impact collisions with neutral atoms, ion-neutral collisions, metastable collisions etc Any of these collisions can result in ionisation, recombination, excitation or relaxation of the particles It is by a combination of these production and loss mechanisms that the plasma is maintained

2.3.2 Ionisation.

Electron impact ionisation is the main process by which the plasmas studied here are sustained In this case a free electron colliding with a neutral atom removes an electron, producing a positive ion and two electrons The two electrons are then accelerated within the plasma by either the electric field or collisions with the oscillating sheath in rf plasmas Once they have acquired sufficient energy they may then cause more ionising collisions. There is a minimum energy required for this to

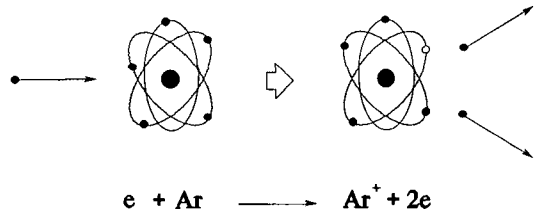

Figure 2 5 Ionisation through electron impact

occur known as the ionisation potential which for argon is 15 7eV It is not only through electron impact collisions that ionisation occurs, though it is the predominant mechanism

2.3.3 Enhanced Ionisation.

This is a process by which electrons can attain ionising potential energies in quite weak electric fields If an electron undergoes an elastic collision at the appropriate time with respect to the phase of the electric field then it is possible for its energy to increase Ideally the electron would collide with an atom, reversing its direction at the same moment the field changes direction In gaining energy this way an rf plasma can be sustained for much smaller electric fields than those required for dc plasmas [3]

2.3.4 Recombination.

Since ionisation is occurring in the plasma producing ions and electrons, recombination between them or losses to the walls must also occur to maintain a stable plasma To conserve momentum and energy, recombination requires three bodies to participate This process only contributes significantly in plasmas above pressures of about 1Torr The electron loss rate is given as

$$\frac{dn_e}{dt} = \alpha n_e n_i \quad , \qquad \textbf{Eqn: 2.4}$$

where α is the recombination coefficient

2.3.5 Excitation and Relaxation.

Electron impact with neutrals does not always cause ionisation In some cases energy is transferred from the impinging electron to a bound electron enabling it to jump to a higher energy level within the atom This is a process known as excitation The opposite of this is relaxation where the excited electron in the atom drops back down to the lower energy level and releases a photon of light equal to the energy difference between the two levels Emission spectroscopy uses this emission of light to detect the presence of various atoms

2.3.6 Diffusion.

Diffusion is a random walk process for particles in a plasma Here a net flux of particles from a dense region diffuses to a less dense region, with the flux proportional to the density gradient The proportionality constant known as the diffusion coefficient is given as,

$$D = \frac{kT}{m\nu} \quad . \qquad \textbf{Eqn: 2.5}$$

This will be different for each of the different species in the plasma When electrons or ions reach the walls of the plasma chamber, they recombine Essentially then the density at the walls is zero so there will be a constant diffusion of particles there Due to their smaller mass, electrons have a higher mobility than ions and diffuse much faster, setting up a space charge separation This will then retard the electrons and increase the ion diffusion so that space charge neutrality is maintained at all points in space This is known as ambipolar diffusion where the electrons and ions diffuse at the same rate determined by the ambipolar diffusion coefficient, which is given as

$$D_a = \frac{\mu_i D_e + \mu_e D_i}{\mu_i + \mu_e} \quad , \qquad \textbf{Eqn: 2.6}$$

where μ_i and μ_e are the ion and electron coefficients of mobilities respectively and are given as

$$\mu = \frac{|q|}{m\nu} \quad . \qquad \textbf{Eqn: 2.7}$$

Ambipolar diffusion is the primary loss mechanism in low pressure plasmas

2.4 Heating Mechanisms.

The exact mechanisms by which the plasma sustains itself, although mainly due to ionisation and excitation, are quite complex At low pressures a mechanism called "sheath heating" is responsible for maintaining the plasma, while at medium pressure localised ionisation dominates At high pressure and voltages secondary electrons emitted from the electrodes cause ionisation throughout the plasma In this case the plasma resembles a dc glow discharge and is known as the γ regime

2.4.1 Sheath Heating.

For a fixed gas, electrode gap and material, and driving frequency, the heating regime can be determined by the gas pressure and current density At low pressures, of the order of 10-40mTorr pressure, 3mAmps/cm^2 with a 7 5cm electrode gap for the experimental system considered here, a collisionless regime for plasma electrons occurs Here, stochastic heating in the sheath dominates and collisional heating due to electron-atom collisions is small The sheaths in an rf plasma move with speeds up to $\sim 5 \times 10^7$ cm/sec Low energy electrons are gently pushed by the bulk electric field towards the electrodes as the sheath retreats during the positive part of the cycle Some electrons move too slowly to catch the retreating sheath and so they bounce and loose energy When the sheath then expands during the negative part of the cycle the electrons are unable to move away and so collide with the sheath as it passes, gaining energy [14,15]

For argon this heating regime is enhanced by a phenomenon known as the Ramsauer effect [16,17] The cross section for elastic collisions, for slow electrons is unusually small in inert gases as shown in Figure 2 6 The low energy group of electrons therefore have an extremely low electron-atom collision frequency These electrons oscillate collisionlessly in the bulk of the plasma, trapped by the ambiploar potential well and unable to gam energy from the sheaths or the rf field The fast

electrons can however overcome these barriers and effectively interact with the argon atoms in ionising collisions. They then compensate for their energy losses through

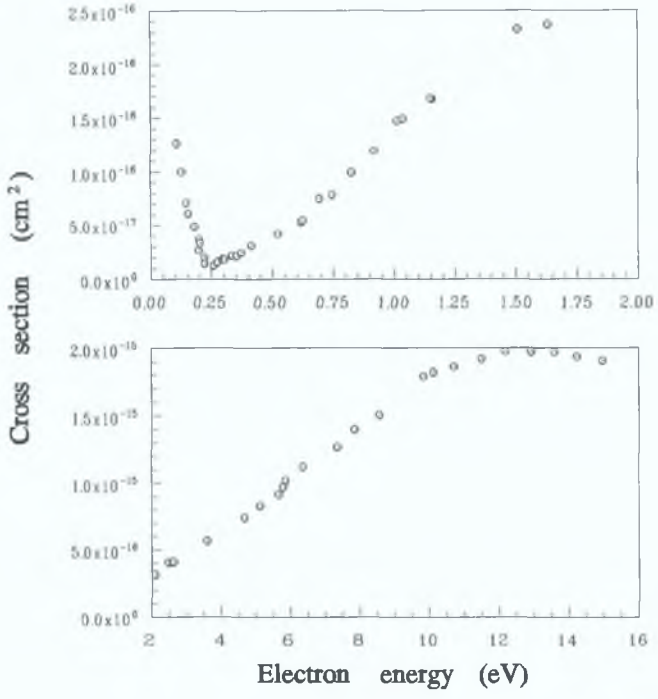

Figure 2.6: Total scattering cross section for argon taken from Golden et al [14].

collisions with the oscillating plasma sheath [18-20]. Most heating occurs during expansion of the sheaths for this process. However a mechanism known as anomalous sheath heating has been shown to occur, where heating during the retreating part of the cycle arises [21]. Since the electrons lag behind the sheath a region of positive space charge forms attracting the electron and heating them in the process.

2.4.2 Bulk Heating.

If the pressure of the plasma is increased above ~50mTorr, again with a 7.5cm electrode gap, for the system used here; the conditions of this regime are determined by the pressure and discharge length, ohmic or bulk heating becomes the dominant heating regime. In this case ionisation occurs locally in the bulk of the plasma as the mean free path of the electrons is less than the chamber dimensions. The electrons are heated by the bulk electric field giving them a higher temperature than they had in the stochastically heated regime. The transition in pressure between

the collisional and non-collisional regimes can be characterised by a parameter pd where p is the gas pressure and d the half width of the bulk plasma [22] The transition normally occurs in the range pd = 0 1 to 0 2 Torr cm

2.4.3 γ Regime

If the pressure of the plasma is increased to >0 5 Torr and the driving voltage also increased the heating mode of the plasma changes abruptly from the α (bulk electron heating) to the γ mode In this regime the ions bombard the surface of the electrodes emitting secondary electrons These electrons are then accelerated by the sheath field to very high energies where they undergo collisions producing more secondary electrons in an avalanche effect The electrons enter the bulk plasma causing ionisation mamly at the plasma sheath boundary but also to some extent in the bulk The ions produced are then accelerated towards the electrodes causing more secondary electrons to be produced The abrupt change in heating mode is also accompanied by a dramatic change in light emission from the plasma, a sharp drop in the electron temperature and an increase in the plasma density [13,23]

2.5 Conclusion.

The basic theory of rf plasmas has been examined The different system configurations have been introduced to show the effect of both chamber geometry and power coupling to the plasma Processes within the plasma have also been reviewed for the benefit of understanding the analysis of the results presented in Chapters 4 to 7 Finally the different heating mechanisms which occur within the plasmas examined in this work have been presented A further analysis of these heating modes is given in Section 4 3 with particular attention paid to the transition from stochastic to bulk heating

References.

[1] J W Coburn, IEEE Trans Plasma Sci 19(6), 1991, 1048-1062

[2] J L Shohet, IEEE Trans Plasma Sci 19(5), 1991, 725-733

[3] B Chapman, *Glow Discharge Processes,* Wiley, New York, 1980

[4] M W Blades, P Banks, C Gill, D Huang, C LeBlanc and D Liang, IEEE Trans Plasma Sci 19(6), 1991, 1090-1113

[5] K Kohler, J W Coburn, D E Horne and E Kay, J Appl Phys 57(1), 1985, 59-66

[6] K F Al-Assadi, Vacuum, 43(4), 1992, 287-290

[7] R Patrick, P Schoenborn and H Toda, J Vac Sci Technol A, 11(4), 1993, 1296-1300

[8] P L G Ventzek, R J Hoekstra, M Gropperhaus and M J Kushner, *Simulations of Inductively coupled plasma for etching applications*, Lam 6th Annual Technical Symposium, Grassau, Germany 1994

[9] G DiPeco, V Vahedi, D W Hewett and T D Rognlien, J Vac Sci Technol A, 12(4), 1994, 1387-1396

[10] Y Ra, S G Bradley and C-H Chen, J Vac Sci Technol A, 12(4), 1994, 1328-1333

[11] G L Moore, *Introduction to inductively coupled plasma emission spectroscopy*, Elsevier, Amsterdam-New York, 1989

[12] M I Boulos, IEEE Trans Plasma Sci 19(6), 1991, 1078-1089

[13] J V Scanlan, PhD Thesis, Dublin City University, 1991

[14] T J Sommerer, W N G Hitchon and J E Lawler, Phys Rev Lett , 63(21), 1989, 2361-2364

[15] T J Sommerer, W N G Hitchon, R E P Harvey and J E Lawler, Phys Rev A , 43(8), 1991, 4452-4472

[16] D E Golden and H W Brandel, Phys Rev 149(1), 1966, 58-59

[17] V E Golant, A P Zhilmsky, I E Sakharov and S C Brown, *Fundamentals of Plasma Physics*, Wiley, New York, 1979, pp49

[18] M Surendra and D.B Graves, Phys Rev Lett 66(11), 1991, 1469-1472

[19] V A Godyak, R B Piejak and B M Alexandrovich, Plasma Sources Sci Technol 1, 1992, 36-58

[20] V A Godyak and R B Piejak, Phys Rev Lett 65(8), 1992, 996-999

[21] M M Turner and M B Hopkins, Phys Rev Lett , 69(24), 1992, 3511-3514

[22] M M Turner, R A Doyle and M B Hopkins, Appl Phys Lett 62(25), 1993, 3247-3249

[23] V A Godyak, R B Piejak and B M Alexandrovich, Phys Rev Lett 68(1), 1992, 40-43

Chapter 3: Plasma Diagnostics.

3.1 Introduction.

The purpose of this chapter is to introduce the different diagnostic techniques used in this work Each different method has its own specific theory associated with it, which shall be examined in detail to extract the means by which the relevant plasma parameters can be calculated

3.2 The Langmuir Probe.

The Langmuir probe due to its simplicity of design and in-situ measurements is one of the most frequently used and useful diagnostics in plasma physics Unlike other analytic techniques it provides local information regarding the various plasma parameters, rather than volume averaged results which are obtained by other methods such as microwave interferometry, emission spectroscopy, etc Although the Langmuir probe is a simple tool, the subsequent analysis of the resulting data is extremely involved and can be subject to much misinterpretation However, extensive investigation into the behaviour of probes within plasmas has produced well established theories making the probe a very powerful diagnostic tool

3.2.1 Probe Theory.

The Langmuir probe diagnostic technique consists of placing a conductor into a plasma, applying a voltage and measuring the resulting current drawn from the plasma with respect to a reference electrode For the system in operation here, the reference electrode is the chamber wall of the system which is connected to ground In this fashion a current-voltage curve is produced from which the various plasma parameters can be calculated Initially when the probe is placed within the plasma a sheath forms around it to shield the bulk plasma from the disturbance Most of the voltage drop will appear across this sheath which is of the order of a few Debye lengths in width [1,2] Since cylindrical probes can be made quite small in comparison to the plasma volume and also due to considerable research already established, they are primarily used No theory exists which adequately describes the behaviour of the I-V characteristic in the plasmas considered here, but the most

complete theory is that of Laframboise, the main drawback being the absence of collisions in his treatment [3-5]

Probe behaviour within a high pressure plasma is quite different to that for a low pressure plasma and so different theories have been developed for each scenario The work here is analysed within the low pressure case where,

$$r_p \ll \lambda \qquad \text{and} \qquad \lambda_d \ll \lambda \qquad \textbf{Eqn: 3.1}$$

where r_p is the probe radius, λ the electron collisional mean fee path and λ_d the Debye length which is given by,

$$\lambda_d = \left(\frac{\epsilon_0 k T_e}{e^2 n_\infty} \right)^{\frac{1}{2}} . \qquad \textbf{Eqn: 3.2}$$

Several other assumptions must also be made for the purpose of simplicity [6]

- The plasma is assumed infinite, homogenous and quasineutral in the absence of the probe
- Maxwellian velocity distributions are assumed for both electrons and ions with temperatures T_e and T_i respectively such that $T_e \gg T_i$
- All charged particles striking the probe are assumed to be absorbed
- No magnetic fields are assumed to be present

It is recognised that the conditions set out above are not always satisfied and discussions of this are included in the text

A typical Langmuir probe I-V characteristic is shown in Figure 3 1, with various regions noted, in Figure 3 1 If the probe is biased strongly negative the probe will collect only ions, although the bias should be large enough to remove any contribution from high energy electrons The current collected by the probe in this region, I_{+sat} is given as,

$$I_{+_{sat}} = \frac{1}{4} n_0 e S \bar{v}_s , \qquad \textbf{Eqn: 3.3}$$

where n_0 denotes the ion density in the undisturbed plasma, S is the sheath area and $\bar{v}_s$ the ion acoustic velocity which is defined as

$$\overline{v_s} = \left(\frac{kT_e}{m_+}\right)^{\frac{1}{2}} \quad . \qquad \textbf{Eqn: 3.4}$$

The ion acoustic velocity is the minimum velocity which the ions must have to enter the sheath [7] As the probe bias is reduced, fast electrons initially begin to contribute most to the collected current The point at which no current is collected is known as the floating potential, V_f At this point the probe potential is sufficiently negative relative to the plasma to repel all the electrons except a small flux equal to the ion

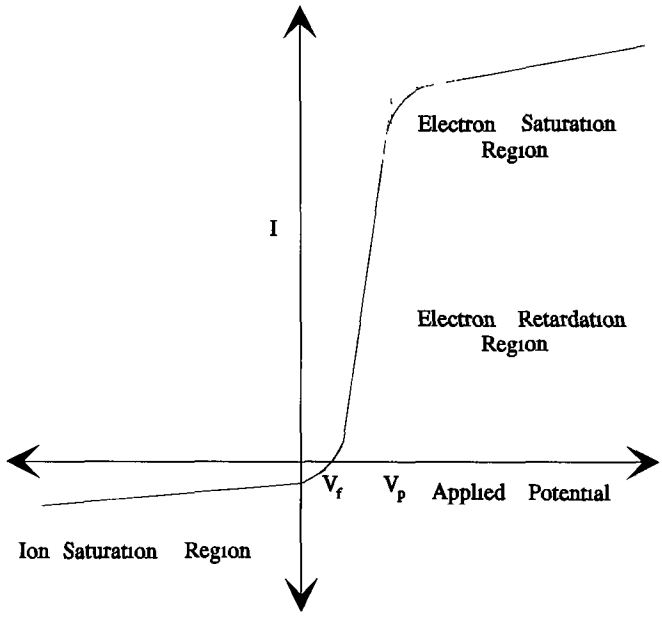

Figure 3 1 Typical current voltage characteristic from a Langmuir probe

flux, so no net current is collected A probe with no electrical connections therefore remains at this potential, which is always negative with respect to the plasma potential

If the probe voltage is biased more positive, the probe begins to collect electrons as more are able to overcome the retarding potential initially the faster ones of the velocity distribution and then the slower ones as the voltage increases In conjunction with this, the thickness of the ion sheath decreases The density of the electrons in this ion sheath is then governed by Boltzmann's law [8] or

$$n_e = n_\infty \exp\left(\frac{eV_p}{kT_e}\right) \quad . \qquad \textbf{Eqn: 3.5}$$

The random current at the sheath edge, like that for the ion current equation (3 3), is given as,

$$I_{e0} = -\frac{1}{4} n_o e \bar{v}_e S \quad , \qquad \textbf{Eqn: 3.6}$$

where S is the area of the sheath and $\bar{v}_e$ is the average electron velocity, calculated from the Maxwell Boltzmann velocity distribution and found to be

$$\bar{v}_e = \sqrt{\frac{8kT_e}{\pi m}} \quad . \qquad \textbf{Eqn: 3.7}$$

The total current to the probe in this region of retarding potential is then [2,6],

$$I_{probe} = I_{+_{sat}} + I_{eo} \exp\left(\frac{eV_p}{kT_e}\right) \quad . \qquad \textbf{Eqn: 3.8}$$

On increasing the probe potential further, a point is reached in the characteristic known as V_p , the plasma potential At this point the probe is at the same potential as the plasma and as a consequence there is no sheath around the probe For this reason ions and electrons migrate to the probe due only to their thermal velocities Since electrons have a higher mobility than ions, the current here is electron dominated At higher positive values of probe voltage, the ions are unable to overcome the potential drop within the sheath This area of the characteristic is called the electron saturation region and the current to the probe given as,

$$I_{e_{sat}} = -\frac{1}{4} n_o e \bar{v}_e S \quad . \qquad \textbf{Eqn: 3.9}$$

From this analysis it can be seen that much information regarding the plasma can be obtained from the current voltage curve. However to calculate parameters such as the electron temperature, density, plasma potential and floating potential, further

examination of the theory is required

3.2.2 Plasma Parameter Analysis.

A cylindrical probe was chosen for the work presented here It has two major advantages over the plane probe which are, a definitive theory describing the behaviour of the sheath [9] and the possibility of using small area probes which cause less disturbance to the plasma Knowing the behaviour of the sheath and thus the ion current expansion it is possible to measure the ion density n_+ as well as the fast electron current to the probe A smaller area probe reduces the depletion of low energy electrons which is particularly beneficial when dealing with low densities and weak magnetic fields The probe theory used in analysing the characteristic is that of Laframboise [9]

From Laframboise theory the expansion of either the ion or the electron current to the probe can be described as a function of the applied voltage

$$\frac{I_+(V)}{I_{+_0}} = f\left(\frac{r_p}{\lambda_d}, \chi\right), \quad \chi < 0 \ , \qquad \textbf{Eqn: 3.10}$$

$$\frac{I_e(V)}{I_{e_0}} = f\left(\frac{r_p}{\lambda_d}, \chi\right), \quad \chi > 0 \ , \qquad \textbf{Eqn: 3.11}$$

where χ , the non-dimensional probe voltage, is given as

$$\chi = \frac{e(V - V_p)}{kT_e} \ . \qquad \textbf{Eqn: 3.12}$$

The function f is derived from numerical fits to Laframboise curves, while I_{+o} and I_{e0} are the following scaling factors,

$$I_{+_0} = n_+ r_p e\left(\frac{2\pi kT_e}{m_+}\right)^{1/2} \qquad \textbf{Eqn: 3.13}$$

$$I_{e_0} = - n_e r_p e \left(\frac{2\pi k T_e}{m_e} \right)^{1/2} . \qquad \textbf{Eqn: 3.14}$$

Since these equations describe the probe behaviour, the calculation of all relevant plasma parameters will require values for the plasma potential V_p , the electron temperature kT_e and the Debye length λ_d To overcome this, estimations are made first from an initial trace of the I-V curve The first derivative of the curve yields a value for the plasma potential while the slope of the exponential section produces a value for kT_e Once $\chi(V)$ is known the most suitable value for r_p/λ_d is chosen by fitting the observed probe current $I(\chi)$ to the theoretically predicted probe current $I(R_p/\lambda_d , \chi)$ For this fitting process χ (V) is taken at a very negative voltage where there would be no contribution by fast electrons to the current Calculation of other parameters such as the electron and ion densities n_e and n_+ , the floating potential and the fast electron contribution can now be made from the first approximations of kT_e V_p and r_p/λ_d [5]

The electron density is found by combining equations (3 10) and (3 13) such that

$$n_e = \frac{-I_e(\chi)}{e r_p \left(\frac{2 \pi k T_e}{m_e} \right)^{1/2} f\left(\frac{r_p}{\lambda_d} \right)} , \qquad \chi > 0 , \qquad \textbf{Eqn: 3.15}$$

where $I_e(\chi)$ is the current at some positive voltage with respect to the plasma potential Similarly the ion density is calculated using equations (3 9) and (3 12)

$$n_+ = \frac{I_+(\chi)}{e r_p \left(\frac{2 \pi k T_e}{m_+} \right)^{1/2} f\left(\frac{r_p}{\lambda_d} \right)} , \qquad \chi < 0 , \qquad \textbf{Eqn: 3.16}$$

with $I_+(\chi)$ measured at a sufficiently negative voltage to remove any contribution from electrons

When determining V_p from the first derivative of the I-V curve, it has been found that the value obtained for the maximum always occurs below the point of

saturation. For this reason it is corrected for using the method of intersecting slopes which predicts,

$$V_p = V_{\max} + kT_e \ln\left(\frac{I_{sat}}{I_{maxderiv}}\right) \qquad \textbf{Eqn: 3.17}$$

where V_{max} is the voltage at the maximum of the first derivative with $I_{maxderiv}$, its corresponding current value and I_{sat} is the electron saturation current. Thus the plasma potential is corrected from its initial estimated value using the value of I_{eo} taken from equation (3.11) using the new value of n_e.

The fast electron density and temperature is calculated from the current to the probe at negative values of χ. However the contribution from the ion and bulk electron current must initially be removed since

$$I(\chi) = I_+(\chi) + I_e(\chi) + I_{fe}(\chi). \qquad \textbf{Eqn: 3.18}$$

To simplify the situation, the calculation of I_{fe} is restricted to the region, $\chi < -10$, as the bulk electron contribution is effectively zero. The fast electron temperature can then be calculated by fitting the current using a least squares exponential regression to

$$I_{fe}(\chi) = I_{0_{fe}} \exp\left(\frac{\chi\, kT_e}{kT_{fe}}\right), \qquad \textbf{Eqn: 3.19}$$

where I_{ofe} is the fast electron thermal flux at the plasma potential and kT_{fe} the fast electron temperature [5].

The electron temperature is recalculated since the ion and fast electron current components can now be removed from the region where the bulk electron temperature was initially calculated.

3.2.3 The Electron Energy Distribution Function.

The most basic characteristic for any gas discharge is the electron energy distribution function (eedf). It provides information regarding the means by which the plasma is sustained and heated and is fundamental in calculating the rate coefficients

for excitation and ionisation. When integrated over, the eedf yields a value for the electron density and reaction cross sections.

$$\langle \sigma v \rangle = \int_{threshold}^{\infty} f(\epsilon)\, \sigma(\epsilon)\, v(\epsilon)\, d\epsilon , \qquad \textbf{Eqn: 3.20}$$

where $f(\epsilon)$ is the normalised eedf, $\sigma(\epsilon)$ is the reaction cross section and $v(\epsilon)$ is the electron velocity.

The second derivative the probe current-voltage characteristic is proportional to the eedf provided that it is isotropic [11], that is

$$n(\epsilon) = n_e\, f(\epsilon) = \frac{2}{eA} \frac{d^2 I_e}{dV^2} \left(\frac{2m\,\epsilon}{e} \right)^{\frac{1}{2}} \qquad \textbf{Eqn: 3.21}$$

where the energy $\epsilon = V - V_p$. So by simply differentiating the probe current twice with respect to the probe bias the eedf is obtained. This differentiation can be by numerical or analogue methods, the former being employed here as it does not mask or suppress the eedf structure.

In calculating the eedf an average of 10^5 data points are taken with a bandwidth of $\Delta\epsilon = 0.5$eV at low energies and $\Delta\epsilon = 1$eV at higher energies. There is no need then to exercise any smoothing techniques.

3.2.4 The Tuned Probe.

Problems are encountered when using a conventional Langmuir probe in a 13.56MHz plasma. Since the plasma potential varies with time so also does the current collected by the probe if it is maintained at a fixed dc bias. This results in an overestimation of the electron temperature kT_e and an underestimation of the electron density n_e. Several methods are available to overcome rf distortion of the probe measurements in the plasma. These include time resolving [12] the I-V characteristic obtained using a conventional Langmuir probe, deconvoluting the effect of the RF potential on the probe characteristic obtained using a capacitive probe with high impedance or combating the RF distortion of the characteristic obtained using a floating double probe [13]. All of these methods can work quite well but they suffer

the problems of being either very complex methods of analysis or are subject to large capacitive loading at 13 56MHz A simple non complex solution is to use a tuned Langmuir probe [14,15], shown in Figure 3 2, to overcome these problems In order to avoid RF convolution of the probe characteristic, the RF voltage across the plasma probe sheath should be less than the electron temperature, approximately 1eV This is done by ensuring that the impedance of the sheath is small compared with the impedance between the probe and ground

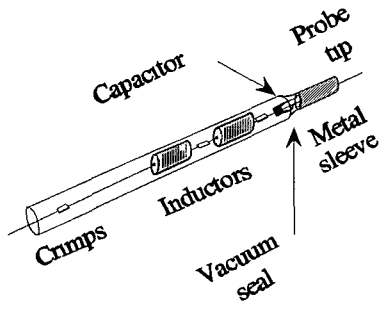

Figure 3 2 The tuned probe

An equivalent circuit of the tuned probe [14,15] is shown in Figure 3 3 Three voltage nodes are shown Point A corresponds to a point outside the plasma,

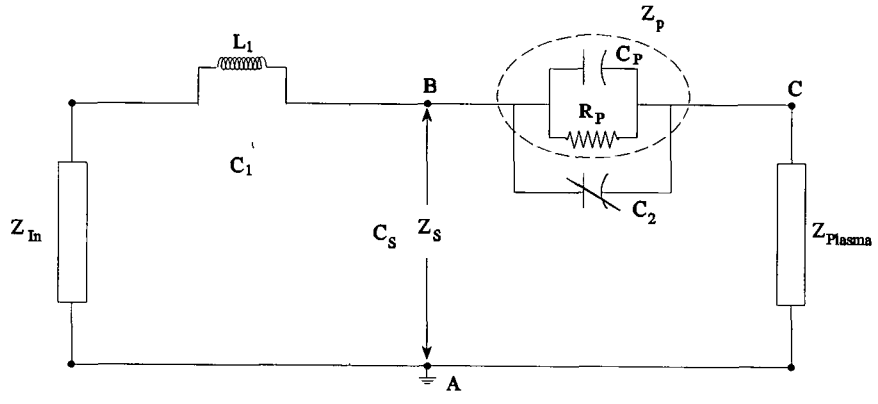

Figure 3 3 Equivalent circuit of the tuned probe

usually the grounded chamber wall Point B corresponds to the probe tip ie the probe collecting surface while point C corresponds to a point in the plasma just

outside the plasma probe sheath The impedance of the plasma probe sheath is denoted by Z_p and consists of a resistive and a capacitive term in parallel, the non-linear nature of this impedance is not discussed When $\omega > \omega_i$, the ion frequency, then the RF sheath is essentially capacitive the value of the sheath capacitance may be estimated as follows

The capacitance of the co-axial sheath is [16]

$$C_p = \left[\frac{2 \pi \epsilon_0 L_p}{\ln \left[\frac{r_s + r_p}{r_p} \right]} \right], \qquad \textbf{Eqn: 3.22}$$

where r_p is the probe radius, L_p the probe length and r_s the sheath thickness Allowing for a probe radius of 0 19mm, the sheath capacitance, C_p for a probe of length 10mm is 0 77pF At 13 56MHz this represents an impedance of $Z_p \approx 1\ 5 \times 10^4 \Omega$ The impedance between the probe collecting surface and the reference point is denoted by Z_s This term consists of the impedance of the rf chokes in parallel with a parasitic capacitance C_s Since Z_p is in series with Z_s the ratio of Z_p/Z_s should be very small to ensure that there is very little rf voltage across the probe sheath junction

The value of Z_p can be reduced by adding a shunt capacitance across the plasma-probe junction [17] An AC shunt can be produced by placing a large conducting surface in contact with the plasma and AC coupling this to the collecting probe This is denoted by C_2 The value of C_2 is only dependant on the plasma parameter λ_d and is independent of the probe voltage, whereas C_p being dependant on the plasma probe sheath thickness is influenced by the probe bias Introducing C_2 in parallel with C_p not only reduces Z_p but also makes the effective probe tip capacitance independent of the probe bias voltage [15,18] The conducting sleeve which constitutes C_2 comprises a stainless steel tube of radius 1 5mm and length 25mm capacitively coupled to the probe tip so that,

$$C_2 = \left[\frac{2 \pi \epsilon_0 L_s}{\ln \left[\frac{\lambda_d + r_p}{r_p} \right]} \right], \qquad \textbf{Eqn: 3.23}$$

r_s is now replaced by λ_d so C_2 = 21 5pF which at 13 56MHz constitutes an impedance of 545Ω Since C_p and C_2 are in parallel their effective capacitance is 22 45pF and their combined impedance is 5 $2x10^2\Omega$

The value of Z_s can be increased by minimising the value of the stray capacitances and maximising the impedance of the inductors at the specific rf frequency To reduce stray capacitances the inductors are placed as close to the probe tip as is possible, values of C_s approach zero effectively when the inductors are immersed in the plasma The impedance of the tuning network is maximised by ensuring that the inductors used have a self resonance close to 13 56MHz This results in an impedance of $\sim 1x10^5\Omega$ at the first harmonic Since Z_s is now $\sim 200Z_p$ a non-convoluted characteristic can be obtained

The inductors were checked to ensure that they resonated at the required frequency This was done by applying a variable frequency signal to the inductor and observing their response using an oscilloscope For the tuned probe here it has been found that the inductors resonate at 13 to 14MHz and at harmonics of this frequency One inductor tuned below 13 56MHz and one above produce the ideal band stop filter The impedance of the filter at 27MHz can be as high as 30% of its value at the fundamental

3.2.4 Hardware of the Probe Diagnostic Unit

The probe diagnostic system used here is a fully automated system [19,20] A personal computer is connected to the data acquisition unit using an input/output card and controlled using a Quick Basic™ program This technique allows non-sequential measurement of the characteristic The software interacts in real time so only data necessary for the evaluation of the plasma parameters is collected The probe current is measured by the voltage drop across a resistor whose value is chosen according to conditions set within the program allowing currents from 30μA up to 300mA to be accurately measured The probe voltage is measured before the resistor to avoid leakage currents The probe unit itself is comprised of two 16 bit analog-to-digital convertors (adc) to measure the voltage and current and send measurements to the computer, and one digital-to-analog convertor (dac) to send the voltage required by the program to the probe The number of averages taken for each point on the

characteristic can be varied within the program but for the work presented here was set to 100 samples In order to prevent errors due to changes in the probe work function, the probe is regularly cleaned using electron bombardment by biasing the probe well above the plasma potential The probe is also held at negative voltages, when possible during scanning, so that it is kept clean through ion bombardment

3.3 Microwave Interferometry

Microwave interferometry is a well established diagnostic technique used for measuring the line integral of the electron density [21] Unlike the probe it is a non-invasive technique and so does not deplete the low energy electron density as the probe can do at very low pressures The theory behind its operation is also less complicated and subject to less misinterpretation

3.3.1 The Microwave Interferometer.

If a microwave signal is passed through an auxiliary transmission path and nulled against that of the signal through the primary path, without a plasma present, the effect of striking a plasma within the transmission path will be to cause a phase shift in the output signal The change in phase is measurable using a variable phase changer, see Figure 3 4 A microwave signal output from the source, passes through

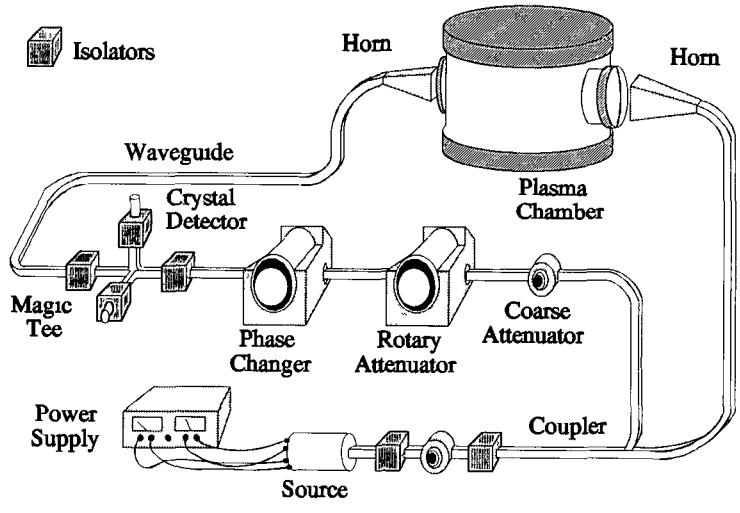

Figure 3 4 Schematic diagram of the microwave interferometer

a coupler which splits the wave between the two paths, the transmission path and the primary path The former path sends the wave along the waveguide to a horn which allows the wave to pass through the plasma and be received by a second horn on the opposite side of the chamber The wave then follows through the waveguide to the "magic T" junction The primary wave travels through several attenuators and a variable phase changer before arriving at the same junction The hybrid magic T allows the waves entering it from opposite sides, arms 2 and 3, to be equally split between arms 1 and 4 However the design of the junction is such that the excited wave in arm 4 will be the sum of the wave in arm 2 to the wave in arm, while the wave excited in arm 1 will be the difference between the waves in arms 2 and 3 [22] If the initial wave from the microwave source is given as

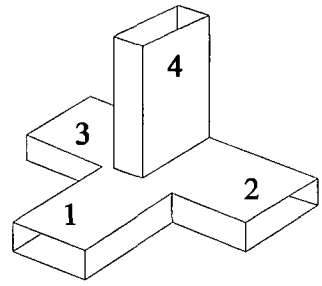

Figure 3 5 Magic T junction

$$A \cos(\omega t), \qquad \textbf{Eqn: 3.24}$$

then the waves entering arms 2 and 3 will be given respectively as

$$\begin{matrix} M \cos(\omega t) \\ R \cos(\omega t + \phi). \end{matrix} \qquad \textbf{Eqn: 3.25}$$

The diodes in the detectors rectify the signal so the output from the arms now is approximatley the sum and difference of the two input waves squared ie the output from arm 1 is now

$$[R \cos(\omega t + \phi) + M \cos(\omega t)]^2, \qquad \textbf{Eqn: 3.26}$$

while that from arm 4 is now

$$[R \cos(\omega t + \phi) - M \cos(\omega t)]^2. \qquad \textbf{Eqn: 3.27}$$

The outputs from the two arms are subtracted from each other and the equation rearranged to give ,

$$-4MR\cos(\omega t)\cos(\omega t + \phi) \qquad \textbf{Eqn: 3.28}$$

Using standard mathematical tables this can be written as

$$-2MR[\cos(2\omega t + \phi) - \cos\phi]. \qquad \textbf{Eqn: 3.29}$$

Since the first part of the equation averages the zero the output signal will be,

$$K\cos\phi, \qquad \textbf{Eqn: 3.30}$$

where K is a constant This type of interferometer setup allows quick and easy measurement of the average electron density of a plasma The results obtained can be directly compared to those of the probe so the optimum pressure range and conditions of the plasma in which the probe operates can be established [23]

3.3.2 Theory of Microwave Interferometry

The interaction of an electromagnetic wave with an electron gas can be described by the Lorentz equation of motion [24],

$$m\frac{dv}{dt} = -eE \quad . \qquad \textbf{Eqn: 3.31}$$

The influence of discrete positive ions and neutral molecules in a plasma can be represented to a good approximation by including a viscous damping term So the equation of motion now becomes,

$$m\frac{dv}{dt} = -eE - \nu m v \quad , \qquad \textbf{Eqn: 3.32}$$

where ν is the collision frequency for momentum transfer Solving this equation for v, using $v = v_o \exp\{j\omega t\}$ gives,

$$v_e = -\frac{eE}{m(\nu + j\omega)} \quad . \qquad \textbf{Eqn: 3.33}$$

where v_e is the electron velocity The current density, J, is defined as,

$$J = \Sigma q n v \quad . \qquad \textbf{Eqn: 3.34}$$

The ions are however assumed to be stationary so J depends only on the electron contribution,

$$J = -e n v_e \quad . \qquad \textbf{Eqn: 3.35}$$

Substitution of Equation 3 26 into 3 28 then results in,

$$J = \frac{ne^2}{m(\omega + jv)} E = \sigma E \quad , \qquad \textbf{Eqn: 3.36}$$

from Ohms law The refractive index of a medium is given as [25],

$$\eta^2 = 1 - j\frac{\sigma}{\epsilon_0 \omega} \quad , \qquad \textbf{Eqn: 3.37}$$

which when solved using the value for σ shown in Equation 3 29 yields [26],

$$\eta^2 = 1 + \frac{\omega_p^2}{\omega^2}\left(\frac{1}{1 - \frac{jv}{\omega}}\right) \quad , \qquad \textbf{Eqn: 3.38}$$

where the plasma frequency ω_p is defined as,

$$\omega_p^2 = \frac{e^2 n}{m \epsilon_0} \quad . \qquad \textbf{Eqn: 3.39}$$

Equation 3 31 gives a direct relationship between the electron density and the refractive index of the plasma Since the plasma has a refractive index different to that of a vacuum, an electromagnetic wave propagating through the plasma will undergo a phase change A comparison of the phases of the two waves will therefore yield a value for the electron density

3.3.3 Average Electron Density.

The phase constants for waves travelling through a vacuum and a plasma are respectively given as [24]

$$\phi_0 = \frac{2\pi}{\lambda} \quad , \quad \phi_p = \left(1 - \left(\frac{\omega_p}{\omega}\right)^2\right)^{1/2} \frac{2\pi}{\lambda} \quad . \qquad \textbf{Eqn: 3.40}$$

The phase difference between the two waves introduced by the presence of the plasma is then

$$\Delta\phi = -\int (\phi_p - \phi_0)\, dx \quad , \qquad \textbf{Eqn: 3.41}$$

where the integration is carried out over the path of the plasma There exists for plasmas, a critical density n_c , below which the plasma is a nearly transparent dielectric and above which the plasma is opaque and highly reflecting This cutoff frequency is given as,

$$\omega_c^2 = \frac{n_c e^2}{\epsilon_0 m} \quad . \qquad \textbf{Eqn: 3.42}$$

If the integration of Equation 3 34, is carried out along the path from transmitting to receiving antenna, it becomes, under the assumption $n \ll n_c$,

$$\Delta\phi \underset{n<n_c}{\rightarrow} \frac{\pi}{\lambda n_c} \int n(x)\, dx \quad . \qquad \textbf{Eqn: 3.43}$$

For this case the phase shift is linearly proportional to the electron density averaged along the integration path, so for a path length L the average density then becomes,

$$\bar{n} = \frac{\int_0^L n(x)\, dx}{L} = \frac{2\epsilon_0 m c}{e^2} \frac{\omega \Delta\phi}{L} \quad . \qquad \textbf{Eqn: 3.44}$$

This may be simplified to,

$$\bar{n}[\mathrm{cm}^{-3}] = 118.4 \frac{\frac{\omega}{2\pi}[\mathrm{Hertz}]\, \Delta\phi[\mathrm{rad}]}{L[\mathrm{cm}]} \qquad \textbf{Eqn: 3.45}$$

This form of the equation allows calculation of the electron density once the phase

difference is known.

3.4 The Current-Voltage Probe.

The current-voltage probe is a device designed to measure the current and voltage applied to the driving electrode. Once both of these parameters are known, the current density, impedance, reactance and the power deposited within the plasma can be found. Accurate measurement of the power is quite difficult to obtain using power meters as losses through the cable and connectors between the meter and the electrode can be quite large.

3.4.1 The Current Probe.

A current pulse transformer is used to measure the current to the driving electrode. It is connected after the matching unit, directly to the driving electrode. This reduces the risk of major losses after the measurement has been taken, as is the case with power meters. The coil itself is basically a Rogowski loop [16]. A metallic former with N turns of wire wrapped around itself is placed around the current carrying wire as shown. The current induces an emf across the ends of the coil, which if the dimensions of the coils are known can be used to calculate the current. The metallic former reduces the number of turns of wire required to measure very low currents. The coil is connected to an oscilloscope and the trace displayed and down-loaded to a computer where a fourier transform is taken to evaluate how the current is distributed among the various harmonics of the 13.56MHz driving frequency.

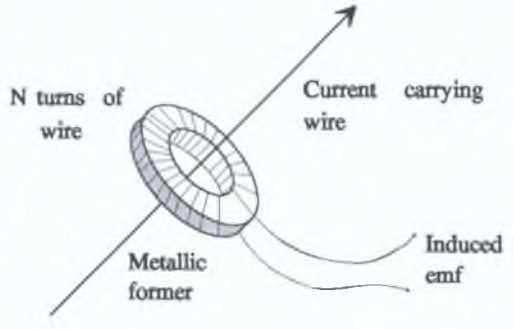

Figure 3.6 : Pearson current coil.

3.4.2 The Voltage Divider.

The voltage applied to the driving electrode cannot be measure using a standard resistive divider oscilloscope probe, as severe loading of the signal occurs.

Instead a capacitive divider network is used. This has the advantage of neglecting the dc component of signal and only transmitting the ac part. The voltage probe is also connected after the matching network but before the current probe. This is to ensure that any loading caused by the voltage probe will not affect the current measurements. The capacitor reduces the magnitude of the voltage by a factor of ~100 at 13.56MHz. This signal is then connected to an oscilloscope with a 50 Ohm input impedance. The voltage is measured across this resistance, and the driving voltage then calculated using calibration tables.

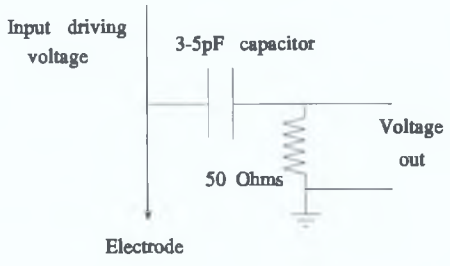

Figure 3.7 : Voltage divider circuit.

3.4.3 Parameter Calculations.

Since both the current and voltage waveforms can be displayed on an oscilloscope and the data down-loaded via an IEEE-488 interface card to a computer, various mathematical functions can be performed to extract information from the data. The phase difference between the two waveforms is initially found so that the power deposited into the plasma itself may be estimated using

$$\text{power} = \frac{V_{peak}\, I_{peak} \cos\phi}{2} \quad , \qquad \textbf{Eqn: 3.46}$$

where ϕ is the phase difference between the current and voltage. The difference in phase is approximately 90° for a capacitively coupled plasma, the deviations from this being due to the resistive component of the plasma which varies with the conditions of the plasma.

Fourier transformation of the current and voltage waveforms yields information regarding the amount of harmonic components present in the driving signal. Although the waveforms appear sinusoidal with a frequency of 13.56MHz, contribution from the 27.1MHz and 40.7MHz harmonics can be quite significant. The fourier transform of a waveform of this type is given as

where f denotes the frequency and t the time. The amplitudes of the different terms

$$H(f) = \int_{-\infty}^{\infty} h(t) \exp^{-j2\pi ft}\, dt \quad , \qquad \textbf{Eqn: 3.47}$$

of the transform indicate the contribution of each of the frequencies to the signal. In this manner it is then possible to design filter circuits to remove these frequencies or account for them in the probe design by incorporating inductors to present a high impedance to these components. The impedance of the plasma can be found once the voltage, current and phase difference between them are known. The impedance Z is complex and defined as

$$Z = R + jX \quad , \qquad \textbf{Eqn: 3.48}$$

where R is the resistive component and X the reactive one. The absolute value $|Z|$ is calculated from the current and voltage such that

$$|Z| = \frac{V}{I} \quad . \qquad \textbf{Eqn: 3.49}$$

Both the resistive and reactive components are used to examine where the power is dissipated within the plasma [27]. They are given respectively as

$$\begin{aligned} R &= |Z| \cos\phi \quad , \\ X &= |Z| \sin\phi \quad . \end{aligned} \qquad \textbf{Eqn: 3.50}$$

Finally, knowing the area of the driving electrode and the current to the plasma, the current density can be calculated. This is also used to assess how the power is deposited within the plasma. The current density is simply the current divided by the electrode area.

3.5 Conclusions.

Using these three diagnostic techniques, much information regarding the plasma can be obtained. The overlap between the data extracted from each method implies that direct comparisons can be made such that failings in any one system can be quickly observed and steps can be taken for its correction. These three techniques

also have the advantage of being able to operate at the same time without causing any interference to each other and in general causing very little disturbance to the plasma

References

[1] B Chapman, *Glow Discharge Process*, Wiley, New York, 1980

[2] F F Chen in *Plasma Diagnostic Techniques*, edited by R H Huddlestone and S L Leonard, Academic Press, New York, 1965

[3] J G Laframboise and L W Parker, Phys Fluids, 16(5), 1973, 629-636

[4] V A Godyak, R B Piejak and B M Alexandrovich, Plasma Sci Sources Technol 1, 1992, 36-58

[5] M B Hopkins and W G Graham, Rev Sci Instrum , 57(9), 1986, 2210-2217

[6] L Schott in *Plasma Diagnostics*, edited by W L Holtgreven, North Holland, Amsterdam, 1968

[7] F F Chen, *Plasma Physics and Controlled Fusion,* Plenum Press, New York, 1980

[8] B Lipschultz, I Hutchinson, B LaBombard and A Wan , J Vac Sci A , 4(3), 1986, 1810-1816

[9] J G Laframboise, UTIAS Report № 100, 1966

[10] M Šícha, P Špatenka and M Tichý, Contrib Plasm Phys 31(1), 1991, 43-47

[11] M J Druyvesteyn, Z Phys , 64, 1930, 781-798

[12] N Hershkowitz, M H Cho, C H Nam and T Intrator, Plasma Chem Plasma Process 8(1), 1988, 35-52

[13] F F Chen, Rev Sci Instrum , 35(9),1964, 1208-1212

[14] R R J Gagné and A Cantin, J Appl Phys 43(6), 1972, 2639-2647

[15] J V Scanlan, PhD Thesis, Dublin City University, 1991

[16] W J Duffin, *Electricity and Magnetism*, McGraw-Hill, New York, 1980

[17] B M Annaratone and N St J Braithwaite, Meas Sci Technol 2, 1991, 795-800

[18] P A Chatterton, J A Rees, W L Wu and K Al-Assadi, Vacuum, 42(7), 1991, 489-493

[19] M. B. Hopkins, W.G. Graham and T.J. Griffin, Rev. Sci. Instrum., 58(3), 1987, 475-476

[20] P Špatenka, R Studený and H Suhr, Meas Sci Technol 3, 1992, 704-708

[21] G Neumann, U Banziger, M Kammeyer and M Lange, Re Sci Instrum 64(1), 1993, 19-25

[22] A J Baden-Fuller, *An Introduction to Microwave Theory and Technique*, Pergamon Press, New York, 1979

[23] L J Overzet, Personal correspondence, University of Texas at Dallas, 1994

[24] M A Heald and C B Wharton, *Plasma Diagnostics with Microwaves*, Krieger Publishing Company, Huntington, New York, 1978

[25] E Hecht, *Optics*, Addison-Wesley, Ontario, 1987

[26] D M Manos, J L Cecchi, C W Cheah and H F Dylla, Thin Solid Films, 195, 1991, 319-336

[27] C Beneking, J Appl Phys , 68(9), 1990, 4461-4473

Chapter 4: Plasma Parameter Measurements in Argon.

4.1 Introduction.

All the diagnostic techniques described in detail in the previous chapter have been applied to the experimental system used here. Plasma parameters were monitored as a function of voltage and current to the plasma and pressure of the plasma. The tuned probe was used to measure the electron temperature, density of ion and electrons, plasma potential, floating potential and the fast electron contributions while microwave interferometry was used to monitor the electron density. The purpose of this chapter is to present the measurements obtained from the plasma and from this examine the fundamental processes within the plasma which are responsible for the behaviour of the plasma.

4.2 The Experimental System.

The plasmas were generated in a parallel plate capacitively coupled asymmetric system. The cylindrical aluminium chamber which was, 180mm in height and 270mm in diameter contained both a driving and ground electrode of diameters 200mm and 240mm respectively. Only the driving electrode was water cooled, the ground electrode as never heated up to such an extent as to warrant cooling. The walls of the chamber and ground electrode were connected together increasing the asymmetry of the system. The spacing between the aluminium electrodes could be varied allowing for gap sizes of 55, 75 and 125mm. The chamber was pumped by a 170 *l*/s turbomolecular pump giving a base pressure of 8×10^{-6} Torr as measured using a Penning gauge. Research quality gas was introduced into the system via a type MK7560 mass flow controller and monitored using an MK247C flowmeter. This type

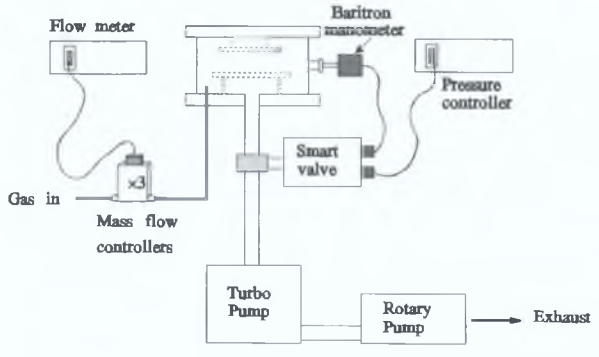

Figure 4.1: Schematic diagram of the gas flow and pressure control of the chamber.

of flow meter allowed for up to four mass flow controllers to be connected and so could be used for mixing gases The pressure of the plasma was set using an MKS 250b meter which in turn was connected to a Baritron capacitance manometer This type of gauge could measure from a few milliTorr to several Torr accurately To acquire the set pressure both the meter and the manometer were connected to a smart valve This type of butterfly valve compared both the set pressure with the actual pressure and opened or closed itself to equate them

Two probes were installed on the chamber, both through "Wilson Seals" These type of connectors allowed the probes to be easily moved about within the plasma so all regions could be examined One probe was installed through the top of the chamber as shown in Figure 4 2 and the other through a side port Because of this arrangement both vertical and horizontal scans of the plasma could be performed

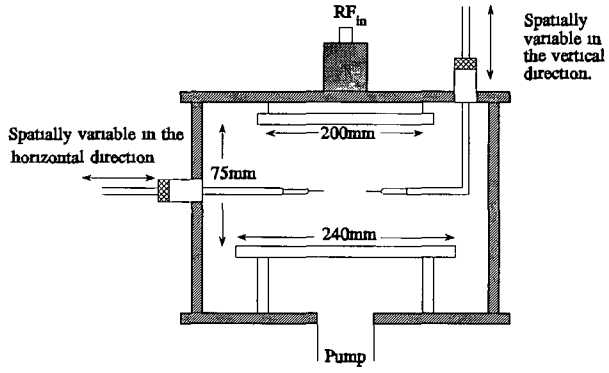

Figure 4 2 Chamber dimensions and probe positions within the chamber

With two probes installed on the chamber it was then also possible to monitor the sheath resistance of the plasma This was done by monitoring the floating potential of the second probe while biasing the first probe It was found that a shift in the floating potential normally occurred as the biased probe as made more positive By using the two probes this shift was measured and accounted for in the probe characteristics

A type ENI (model ACG-3) rf generator was used to produce the plasma It was connected directly to a π-type matching network shown in Figure 2 4, Section 2 2 2, to optimise the power deposited within the plasma A shunt circuit composed of an inductor and variable capacitor was connected to the top electrode This was incorporated to ensure that the current measured by the current probe was that within the plasma only rather than a combination of that current plus any stray current in chamber The matching unit connected directly from the power supply to the

current/voltage probe which in turn was connected to the electrode immediately before the plasma The current/voltage probe was connected to a HP5450 400MHz scope which was interfaced using a gpib card to a computer From the data which was transferred calculations to estimate the amount of power deposited into each of the harmonics of the rf wave were made as well as the peak to peak current and

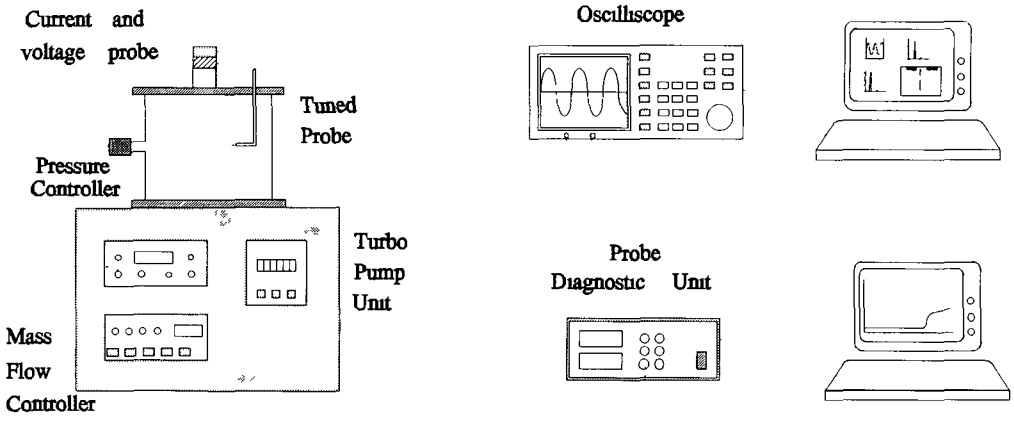

Figure 4 3 Schematic diagram of the Langmuir probe and current/voltage probe connections to the plasma

voltage of each harmonic The Langmuir probe was connected to a diagnostic unit which too was interfaced to a computer, though in this case via a Blue Chip I/O card The card relayed voltage and current measurements from the diagnostic unit to the computer so calculations of electron temperature, plasma potential, floating potential, densities etc could be made from the IV characteristic

Two windows of diameter 75mm on opposite sides of the chamber were used to pass microwaves from the interferometer through the plasma The horns of the interferometer were than placed up against the windows as shown in Figure 3 4, Section 3 3 1 Eccosorb sponge was then placed around the horns to remove any spurious reflections of the microwaves from the windows, to prevent them from being emitted into the laboratory All the sections of the interferometer were joined together tightly to reduce any mismatches in the waveguide as this would produce backward

reflections Isolators were placed throughout the whole of the interferometer as well to remove any reflected signals which might be present An 11 GHz signal was used to measure the electron density of the plasma This frequency signal was obtained using a YIG oscillator Since this source of microwaves produces a variable frequency signal from 7 - 16 GHz, it was necessary to calibrate the frequency as a function of the input current using a frequency meter A linear relationship between the two was found as shown in Figure 4 4 All the components of the interferometer were accurate over the 8 - 12 GHz range so the 11 GHz signal was fully compatible Two HP 8474B crystal detectors were connected to the arms of the "Magic T" junction, shown

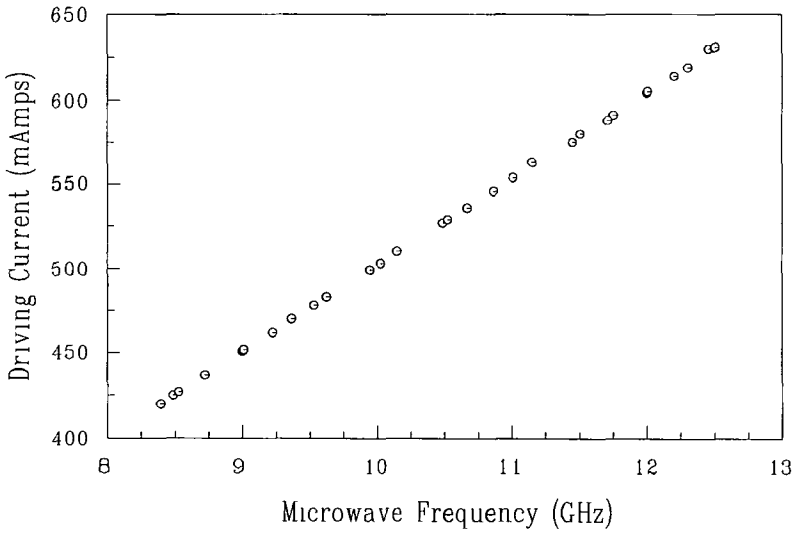

Figure 4 4 Yig oscillator calibration curve of driving current versus output frequency

in Figure 3 5, Section 3 3 1, to measure the output signals The detectors converted the signals into dc outputs which were then amplified and subtracted using an EG&G 5113 preamplifier The result was then displayed on an oscilloscope

4.3 Results and Discussion.

When making probe measurements the electrode sheath differential resistance R_e must be considered since it makes up part of the probe current path In dc plasmas this does not present itself as a problem because the conduction current of the sheaths

is approximately equal to the discharge current and so R_e is negligible However in rf plasmas the sheaths are mainly capacitive, so the conduction current of the sheaths and the discharge current are not longer equal resulting in R_e being comparable to the probe sheath resistance R_p This being the case distortion to the I curve of the probe will occur The probe sheath resistance is given as [1],

$$R_p = \left(\frac{dV_p}{dI_p}\right)^{-1} = \frac{kT_e}{eI_e} \propto \frac{T_e^{1/2}}{n_e} \quad , \qquad \textbf{Eqn: 4.1}$$

for a maxwellian distribution only, where T_e is the bulk electron temperature and I_p the probe current From this it can be seen that R_p has its minimum value at the plasma potential, so most distortion to the eedf will occur at low energies In a two temperature plasma this effect is even greater since the electron sheath resistance will be dependant on the fast rather than the bulk electrons since only these electrons will be able to overcome the electrode floating voltage

The resistances R_e and R_p are related to the areas of the electrodes According to Godyak et al [1],

$$\frac{A_p}{A_e} \ll \left(\frac{m_e T_{e_{bulk}}}{M T_{e_{fast}}}\right)^{1/2} \cdot \frac{n_{fast}}{n_{bulk}} \qquad \textbf{Eqn: 4.2}$$

where A_p and A_e are the probe and electrode areas respectively For argon at 10mTorr here $T_{e\,bulk} \approx 1\ 2eV$, $T_{e\,fast} \approx 3\ 5eV$ and $n_{fast} = 0\ 1\ n_{bulk}$, the ratio of probe to electrode areas, $A_p/A_e \ll 10^{-4}$ However for the system used here and described in Section 4 2, $A_p/A_e \approx 10^{-4}$, resulting in some distortion Figure 4 5 shows R_p, measured using the double probe technique describe in the latter section, as a function of pressure at constant current The increase in R_p stems from the decrease in density over this range With the voltage held constant and the pressure varied the electron density increased and R_p subsequently decreased, see Figure 4 10 Although the sheath resistance is not fully understood its importance is clear for systems which do not satisfy the criterion of Equation 4 2, it is essential to measure R_p to correct the I curve The sheath resistances for this system are quite small, although neglecting them leads to a shift in plasma potential of ~2Volts and an increase in the electron

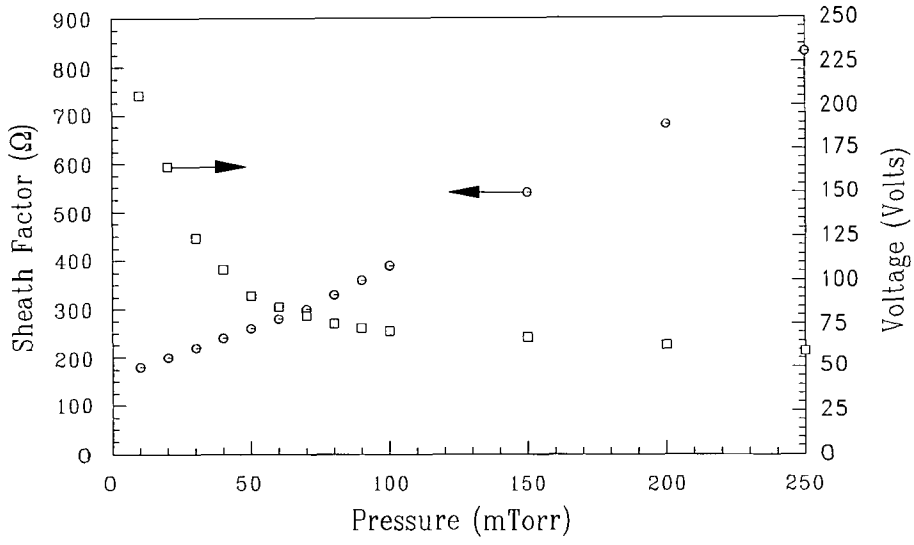

Figure 4 5 Graph of sheath resistance and driving voltage versus pressure for an argon plasma with current density 3mAmps/cm^2

temperature, so for systems with much smaller electrode areas this effect will be significant Finally the probe resistance due to the inductors is $\sim 8\Omega$ and so negligible when compared to the probe sheath resistance

For all the results presented here the probe sheath resistance was calculated and the probe measurements corrected accordingly The variation of electron temperature with pressure is shown in Figure 4 6 A number of points can be made about these measurements Firstly, the temperature increases from $\sim$ 1eV at 10mTorr to $\sim$3eV from 50 to 250mTorr The change between the two temperatures occurs quite abruptly, the reason for this being the transition from stochastic to bulk heating as the primary heating mechanism of the plasma At low pressure the bulk electrons have relatively low energy so the plasma is sustained by fast electrons gaining energy at the plasma sheath boundary As the pressure increases so too do the number of collisions between the electrons and the argon atoms resulting in a higher average energy and more uniform distribution of energy amongst the electrons Another point to note about Figure 4 6, is the repeatability of the data presented Three sets of separate results obtained over a four week period are shown The consistency of the measurements demonstrate how the probe is becoming a reliable diagnostic technique for rf discharges

With the pressure being increased it would be assumed that the electron and

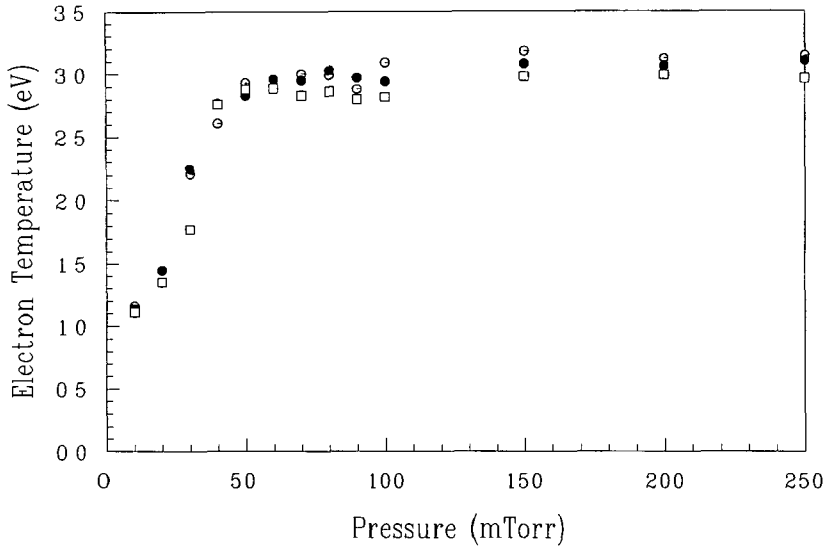

Figure 4 6 Electron temperature versus pressure for argon The data shown was taken on the 29/7/93, 10/8/93 and 27/8/93

ion densities too would increase However as shown in Figure 4 7 this is not the case over the pressure range examined Three sets of measurements are also shown on this graph, each one using a different probe based diagnostic technique to calculate the density The first method *Ne (probe)*, which is a standard approach, consists of calculating the random flux to the probe biased above the plasma potential [2] The

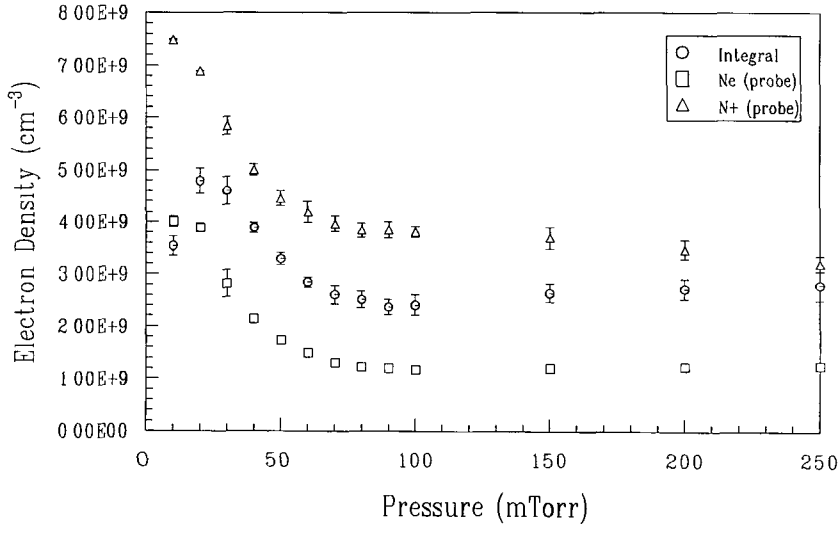

Figure 4 7 Graph of electron density versus pressure for argon Results of three different techniques to measure the density are shown

second method *Ni (probe)* calculates the ion density to the probe when biased very negatively [3] so as to ensure no fast electrons are present Since argon is an electropositive gas both n_e and n_+ should be equal Finally the integral of the eedf has also been calculated to give a value for the electron density It can clearly be seen in Figure 4 7 that all of the measuring techniques show a decrease in the density as the pressure is increased As the plasma undergoes the transition from stochastic to bulk heating, the energy of the bulk electrons increases, but the energy of the fast electrons decreases since they are cooled by the bulk plasma and cannot traverse the plasma This results in an overall decrease in the number of electrons with energies above the ionisation potential in turn causing the electron density to decrease It has been stated previously by Godyak et al [4], that the integral of the eedf is a more accurate measure of the electron density which for the case here, as seen in Figure 4 7, lies between the other two measurements, possibly indicating that the other two techniques either overestimate or underestimate the density The microwave interferometer was also used to examine the behaviour of the density as a function of pressure The results shown in Figure 4 8, also show a decrease as the pressure was increased

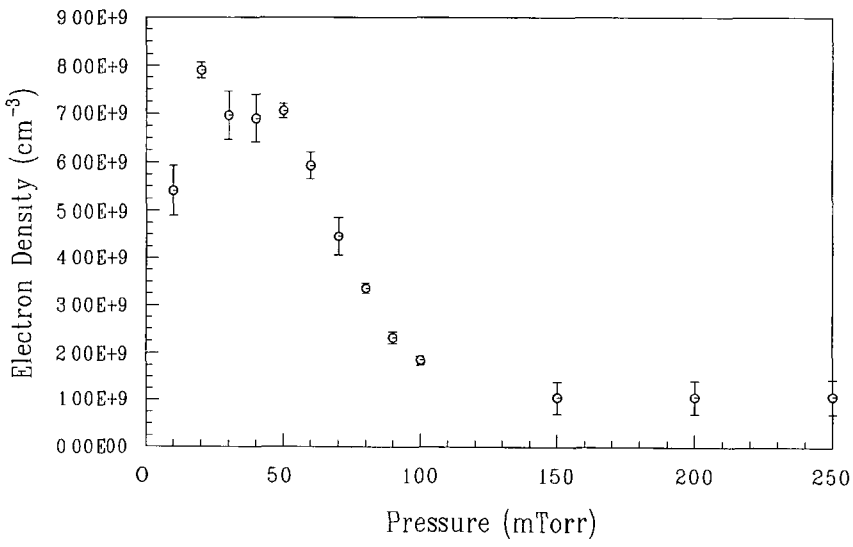

Figure 4 8 Graph of electron density versus pressure measured using a microwave interferometer

Absolute density measurements can not be taken from these results as further calibration [5] of the interferometer is required The system was also subject to vibrational disturbances and external noise when these measurements were taken

Future work includes both calibrating and stabilising the entire system sufficiently to remove all of these effects and get better agreement between the probes and microwave interferometer Previous studies between the probe and microwave interferometer density measurements in oxygen [6] and in argon [7] up to approximately 300mTorr, have shown excellent agreement However at pressure higher than 300mTorr, the probe began to underestimate the density by a factor of 2, see Section 7 3

The electron energy distribution functions from which the integral densities were taken are shown in Figure 4 9 The decreasing density with increasing pressure is quite clear, so too is the abrupt change in temperature of the bulk electrons as the eedfs change from a bi-maxwellian to a Druyvesteyn shape The temperature measured from the eedf agrees quite well with that obtained from the I curve with both giving a value of $\sim$1eV for the bulk electrons The fast electron temperature calculated from the eedfs shown is $\sim$4eV at 10mTorr The change in the eedf occurs as the primary plasma heating mechanism changes from stochastic to bulk heating The large observable difference is accentuated by the Ramsauer effect which is prominent in most noble gases [8,9] This effect produces a minimum in the scattering cross section for argon, see Section 2 4 1, Figure 2 6 Electrons with energies near this minimum have very low electron-neutral collision frequencies For the eedf at 10mTorr shown in Figure 4 9, the mean energies corresponding to the temperature of the slow and fast electrons are $\langle\epsilon_{slow}\rangle$ = 1 5eV and $\langle\epsilon_{fast}\rangle$ = 6 0eV respectively The densities for these two distinct groups of electrons were also calculated from the eedf and found to differ by an order of magnitude as expected with $n_{slow} = 3\ 3\times10^{9}$ cm^{-3} and $n_{fast} = 3\ 3\times10^{8}$ cm^{-3} The electron-neutral collision frequency is given as,

$$\nu_{en} = v_E\ \sigma_{tot}\ n_0 \qquad \textbf{Eqn: 4.1}$$

where v_E is the electron velocity, σ_{tot} is the total collision cross section and n_0 is the neutral density This results in $\nu_{en} \approx 9\times10^{6}$ s^{-1} for the low energy group Their mean free path is then $\sim$7cm which is much greater than the plasma half-width d $\sim$ 3cm The fast electrons, because of their greater mean energy have an electron neutral collision frequency an order of magnitude greater with $\nu_{en} \approx 9\times10^{7}$ s^{-1} and a

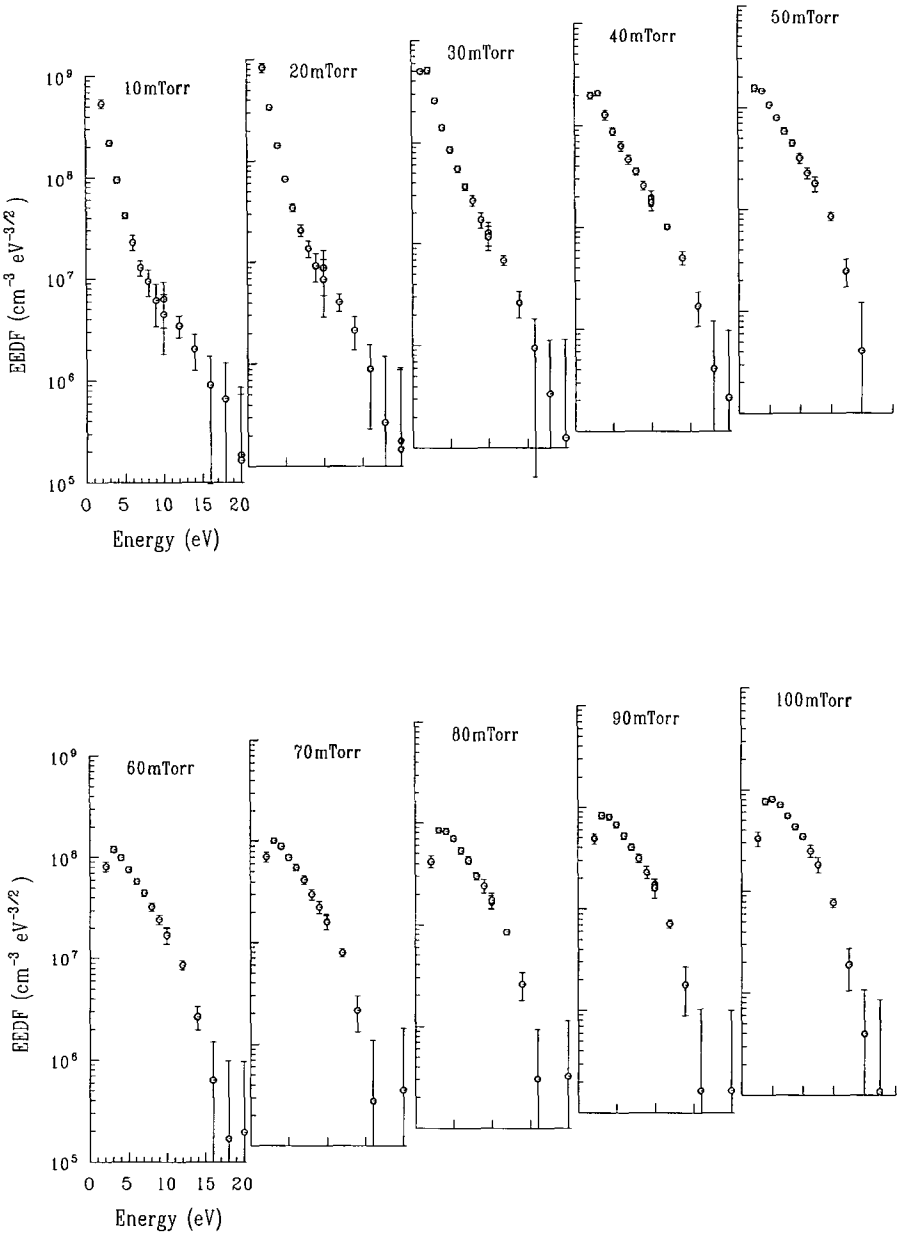

Figure 4 9 Electron energy distribution functions taken in argon at constant current

corresponding mean free path of only 1 5cm The bulk electrons, because of their low ν_{en} , oscillate collisionlessly in the weak rf field unable to gain any energy from either the field or the oscillating plasma sheaths since they have only low energy they are unable to overcome the dc ambipolar potential barrier in the plasma body and so cannot reach the sheaths to be stochastically heated [10] However the fast electrons

interact with the neutral argon atoms through elastic and ionising collisions, and compensate for their losses through stochastic heating at the plasma sheath boundary [11] This transition has been observed by others [12-14] using computational models The Ramsauer minimum was also removed to observe any effects on the eedf It was found that without this feature the bulk electron temperature increased while the fast electron temperature remained the same and the transition between the two heating modes was not nearly so abrupt With the voltage of the plasma held constant and the current density changing, the pressure was varied to see if the same transitions between heating modes were observed and also to examine the variations of sheath factor, electron temperature and density under these new conditions Figure 4 10 shows the relationship between the sheath resistance, the current and the pressure while the voltage was kept constant The current increased as would be expected while the sheath resistance being dependant on the electron density decreased as the

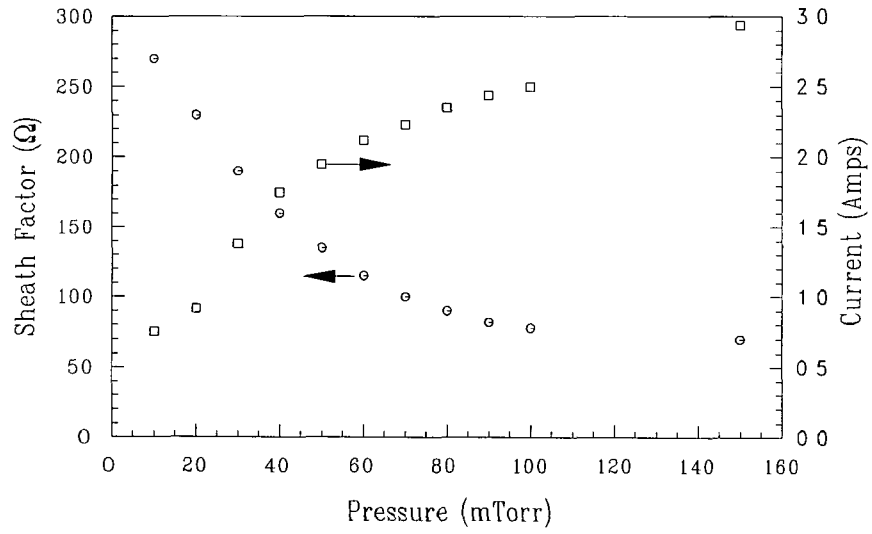

Figure 4 10 Graph of sheath factor and current versus pressure for argon with a driving voltage of 150Volts

pressure was increased The bulk electron temperature again increased as the pressure was increased though not as abruptly as in the constant current case Since the current to the plasma increased causing an increase in the current density, the electron density also increased as would be expected These features are clear from the eedfs, shown in Figure 4 11 The transition from stochastic to bulk heating can also be seen to occur at ~40mTorr as was the case previously It has been already stated [13] that

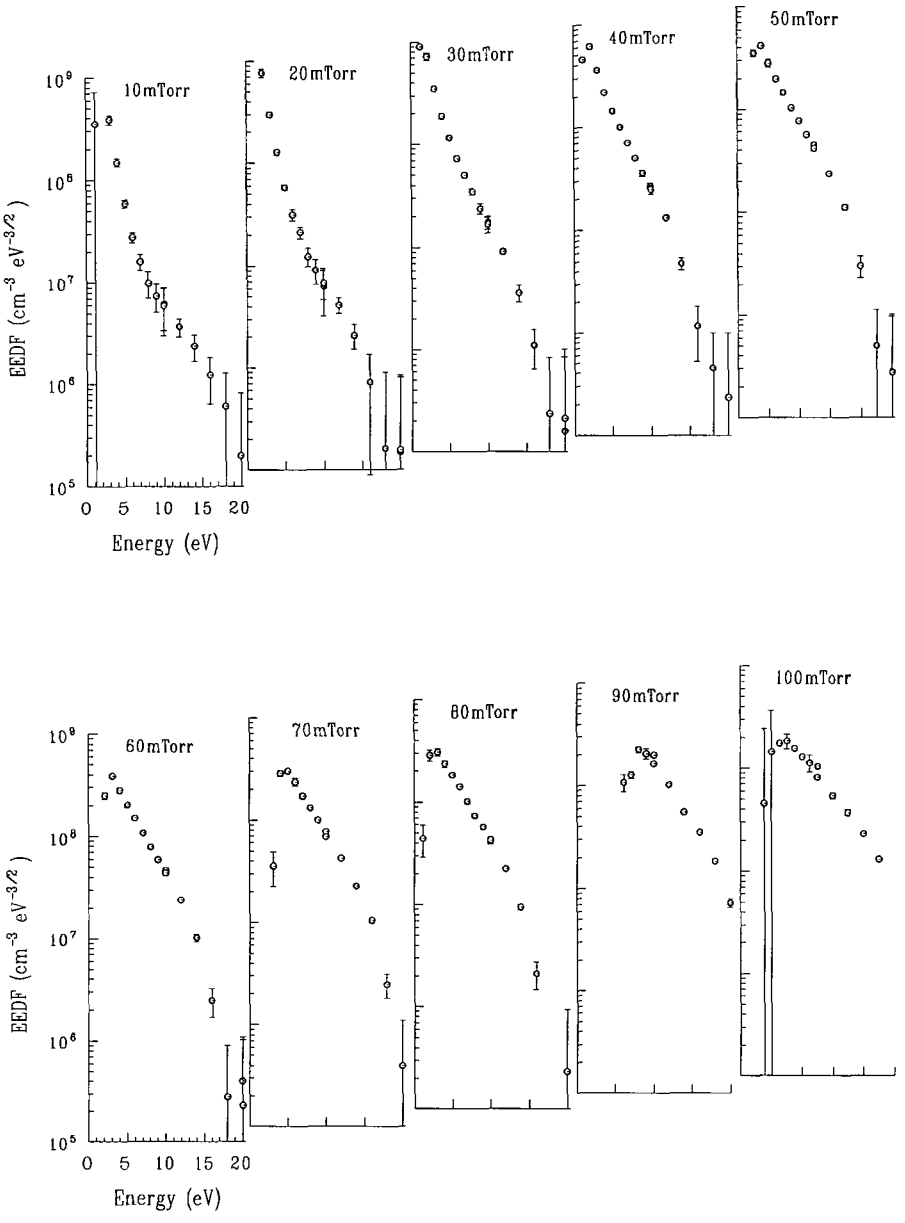

Figure 4 11 Electron energy distribution functions taken in argon at 150Volts

the pressure at which this transition occurs depends on the pressure p and half-width d of the bulk plasma For the system here that corresponds to a value $pd \approx 0$ 14 Torr cm which is in excellent agreement with the findings of others [1] To investigate this further the electrode gap was changed to both 5 5cm and 12 5cm, and the eedfs over a range of pressures, at constant current were taken The change between

heating modes was found to occur at between 40 and 50mTorr giving rise to a *pd* of 0 11 Torr cm for the 5 5cm case In the 12 5cm electrode gap experiments the transition occurred at ~20mTorr resulting in a *pd* of ~0 11 Torr cm also Experiments on a system with a 4cm electrode gap showed a transition between heating modes at 100 mTorr resulting in a *pd* of 0 15 Torr cm [15]

4.4 Conclusions.

It can first be concluded by the repeatability of the probe data collected and its agreement with the work of others that the probe is now a reliable diagnostic technique from which credible measurements can be taken The sheath factor should be taken into account when measuring the I curve and the eedf neglecting it introduces error the electron temperature is overestimated and the plasma potential shifted The temperature of the bulk electrons increases abruptly with increasing pressure as bulk heating takes over from stochastic heating as the primary heating mechanism of the plasma This transition is obvious from the eedfs which show a change from a bi-maxwellian to a Druyvesteyn shaped curve The occurrence of the transition was shown to depend only on the pressure of the plasma and the half-width of the bulk plasma Two experiments, one carried out at constant voltage and the other at constant current both showed a change in heating mode at ~40 mTorr when an electrode gap of 7 5cm was used, while experiments carried out using different electrode gaps but at constant current changed heating modes at different pressures The transition should occur for a *pd* of 0 1 to 0 15 Torr cm which was quite clearly the case here Finally the electron density was found to decrease while the pressure was increased, the reason being that as the transition from one type of heating to another occurred, less electrons with energies sufficient to cause ionisation were available resulting in a general decrease in ionisation throughout the bulk plasma even though the average energy of the bulk electrons increased

References.

[1] V A Godyak, R B Piejak and B M Alexandrovich, Plasma Sources Sci Technol , 1, 1992, 36-58

[2] M B Hopkins and W B Graham, Rev Sci Instrum , 57(9), 1986, 2210-2216

[3] J G Laframboise, University of Toronto Institute for Aerospace Study Report № 100, 1966

[4] V A Godyak, R B Piejak and B M Alexandrovich, J Appl Phys , 73(8), 1993, 3657-3663

[5] L J Overzet, J C Miller, T J Morel and B E Cherrington, Conference paper at the 43rd Annual Gaseous Electronics Conference, Urbana, Illinois, 1990

[6] L J Overzet and M B Hopkins, J Appl Phys , 74(7), 1993, 4323-4330

[7] G Neumann, U Banziger, M Kammeyer and M Lange, Rev Sci Instrum , 64(1), 1993, 19-25

[8] V E Golant, A P Zhilinsky, I E Sakharov and S C Brown, *Fundamentals of Plasma Physics*, Wiley and Sons, New York, 1979

[9] D E Golden and H W Bandel, Phys Rev 149(1), 1966, 58-59

[10] V A Godyak and R B Piejak, Phys Rev Lett , 65(8), 1990, 996-999

[11] T J Sommerer, W N G Hitchon and J E Lawler, Phys Rev Lett , 63(21), 1989, 2361-2364

[12] M Surendra and D B Graves, Phys Rev Lett , 66(11), 1991, 1469-1472

[13] M M Turner, R A Doyle and M B Hopkins, 62(25), 1993, 3247-3249

[14] J V Scanlan, M M Turner and M B Hopkins, Conference paper at the 10th International Conference on Gas Discharges and their Applications, Swansea U K , 1992, 436-439

[15] R A Doyle, M B Hopkins and M M Turner, Conference paper at the 45th Annual Gaseous Electronics Conference, Boston, Massachusetts, 1992

Chapter 5: Spatial Measurements in Argon.

5.1 Introduction.

This chapter focuses on spatial measurements taken throughout an argon plasma using a tuned probe Because of the geometry of the experimental chamber used spatial measurements across the plasma within a fixed plane between the electrodes, could be taken Measurements were also obtained as a function of position between the two electrodes In this manner the electron temperature and density could be examined in different regions of the plasma under a variety of different conditions

5.2 The Experimental System.

The experimental setup was the same as used previously, see Section 4 2 An electrode gap of 7 5cm was chosen as this put the horizontal probe in the centre of the plasma Both probes were variable in position as they were connected to the chamber using Wilson seals The horizontal probe was redesigned with the sleeve and probe tip perpendicular to the glass body of the probe This was done to ensure that both the probe tip and sleeve were the same distance from the wall of the chamber, see Figure 5 1 Since double O-ring Wilson seals were used as connectors very little leakage into the chamber occurred when the probes were moved, although a delay was left between moving the probes and taking results to ensure that any air which may have entered the chamber was removed by the pump Power was applied to the top electrode which was water cooled and the current and voltage applied were monitored

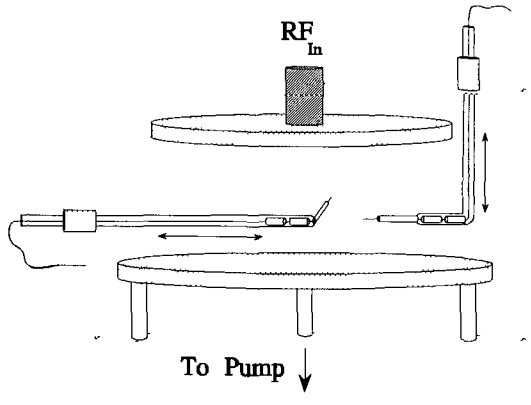

Figure 5 1 Orientation of the probes within the plasma

It was possible using the vertical probe to measure from the driving to the ground electrode However, the large diameter of the plasma chamber, 27cm from wall to wall, meant that measurements could only be taken from the wall to the centre

of the plasma. Since the walls of the chamber were all at ground potential, with no bias towards a particular section, azimuthal symmetry could be assumed. The probe did not disturb the plasma significantly during these spatial measurements.

5.3 Results and Discussion.

Spatial measurements were taken both across the plasma in a plane parallel to the electrodes, the r direction, and in a plane perpendicular to the electrodes, the z direction. For the purpose of mathematical discussion later in this chapter the cylindrical coordinates used are shown in Figure 5.2 with respect to the driving and ground electrodes and the walls of the chamber. Various plasma parameters measured as a function z, at pressures of 10 and 150 mTorr in argon, are shown in Figure 5.3. These pressure values were selected since at 10 mTorr the plasma is stochastically heated while at 150 mTorr the plasma is bulk heated. Therefore observations of any spatial anomalies associated with the different plasma heating mechanism could be made. Firstly it can be seen that the electron temperature in Figure 5.3, remains constant throughout the bulk of the plasma for both pressures [1]. The temperature deviates from its constant 1.1eV at 10 mTorr and 2.9eV at 150 mTorr, at the sheath regions of the plasma. The sheath temperature values recorded are not assumed to be correct as the voltage drop across the sheaths was quite large which caused distortion to all probe measurements taken in this region. A constant temperature across the bulk plasma is to be expected from an argon plasma as visually this region of the plasma appears quite uniform and homogenous unlike hydrogen plasmas where a bright region within the bulk, outside of the sheath regions, can also be seen. The plasma potential is plotted as a function of z in Figure 5.3. Again the extent of the sheath regions can be seen as here the measured value of plasma potential deviates by a large amount from the bulk plasma values. A virtually field free bulk plasma is apparent from the data shown with a

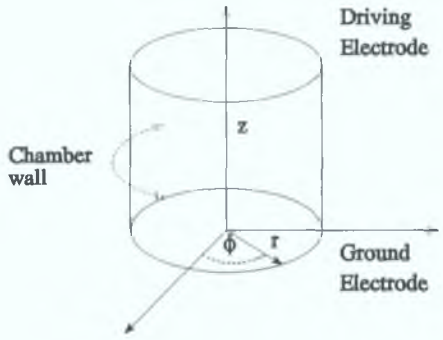

Figure 5.2: Cylindrical coordinate system.

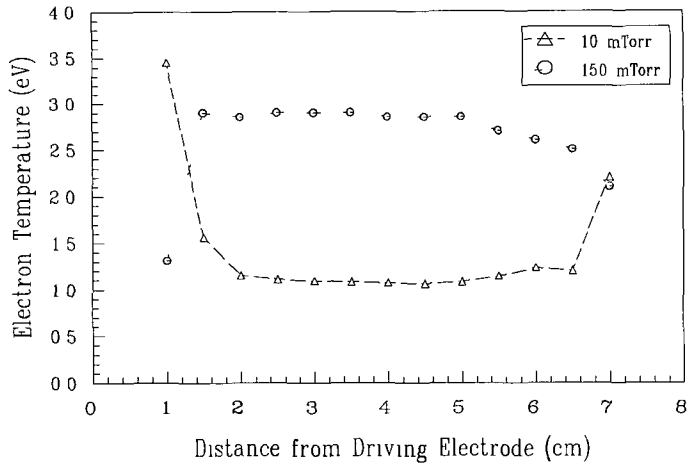

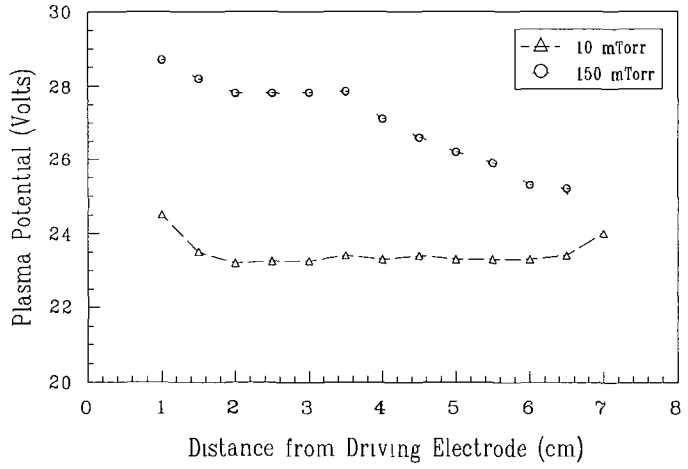

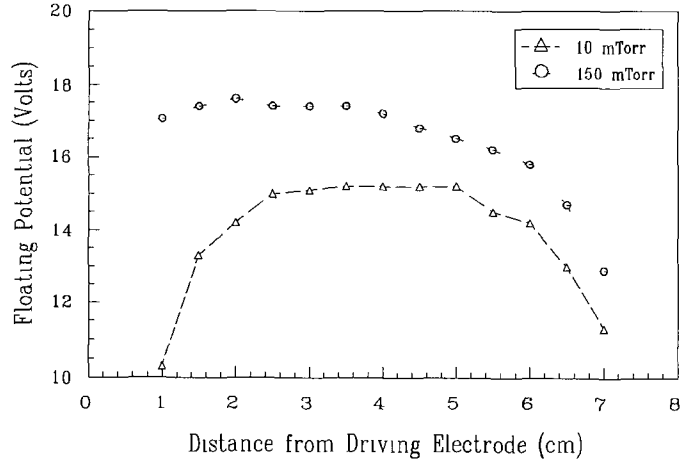

Figure 5 3 Electron temperature plasma potential and floating potential shown as a function of z for an argon plasma at 10 and 150mTorr with constant current density

maximum dc field of 0 5 V/cm at 10 mTorr and 1 V/cm at 150 mTorr The slight increase between these two values is due to the increased number of collisions within the bulk plasma at higher pressures [2] Finally the floating potential remains almost constant throughout the centre of the plasma It deviates more rapidly than the plasma potential and the electron temperature from its uniform value This is due to the changes in the electron temperature as a function of z By definition the floating potential is the potential which an unbiased body in the plasma will attain It therefore depends on both the density of charged particles present and their mobilities as equal fluxes of both positive and negative particles must be collected by the probe The floating potential in an rf argon plasma is always negative with respect to the space potential in order to attract the slower ions and repel to some extent the electrons Nearer to the sheath regions, particularly at low pressures, more fast electrons are present and able to overcome the potential of the probe This results in a decrease of the floating potential to repel some of these electrons and maintain zero net collected current

A radial scan was also performed on the plasma The data was taken from the wall of the chamber to the centre of the plasma only Figure 5 4 shows some of the plasma parameters measured as a function of radius, again for the two pressures, 10 and 150 mTorr The electron temperature variation is shown in Figure 5 4 For both pressures the temperature remains constant within the bulk region Combining these results with those of the temperature variations in the z direction, show quite clearly that the argon plasma is homogenous outside of the sheaths regions The temperature is $\sim$1 2eV and 2 9eV for 10 and 150 mTorr respectively, which shows good agreement between the two probes used The plasma potential is shown as function of r in Figure 5 4 At both 10 and 150 mTorr some noise is observed in the data from 0 to 4 cm due to the sheath at the wall The reasons for such a large sheath area can easily be explained The distance between the wall and the ground electrode is 1 5cm, however the driving electrode is smaller in diameter than the ground electrode such that its distance from the wall is 3 5cm, causing the sheath to stretch to $\sim$4cm As was the case with the plasma potential variation with z, the plasma is virtually field free with a maximum change in the dc field of $\sim$0 5 V/cm The floating potential decreases from the centre of the plasma to the walls of the chamber

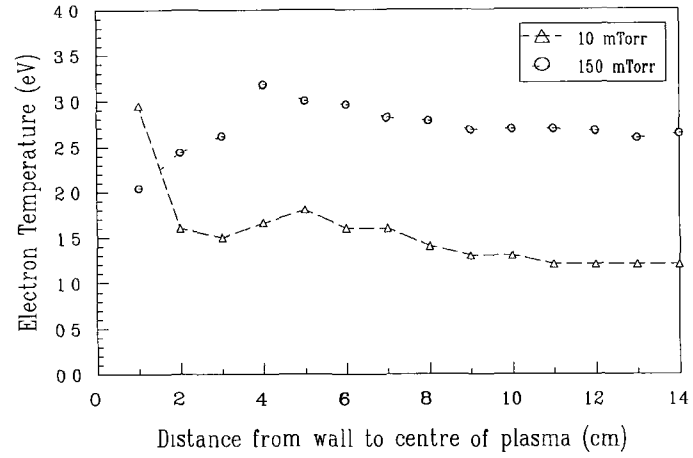

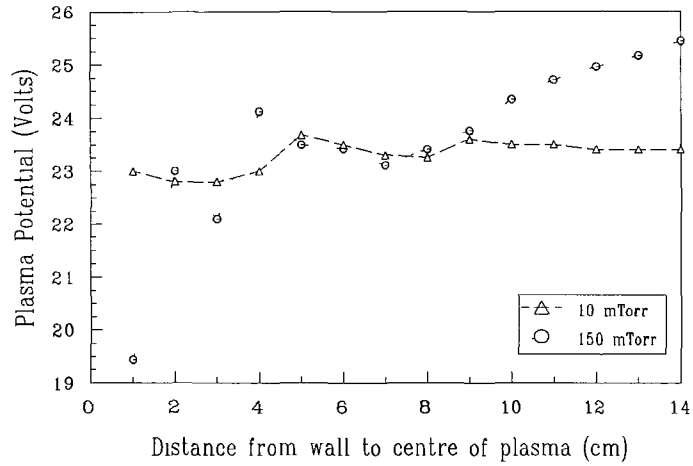

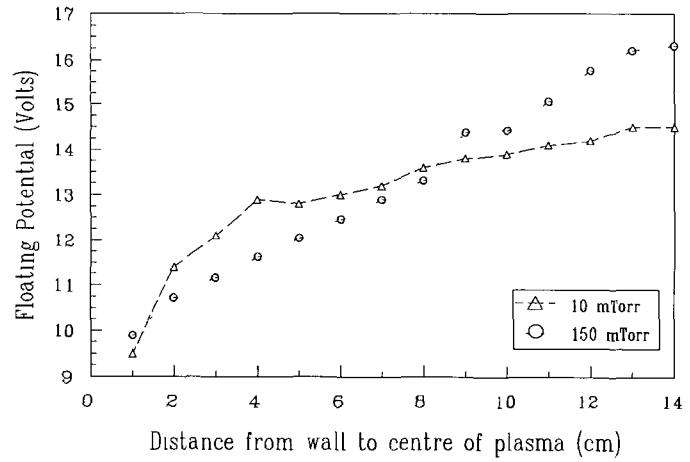

Figure 5 4 Electron temperature, plasma potential and floating potential as a function or r for an argon plasma 10 and 150 mTorr with constant current

The variation of electron density with position in the plasma is now examined as a function of both z and r and compared to theoretical predictions Figure 5 5 shows the change in electron density as function of z, the distance from the driving to ground electrode, for both 10 and 150 mTorr The density decreases from the centre of the plasma towards the walls at 10 mTorr, see Figure 5 5, showing ambipolar diffusion dependence The diffusion equation which is both temporally and spatially dependant is given as,

$$n(r,z,t) = T(t)\, R(r)\, Z(z) \quad , \qquad \textbf{Eqn: 5.2}$$

where T denotes the temporal and RZ the spatial contributions with no azimuthal dependence By separation of variables the spatial part of the diffusion equation may be written as,

$$\nabla^2(RZ) = -\frac{RZ}{D\tau} \quad . \qquad \textbf{Eqn: 5.2}$$

Since the plasma under examination was produced in a cylindrical chamber the latter equation is written as,

$$-\frac{R(r)Z(z)}{D\tau} = Z(z)\left[\frac{1}{r}\frac{\partial}{\partial r}\left(r\frac{\partial R}{\partial r}\right)\right] + R(r)\left[\frac{\partial^2 Z}{\partial z^2}\right] \quad . \qquad \textbf{Eqn: 5.4}$$

The data shown in Figure 5 5 was taken in the z direction so both radial and azimuthal symmetry were assumed For the axial dependence of the electron density,

$$\nabla^2 Z = \frac{\partial^2 Z}{\partial z^2} = -\frac{1}{D\tau} Z(z) \quad . \qquad \textbf{Eqn: 5.5}$$

The solution to this equation is in the form of,

$$Z(z) = A\cos\left(\frac{z}{(D\tau)^{1/2}}\right) + B\sin\left(\frac{z}{(D\tau)^{1/2}}\right) \quad . \qquad \textbf{Eqn: 5.6}$$

The boundary conditions are such that there are no electrons at z = 0 and z = L, where L is the chamber length This implies that at A = 0 and

$$\frac{L}{(D\tau)^{1/2}} = n\pi \quad ,$$

$$\Rightarrow \tau = \left(\frac{n\pi}{L}\right)^2 \frac{1}{D} \quad . \qquad \textbf{Eqn: 5.7}$$

Using the first harmonic (n = 1), substitution of this into equation 5 5 yields the results,

$$Z(z) = A\sin\left(\frac{z\pi}{L}\right) \qquad \textbf{Eqn: 5.8}$$

where A is a constant equal to the maximum electron density [3]

As can be seen in Figure 5 5a, at 10 mTorr both the experimental and the

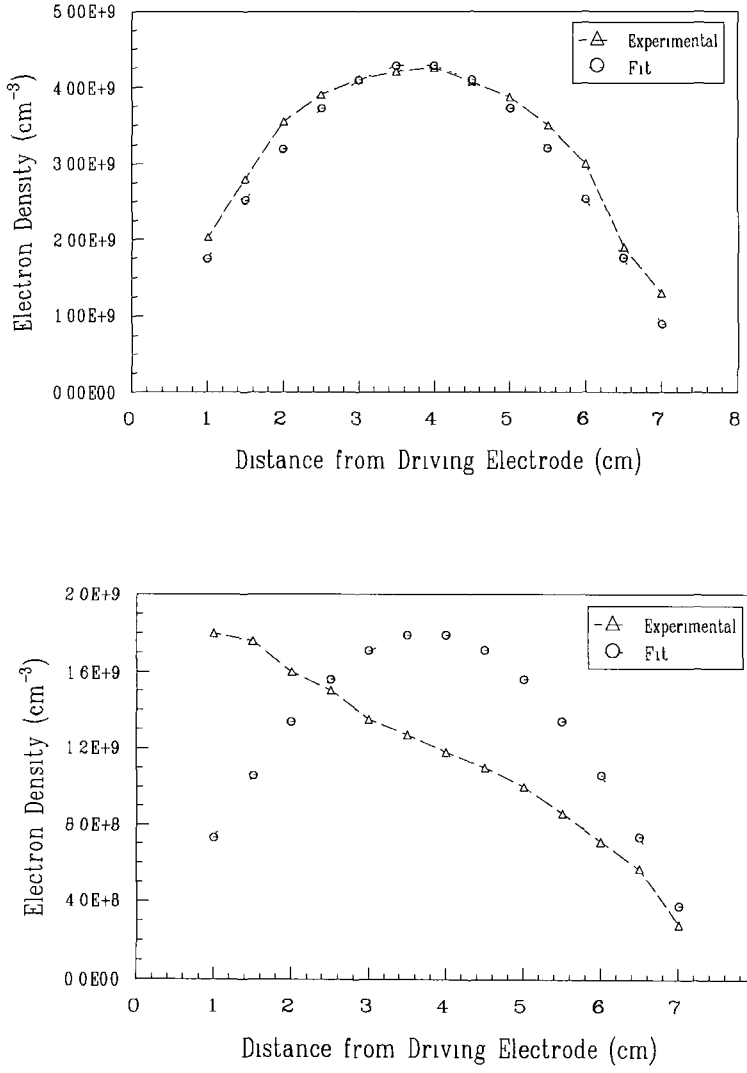

Figure 5 5 Electron density as a function of z in argon at 10 and 150mTorr compared to the theoretical prediction derived from the diffusion equation

theoretical results agree quite well [4,5] However at 150 mTorr major discrepancies can be seen between the two sets of data The reason for this is that the theoretical approach assumes that ionisation occurs at a point in the centre of the discharge which is not always true In the system under examination here, the driving electrode and ground electrode sheaths are not the same and so ionisation is biased towards the driving electrode PIC simulations of Krimke et al [6] in an asymmetric argon plasma have also shown an electron density tending towards the driving electrode This is shown to be the case here since at 150 mTorr, the experimental density as a function of r agrees quite well with the theoretical data as the walls of the chamber are of uniform bias The electron density as a function of r is shown in Figure 5 6 for both 10 and 150 mTorr Both pressures show a decrease in density from the centre of the

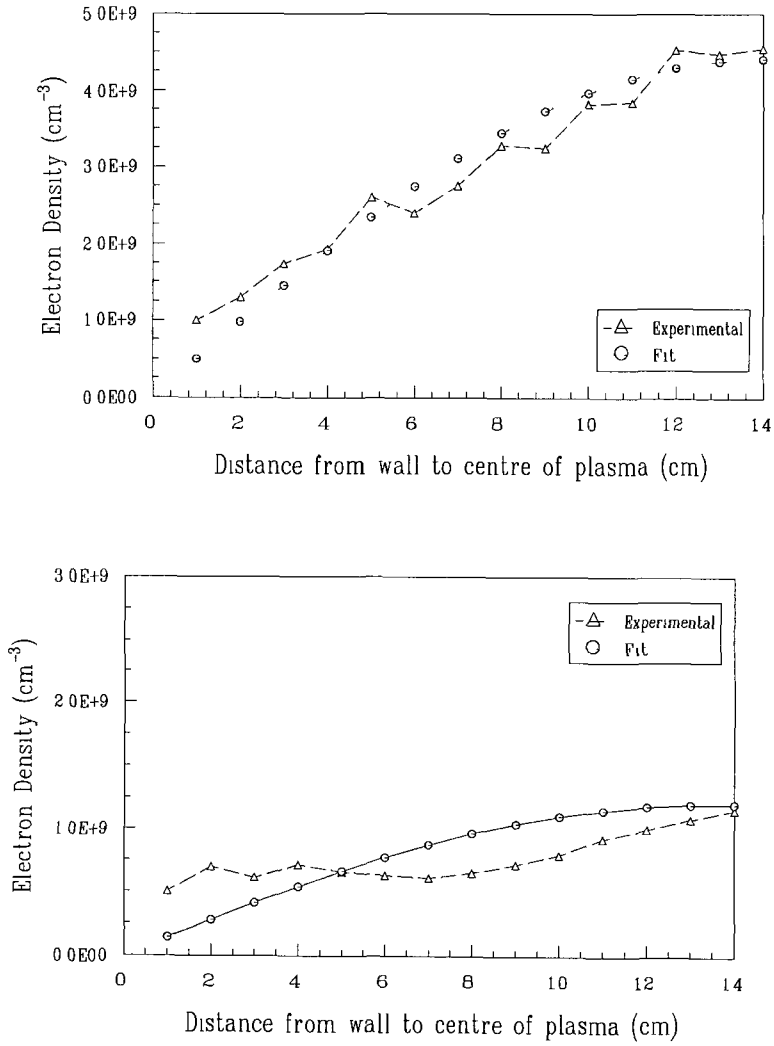

Figure 5 6 Electron density as a function of r for argon at 10 and 150mTorr compared to the theoretical predictions derived from the diffusion equation

plasma to the walls Again using the diffusion equation of Equation 5 3, but this time ignoring the z and ϕ dependence by assuming symmetry in these directions and examining the radial contribution only, on evaluation yields,

$$\frac{\partial^2 R}{\partial r^2} + \frac{1}{r}\frac{\partial R}{\partial r} + \frac{R(r)}{D\tau} = 0 \quad . \qquad \textbf{Eqn: 5.9}$$

The first harmonic solution to this is a Bessel function of zero order, $J_0\,(r/D\tau)^{1/2}$ This is simply a damped sine wave described by the equation,

$$R(r) = C_o \sum_{k=0}^{\infty} \frac{1}{(k!)^2}\left(-\frac{r^2}{4}\right)^k \quad , \qquad \textbf{Eqn: 5.10}$$

where C_0 is a constant This bessel function profile has been observed by others in both experiments and simulations [7,8]

The variation of electron density as a function of position in the plasma can also be seen in the electron energy distribution functions Figure 5 7 shows a surface plot of the eedf from the driving to ground electrode at 10 mTorr The constant temperature in the bulk of the plasma and the change in density along this axis of the

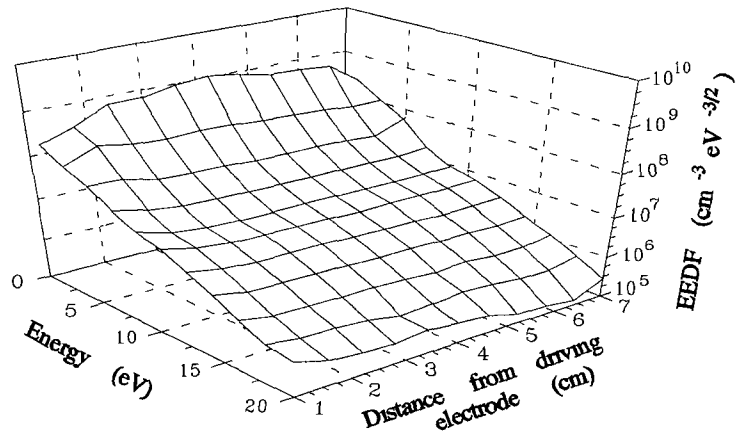

Figure 5 7 Electron energy distribution function as a function of z for argon at 10mTorr

plasma can be seen At 150 mTorr, Figure 5 8, the overall electron density is reduced, see Section 4 3, the eedfs showing a shift in ionisation towards the driving

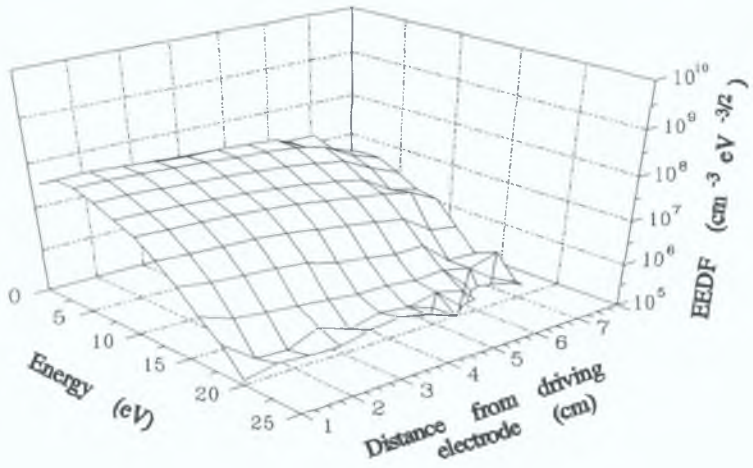

Figure 5.8: Electron energy distribution function as a function of z for argon at 150mTorr.

electrode. Again the constant temperature of the bulk plasma and its Druyvesteyn profile can be seen. The eedfs from the radial scan across the plasma also agree with the results already presented. Figure 5.9 shows a surface plot, at 10 mTorr, of the eedfs taken from the wall to the centre of the plasma. The sheath regions shows some

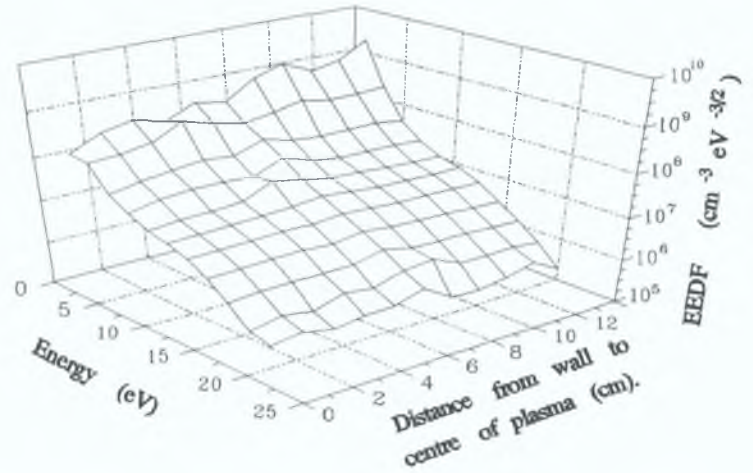

Figure 5.9: Electron energy distribution functions variation with z for argon at 10mTorr.

noise from the wall out to ~4cm, while in the bulk of the plasma the eedfs are bi-Maxwellian with an increasing density towards the centre of the plasma. As was the case before, at 150 mTorr the density is reduced, the eedfs now have a Druyvesteyn profile and consequently a higher electron temperature. The density falls off towards

the walls, its decrease in the form of a Bessel function is not obvious

5.4 Conclusion.

The results presented here show clearly the variation of some of the plasma parameters as a function of position within an argon plasma Two pressures were chosen for the spatial measurements, 10 and 150 mTorr, to examine if any spatial anomalies were heating mode dependant At 10 mTorr the plasma was predominantly stochastically heated while at 150 mTorr it was bulk heated The results show that for both pressure the temperature stays constant within the bulk of the plasma outside of the sheath regions This was found to be true both along the z and r axis The bi-Maxwellian tending to Druyvesteyn profile of the plasma was apparent in the eedf agreeing with the data presented in the previous chapter The plasma potential also showed no great variation leading to the conclusion that the plasma is virtually field free and homogenous Finally the electron densities which did vary as a function of position within the plasma were compared with the theoretical expectations of the diffusion equation At 10mTorr the agreement between the experimental and theoretical was quite good for the data taken as a function z However for the scan at 150 mTorr the comparison between the two was not so good since the theory assumed ionisation at a point source in the centre of the discharge This can not be assumed in this case since the electrodes and consequently the sheath regions were of differing sizes For the radial scan however, the data taken for both pressures agreed with the theoretical expectations A first order bessel function, as was expected, fit quite well to the experimental measurements

References.

[1] V A Godyak and R B Piejak, Appl Phys Lett , 63(23), 1993, 3137-3139

[2] J V Scanlan, PhD Thesis, Dublin City University, 1991

[3] F F Chen, *Introduction to Plasma Physics and Controlled Fusion 2nd Ed* , Plenum Press, New York, 1990

[4] L J Overzet and M B Hopkins, Appl Phys Lett , 63(18), 1993, 2484-2486

[5] U Flender and K Wiesemann, J Phys D Appl Phys , 27, 1994, 509-521

[6] R Krimke, H M Urbassek, D Korzec and J Engemann, J Phys D Appl Phys , 27, 1994, 1653-1659

[7] G Oelerich-Hill, I Pukropski and M Kujawka, J Phys D Appl Phys , 24, 1991, 593-601

[8] C Chan, Z-J Jin and C Whitaker, J Appl Phys , 62(5), 1987, 1633-1638

Chapter 6 : Argon Plasmas with Transverse Magnetic Fields.

6.1 Introduction.

Magnetic fields are often used in the field of plasma physics to both confine and enhance ionisation within the discharge For the case of multicusp ion sources, fast electrons are prevented from recombining with the chamber walls by a strong multipole arranged magnetic field These systems are used for the production of negative ions which are subsequently converted into high energy neutral beams for injection into fusion reactors [1]

Of more relevance to this work are magnetron sputtering systems which employ axial magnetic fields to enhance ionisation and decrease wall recombination wall losses [2-4] A field is applied along the discharge axis as shown below Electrons travelling parallel to the field will be unaffected since vector product V x B will be zero However, electrons travelling at an angle θ will be subject to a force BeV Sinθ perpendicular to the field

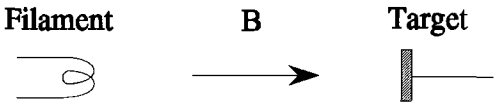

If the electron makes no collisions it will move with circular motion around B with a radius of,

$$r = \frac{m_e V Sin\theta}{Be} \quad . \qquad \textbf{Eqn : 6.1}$$

Coupling this motion with its velocity VCosθ parallel to B will result in helical motion of the electron This effect serves to increase the electron mean free path and reduce the net velocity of the electrons towards the walls hence decreasing recombination losses [5] Increasing the electron mean free path results in more ionisation and excitation of neutrals through collisions, in turn allowing the operating pressure of the system to be reduced Consequently if the number of collisions between particles increases, the pressure at which the transition from stochastic to bulk heating occurs must change since it is primarily dependant on such collisions, see Section 4 3 This chapter serves to compare both experimental and computational

work on the effect of the application of a transverse magnetic field to a low pressure (~ 10mTorr) rf generated argon plasma with particular attention paid to the effect the field has on the density and heating modes of the plasma

6.2 Confinement by a Magnetic Field.

Particles in a plasma diffuse to regions of lower density along a density gradient ∇n, see section 2 3 6 In travelling through the plasma they also undergo collisions, the distance between collisions being λ_m , the mean free path The rate of plasma loss by diffusion can be reduced by the application of a magnetic field Consider a weakly ionised plasma with a magnetic field B along the z direction Charged particles will move along B by diffusion and mobility since B does not affect motion in the parallel direction The particle motion is described as,

$$\Gamma_z = \pm \mu n E_z - D \frac{\delta n}{\delta z} \quad , \qquad \textbf{Eqn : 6.2}$$

where Γ_z is the flux of a species in the z direction, and μ and D are the mobility and diffusion coefficients respectively If there were no collisions at all the particles would continue to gyrate around the same lines of force such that no particles would diffuse in the perpendicular direction However there will be particle drifts across B due to the electric field If no collisions take place though the particles will migrate across B along the gradients to the walls If collisions do take place the colliding ions will change their phase of rotation, their guiding centre will shift position and they will undergo a random walk The particles will then diffuse in a direction opposite to the density gradient ∇n and the step length will no longer be λ_m , the mean free path for collisions, but the Larmor radius, r_L [5-7] This means that diffusion across B can now be controlled by increasing or decreasing r_L , which in effect means altering B as is necessary The fluid equation of motion can be written, for the perpendicular component as,

$$mn \frac{d\mathbf{v}_\perp}{dt} = \pm en(E + \mathbf{v}_\perp \times B) - kT \nabla n - mn\nu \mathbf{v} = 0 \quad , \qquad \textbf{Eqn : 6.3}$$

where ν denotes the collision frequency Assuming that ν is sufficiently large for the $dv_\perp/dt$ term to be negligible, the plasma is isothermal with x and y components,

$$m n \nu v_x = \pm e n E_x - kT\frac{dn}{dx} \pm e n B v_y \quad ,$$
$$m n \nu v_y = \pm e n E_x - kT\frac{dn}{dy} \mp e n B v_x \quad . \qquad \textbf{Eqn : 6.4}$$

Using the definition for diffusion and mobility given in Equations 2 5 and 2 7, the x and y components may then be written as,

$$v_x = \pm \mu E_x - \frac{D}{n}\frac{\delta n}{\delta x} \pm \frac{\omega_c}{\nu} v_y \quad ,$$
$$v_y = \pm \mu E_y - \frac{D}{n}\frac{\delta n}{\delta y} \mp \frac{\omega_c}{\nu} v_x \quad , \qquad \textbf{Eqn : 6.5}$$

where ω_c , the cyclotron frequency is given as,

$$\omega_c = \frac{|q|B}{m} \quad . \qquad \textbf{Eqn : 6.6}$$

By substituting for v_x a solution for v_y may be found and vice versa

$$v_y(1 + \omega_c^2\tau^2) = \pm \mu E_y - \frac{D}{n}\frac{\delta n}{\delta y} - \omega_c^2\tau^2\frac{E_x}{B} \pm \omega_c^2\tau^2\frac{kT}{eB}\frac{1}{n}\frac{\delta n}{\delta x} \quad ,$$
$$v_x(1 + \omega_c^2\tau^2) = \pm \mu E_x - \frac{D}{n}\frac{\delta n}{\delta x} + \omega_c^2\tau^2\frac{E_y}{B} \mp \omega_c^2\tau^2\frac{kT}{eB}\frac{1}{n}\frac{\delta n}{\delta y} \quad . \qquad \textbf{Eqn : 6.7}$$

These two equations may now be split up into several components The last two terms of both equations contain the E×B and diamagnetic drifts [7]

$$v_{E_x} = \frac{E_y}{B} \quad , \qquad v_{E_y} = -\frac{E_x}{B} \quad ,$$
$$v_{D_x} = \mp\frac{kT}{eB}\frac{1}{n}\frac{\delta n}{\delta y} \quad , \qquad v_{D_y} = \pm\frac{kT}{eB}\frac{1}{n}\frac{\delta n}{\delta x} \quad . \qquad \textbf{Eqn : 6.8}$$

The first two terms of Equation 6 7 can be simplified by redefining the mobility and diffusion coefficients to,

$$\mu_\perp = \frac{\mu}{1 + \omega_c^2 \tau^2} \quad , \quad D_\perp = \frac{D}{1 + \omega_c^2 \tau^2} \quad , \qquad \textbf{Eqn : 6.9}$$

such that $v_\perp$ can now be written as,

$$v_\perp = \mu_\perp E - D_\perp \frac{\nabla n}{n} + \frac{v_E + v_D}{1 + \left(\frac{\nu^2}{\omega_c^2}\right)} \quad . \qquad \textbf{Eqn : 6.10}$$

The perpendicular velocity component can be divided into two parts Firstly there are the v_D and v_E components which are perpendicular to the gradients in density and potential These drifts are slowed down through collisions with the neutral particles, the drag factor $1 + \nu^2/\omega_c^2$ becoming one as the collision frequency ν tends to zero Secondly there are the mobility and diffusion drifts parallel to the gradients in density and potential These have the same form as in the B = 0 case except now they are reduced by a factor $1 + \omega_c^2 \tau^2$ The magnetic field has little effect on diffusion when this term is much less than one However the rate of diffusion across B is retarded significantly when $\omega_c^2 \tau^2 \gg 1$ In this case the role of the collision frequency ν is reversed For diffusion parallel to the magnetic field, $D \propto \nu^{-1}$ since collisions retard motion In the limit $\omega_c^2 \tau^2 \gg 1$ for diffusion perpendicular to the magnetic field,

$$D_\perp = \frac{D}{\omega_c^2 \tau^2} = \frac{kT\nu}{m\omega_c^2} \quad . \qquad \textbf{Eqn : 6.11}$$

Collisions are needed for cross field migration, hence $D_\perp \propto \nu$ In parallel diffusion the electrons move much faster than the ions because of their greater thermal velocities so $D \propto m^{-1/2}$ However in perpendicular diffusion electrons escape more slowly because of their smaller Larmor radius and $D \propto m^{1/2}$ This reduction in diffusion leads to an increase in the density of the plasma This has implications for the plasmas examined here as the increase in density changes the mechanism by which the plasma is heated at certain pressures

6.3 Experimental System.

Two tesla coils used to generate a uniform transverse magnetic field were applied to the plasma The coils consisted of 380 turns of insulated copper wire

wound on a 16cm diameter core The coils were then placed approximately 30cm apart on either side of the chamber and connected up to the power supplies as shown in Figure 6 1, producing a uniform field The current to the coils was varied from 0 to 8 amps with 25 volts the maximum voltage applied The field produced then ranged from 0 to 18 5 Gauss at the centre of the plasma where the probe was positioned see Figure 6 2 When greater than 8amps was applied to the coils, the heat produced by them caused a decrease in the current such that the field could not be kept stable and so fluctuation occurred In order to produce much higher fields, bar magnets were arranged on either side of the chamber and used in conjunction with the coils Between five and eight magnets were evenly spaced apart along each side producing a very uniform field which could then be

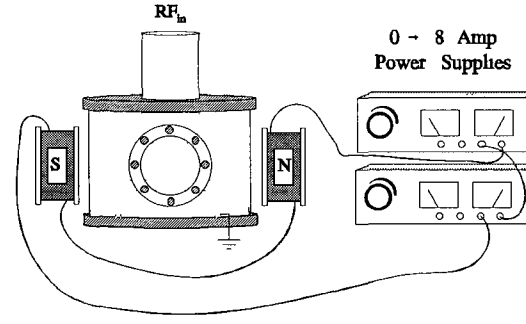

Figure 6 1 Experimental system

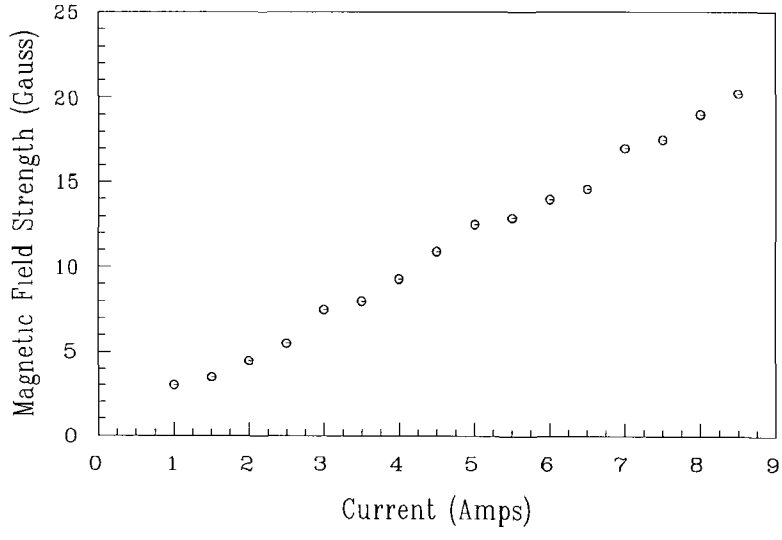

Figure 6 2 Graph of the field produced as a function of coil current

varied from 25 to 55Gauss A hall effect magnetometer was used to measure the magnetic field strength within the chamber and the tuned probe described previously used to measure the plasma parameters including the eedf [8,9] The strength of the

maximum applied magnetic field was such that the Larmor radius of the electrons was greater than the probe radius so the effect of the field on the probe measurements was minimal The plasmas were generated in the parallel plate, capacitively coupled, asymmetric system described earlier in section 4 2 A gap of 7 5cm was chosen as the electrode spacing as the transition from stochastic to bulk heating could clearly be seen here The current density and voltage to the plasma were measured using the current-voltage probe described in section 3 4 An 11GHz microwave signal was used to measure the electron density The microwave setup is shown in Figure 3 4 The magic T and the isolators were shielded from the magnetic field by μmetal At the higher magnetic fields, 25-55gauss, this section of the interferometer was removed and no measurements were taken as the close proximity of the magnets would have caused permanent damage to the isolators even with μmetal present

6.4 Results and Discussion.

A current of 1Amp was applied to the plasma giving rise to a current density of 3mA/cm^2 The pressure was kept at 10mTorr and the magnetic field varied to examine its affect The voltage across the plasma and power deposited were also monitored while probe and microwave measurements were taken It was assumed from the analysis of diffusion across a magnetic field, Section 6 2, that the mobility of the electrons would decrease and the plasma heating would change from being stochastic to collision dominated From the eedf in Figure 6 3 it can be seen that at zero magnetic field the plasma remained bi-maxwellian with two distinct groups of electrons present, the bulk electrons with a temperature of $\sim$1 4eV and the fast electrons with temperature $\sim$3 1eV When the magnetic field was applied the electrons moved in helical orbits increasing the distance they travel and in doing so increasing their chances of making a collision The fast electrons caused stochastic heating through repeated collisions with the sheaths As the field intensity increases the fast electrons become well confined to the sheath regions such that heating in the centre of the plasma where the eedfs were taken consists entirely of the ohmic contribution At high magnetic fields $\sim$20 Gauss the bi-Maxwellian nature of the plasma has almost completely disappeared being replaced by a uniform distribution with a temperature of 2 8eV, the concave shape of the distribution being characteristic

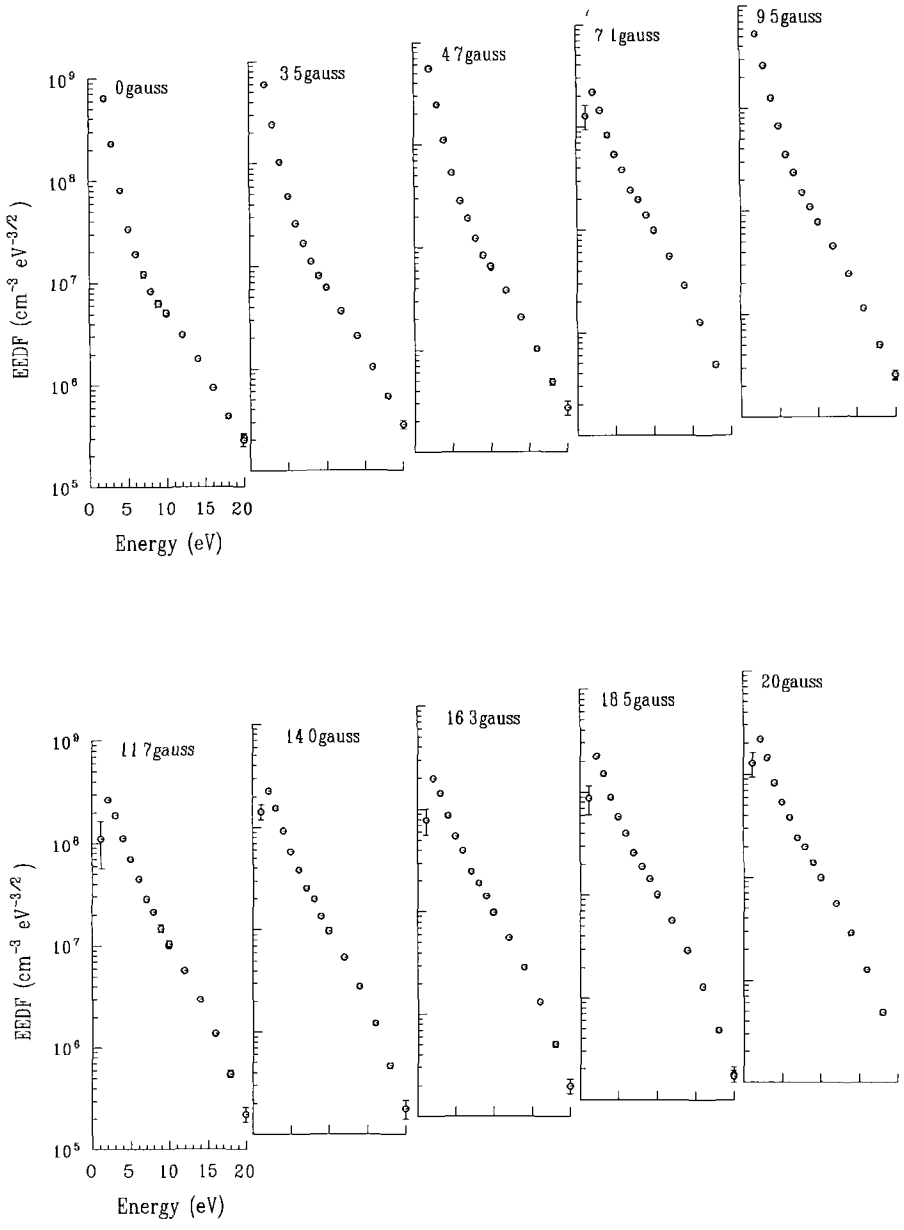

Figure 6 3 Electron energy distribution functions in an argon plasma with a transverse magnetic field

of a collision dominated regime These results agree quite well with the PIC/MCC simulations performed through which the average electron energy was examined [10] It was found that again ohmic heating in the bulk dominated as the magnetic field was increased Electron cyclotron resonance is not visible in the eedfs The reason for this is possibly that the low energy electrons are confined to a field free region and so resonance will be unimportant while the fast electrons which see the effects of resonance have a very low density and are highly non-maxwellian However at fields

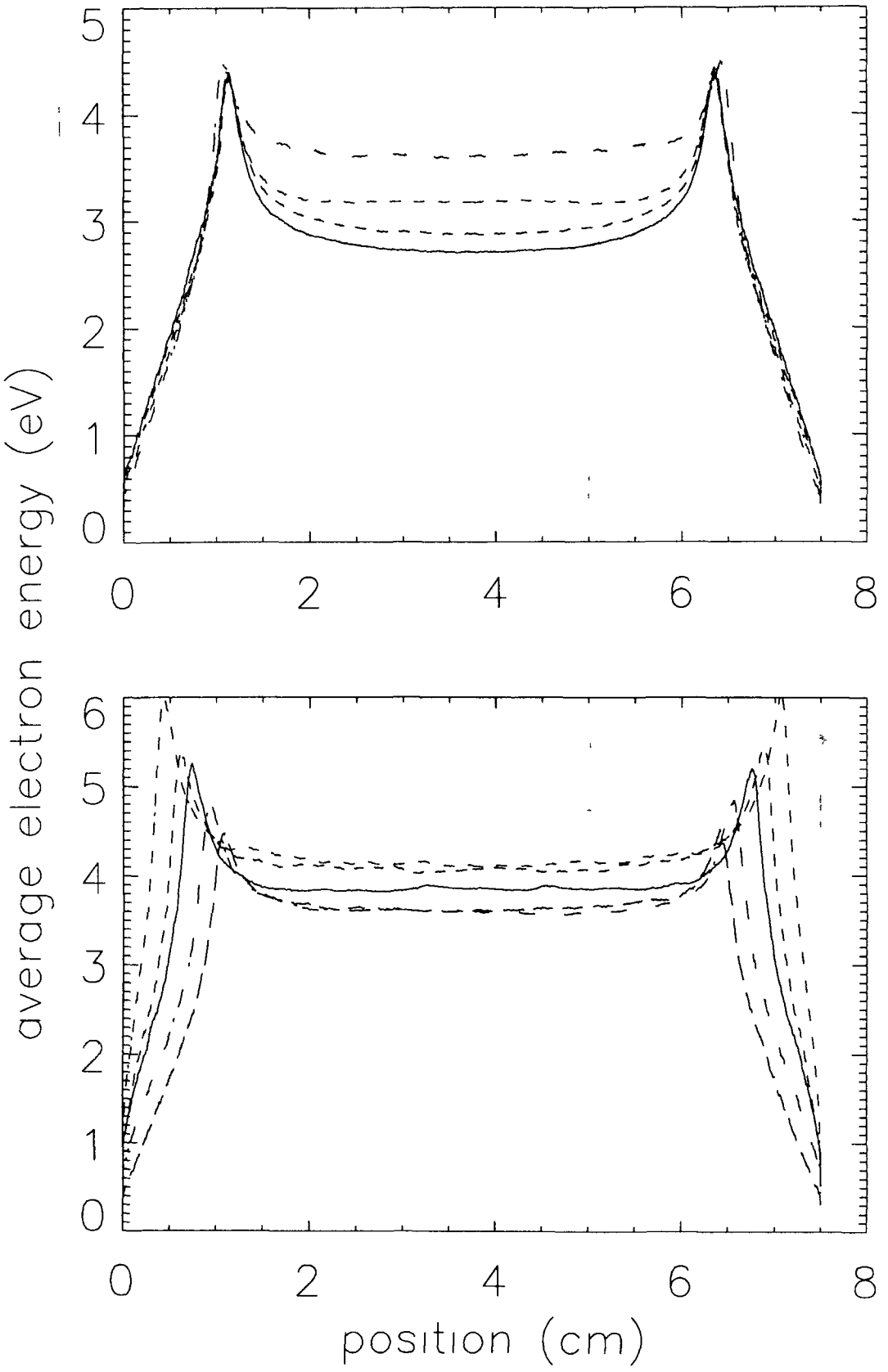

Figure 6 4 PIC/MCC simulations taken from Hutchinson et al [10] Simulated average electron energy across the glow for magnetic fields from 0 to 7 Gauss (solid, dash, dot-dash, treble-dot-dash lines correspond to 0 2, 5 and 7 Gauss [a] and 7 to 30 Gauss (long-dash, treble-dot-dash, solid dash and dot-dash lines correspond to 7, 10, 15 20 and 30 Gauss

of approximately 10 Gauss the average electron heating near the sheaths decreased as some fast electrons with Larmor radius of 0 5cm penetrated the bulk and were cooled yielding a decrease in the total electron heating [11,12] In addition to enhancing ohmic heating it has also been proposed by Lieberman et al [13] that increased magnetic fields can cause electrons to undergo repeated collisions with the same sheath, provided that their Larmor radius is small compared to the half width of the plasma This would then lead to enhanced stochastic heating of the electrons within the sheath These electrons however remain confined to the sheaths and so are not observable in the eedf from the experimental results

However Figure 6 4 taken from the PIC/MCC simulation shows the average electron energy throughout the plasma for varying magnetic fields The increase in the bulk electron energy is clearly observable At fields greater than 10 Gauss the average energy of the electrons in the sheaths increases notably as the Larmor radius of the electrons becomes less than the width of the sheath region This is thought to be due to the gyrating electrons colliding more than once with the moving sheath as shown in Figure 6 5 For the case of no magnetic field, if the sheath moves towards the electron its energy increases, while if it moves away the energy decreases Though some electrons gain while others lose energy, the net effect is an increase in energy

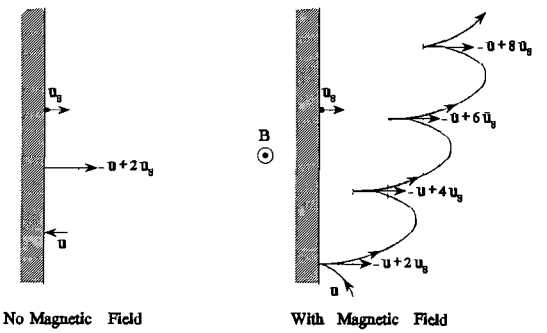

Figure 6 5 Electron energy gain at the sheath edge for unmagnetised and magnetised plasmas Taken from Ref [13]

In the case of a magnetic field several collisions with the sheath are possible Assume an electron incident on the sheath edge has velocity u and the sheath is moving with velocity u_s An electron reflected from the sheath will then have velocity $u_{total} = -u + 2\Delta u$, where $2\Delta u$ is the total velocity change from all the collisions with the sheath The increase in the average electron energy in the sheaths is thought to be due to this repeated sheath collision process

In the unmagnetised plasmas the electron density was found to be $\sim 4 \times 10^9 cm^{-3}$

from both probe and microwave interferometry techniques This density then decreased as the magnetic field increased This drop in density as seen in Figure 6 6, is associated with the transition from stochastic to bulk heating Although the average

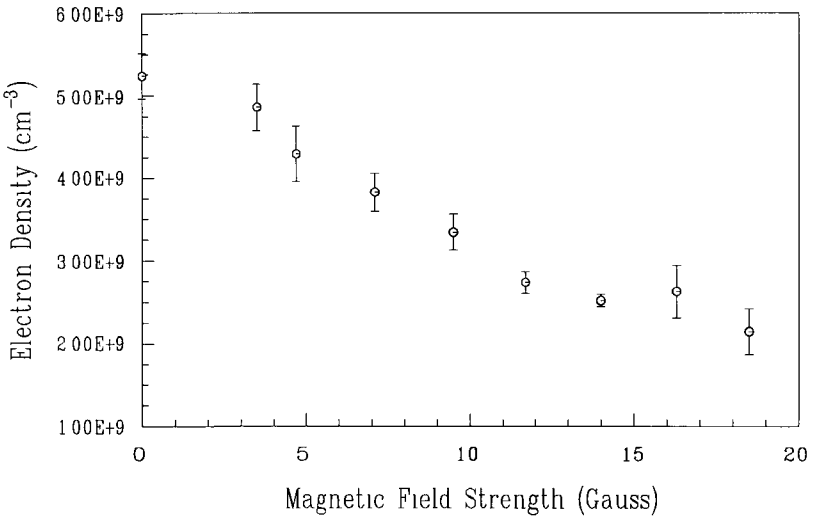

Figure 6 6 Electron density as a function of magnetic field strength measuring using the microwave interferometer

electron energy increases the stochastically heated electrons can no longer penetrate into the bulk plasma This results is a decrease in the density of electrons within the bulk as there are fewer electrons present with energies in excess of the ionisation

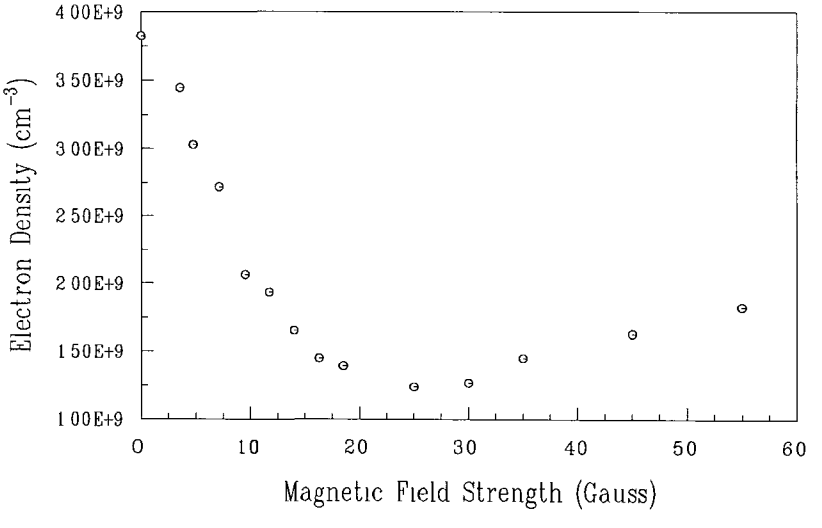

Figure 6 7 Electron density as a function of magnetic field strength measured using a Langmuir probe

threshold. The bulk ionisation rate therefore decreases and there is a drop in the bulk electron density. This feature is also present for an unmagnetised plasma as the transition from stochastic to bulk heating occurs, see Section 4.3. As the magnetic field increases though above ~ 20 Gauss the density begins to increase again as diffusion of electrons to the walls reduces and the bulk ionisation rate increases. This is clearly visible in Figure 6.7 which shows the electron density measurements taken from the probe. The decrease in density agrees quite well with the microwave measurements. The absolute values of density as measured by the two techniques varies slightly though because the microwave method measures the line average density while the probe measures the bulk density. The size of the plasma varies slightly as the pressure or magnetic field changes, so an absolute knowledge of this value is not known leading to discrepancies in the calculated density from the microwave technique.

6.5 Conclusions.

A small magnetic field applied parallel to the electrodes of a capacitively coupled low pressure rf plasma has several effects on both the heating modes and density of the discharge. Firstly, with no magnetic field applied repeated scattering of the fast electrons from the sheaths heat the plasma at low pressures. With a field applied the induced cyclotron motion of the electrons prevents their bouncing from opposite sheaths therefore disrupting the stochastic heating mechanism. As less electrons diffuse to the walls bulk heating takes over as the dominant process. This transition is clearly visible from the eedfs shown in Figure 6.3. The drop in electron density associated with this transition being clearly visible from both probe and microwave interferometry techniques of measuring electron density. With the field strength increased further the density increases as the bulk ionisation rate rises and losses to the walls decrease. Secondly at field strengths above 7Gauss the PIC/MCC simulations show that motion of the electrons in cyclotron orbits can lead to enhanced sheath heating as electrons repeatedly bounce off the same sheath [13]. The electrons however are confined to the sheath regions and so are not examinable by the probe techniques employed here. Finally it was also found that at fields of ~ 10 Gauss there is a slight decrease in the average electron heating near the sheaths. This is due to

sheath accelerated electrons penetrating into the bulk and cooling down [11,12]

References.

[1] M B Hopkins and W G Graham, J Phys D Appl Phys , 20, 1987, 838-843

[2] Y Li, S Lizuka and N Sato, Appl Phys Lett , 65(1), 1994, 28-30

[3] A D Kuypers, E H A Granneman and H J Hopman, J Appl Phys 63(6), 1988, 1899-1903

[4] T E Wicker and T D Mantei, J Appl Phys 57(5), 1985, 1638-1647

[5] B Chapman, *Glow Discharge Processes*, Wiley and Sons, New York, 1966

[6] V E Golant, A P Zhilmsky, I E Sakharov and S C Brown, *Fundamentals of Plasma Physics*, Wiley and Sons, New York, 1979

[7] F F Chen, *Introduction to Plasma Physics and Controlled Fusion*, Plenum Press, New York - London, 1990

[8] F F Chen, *Plasma Diagnostic Techniques* edited by R H Huddelstone and S L Leonard, Academic Press, New York, 1965

[9] R J Armstrong, K-B Liland and J Trulsen, Physica D, 60, 1992, 160-164

[10] D A W Hutchinson, M M Turner, R A Doyle and M B Hopkins, to be published

[11] M Surendra and D B Graves, Phys Rev Lett 66(11), 1991, 1469-1472

[12] M Surendra and D B Graves, IEEE Trans Plasma Sci 19 (2), 1991, 144-157

[13] M A Lieberman, A J Lichtenberg and S E Savas, IEEE Trans Plasma Sci 19 (2), 1991, 189-195

Chapter 7: Collaborations.

7.1 Introduction.

The probes and associated diagnostic units have in the course of this work been used by different research groups on a variety of different systems These include, the GEC reference cell in The University of Texas at Dallas, a thin film evaporation chamber in Eolas, Dublin and finally a research system in Bochum, Germany A range of gases, pressures and powers were tried to characterise the different plasmas in each process The purpose of this chapter is to review the results obtained from each of these systems

7.2 The GEC Reference Cell.

The GEC reference cell was developed at the 1988 Gaseous Electronics Conference (GEC) The basic purpose of this cell is to provide an experimental platform for the comparison of different plasma measurements made on a common chamber geometry but by different research groups [1,2] Initially the current and voltage properties of the discharge, were examined, but as time progresses measurement techniques are being developed to characterise other parameters such as density, optical emission, etc The reference cell, shown in Figure 7 1, consists of a stainless steel chamber with parallel plate electrodes, each with a 102cm diameter Although most chambers use high purity aluminium electrodes, the cell in Texas uses stainless steel ones in order to allow for the inclusion of a pinhole aperture as an inlet to an ion energy analyser All ports and flanges are ultrahigh vacuum sealed producing a low base pressure in the range of $\sim 10^{-7}$ Torr with a 300 *l*/s turbomolecular pump Gas is injected into the chamber from a showerhead inlet incorporated into the top electrode

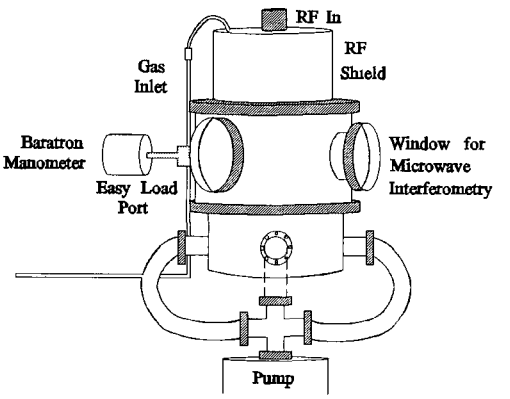

Figure 7 1 Schematic diagram of the GEC reference cell in the University of Texas at Dallas

This electrode is also the driving electrode for the Texas cell The electrode spacing is variable from 12 7 to 63 5mm although was set to 25 4mm for the work presented here Each electrode is isolated from the chamber by an electrical insulator so that either electrode can be driven, biased, or allowed to float Ground shields surrounding the insulators extend from the mount to the plane of the electrode The shields reduce sputtering of the insulator and provide a more uniform electric field between the electrodes Eight ports are arranged around the chamber to provide optical access to the entire discharge A tuned probe, see Section 3 2, was installed on the GEC cell in the University of Texas at Dallas [3] Argon and nitrogen plasmas were examined and density measurements taken from the probe were compared to that from a microwave interferometer An 8 6GHz signal was used in the interferometer here but in all other respects the experimental apparatus was identical to that described in Section 3 3

7.3 Results and Discussion.

The results shown here are a combination of data taken when the probe was initially installed and measurements taken more recently Figure 7 2 shows a comparison between the electron density measured by the probe and that measured

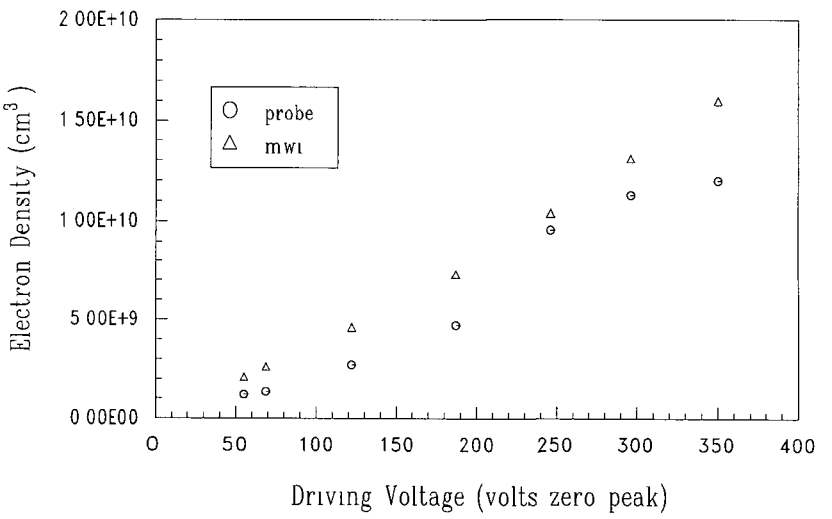

Figure 7 2 The electron density as a function of driving voltage measured in argon by a tuned probe and a microwave interferometer

by the microwave interferometer for an argon plasma at 100mTorr with varying rf voltage The two sets of data agree quite well for the range of voltages examined A previous study [4] showed agreement between the two up to 500 Volts at this pressure At higher pressures though with varying voltage discrepancies between the two occurred at 250mTorr the probe underestimated the density by a factor of 2 while at 500mTorr this rose to a factor of almost 4 For nitrogen plasmas at 100 mTorr the probe began to underestimate the electron density at 200 Volts see Figure 7 3 The reason for these difference is probably due to the increased number of collisions in the plasma Since the theory used to calculate the densities from the

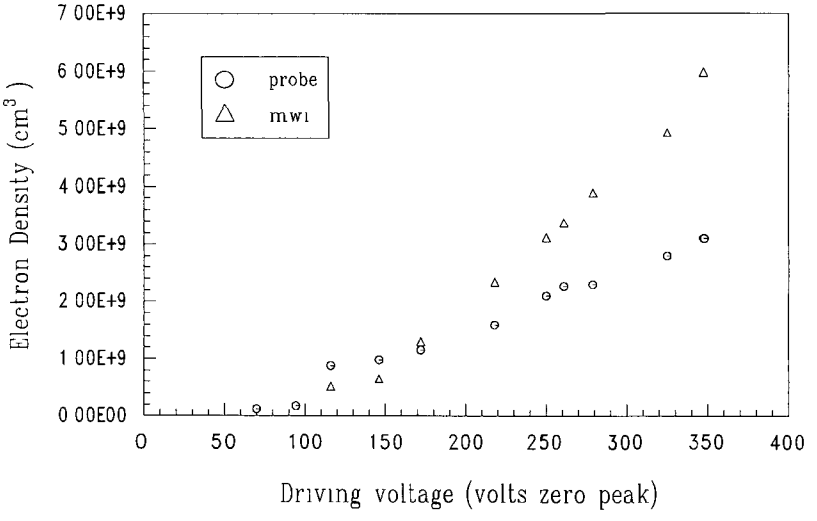

Figure 7 3 Electron density in Nitrogen measured using a tuned probe and a microwave interferometer

probe trace is that of Laframboise, see Section 3 2 2, the ion collisions in the sheath at high pressure are neglected Although the probe is operated in the sheath limited case and should be non-collisional this situation would be very rare Only a small number of collisions in the region of the probe would be sufficient to alter the trajectories of ions which should be collected at very negative potentials, thus reducing the measured density When the probe is strongly biased positive it can cause a depletion to the local electron density These two factors result in discrepancies between the probe and microwave interferometer measured densities The eedfs taken in argon and shown in Figure 7 4 show the transition from stochastic to bulk heating The pressure threshold at which this occurs being ~70 mTorr This

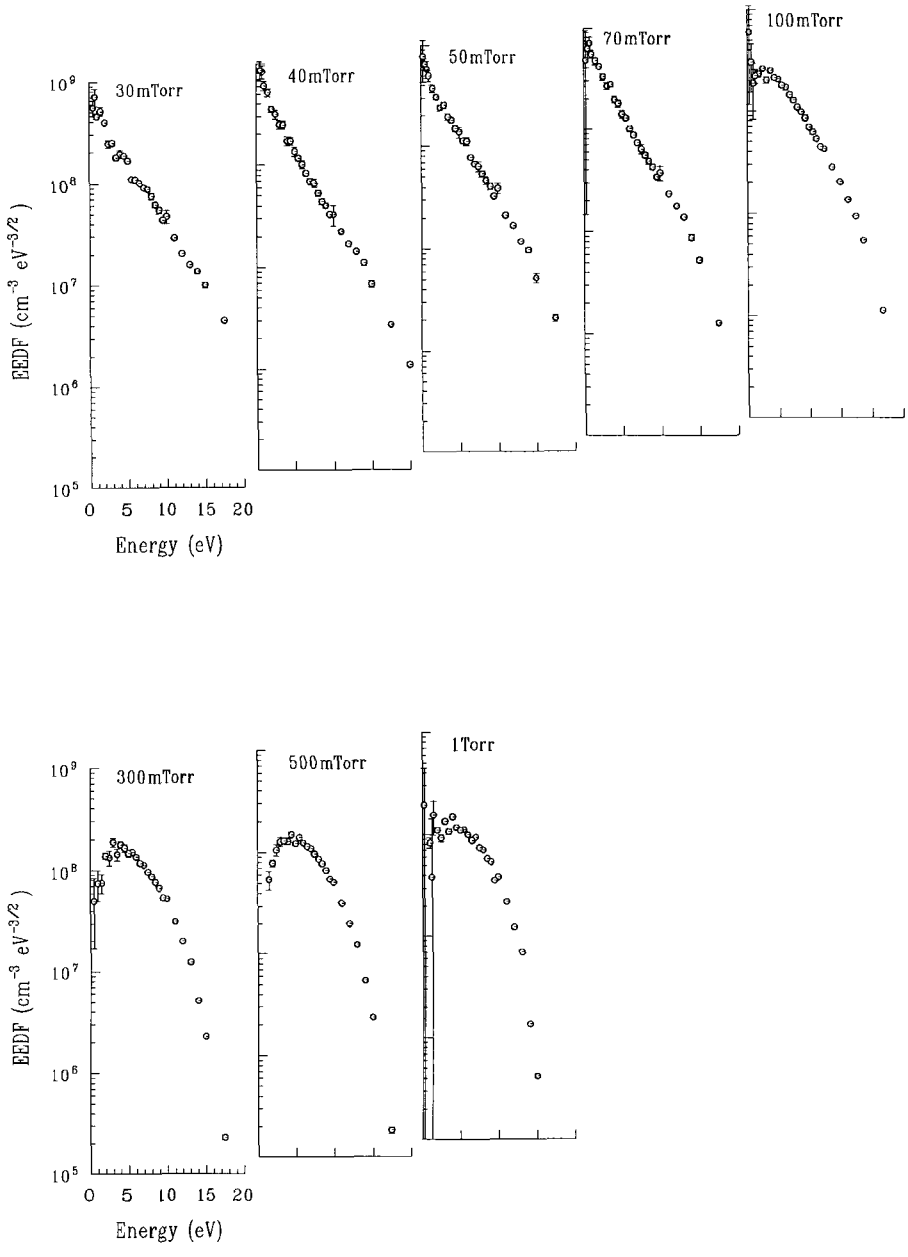

Figure 7 4 EEDFs taken in argon in the GEC reference cell All the data was taken for a current of 175mAmps and electrode gap of 25 4mm

agrees quite well with the work of Godyak et al [5] and Turner et al [6], where the transition in heating modes was found to be dependant on the pressure and length of the discharge, see Section 4 3 The product of these two values, pressure (Torr) and length (cm) at the transition, which should be in the region of 0 14 to 0 18 in this case is ~0 14 Torr cm At pressure greater than 70mTorr, bulk heating quickly takes

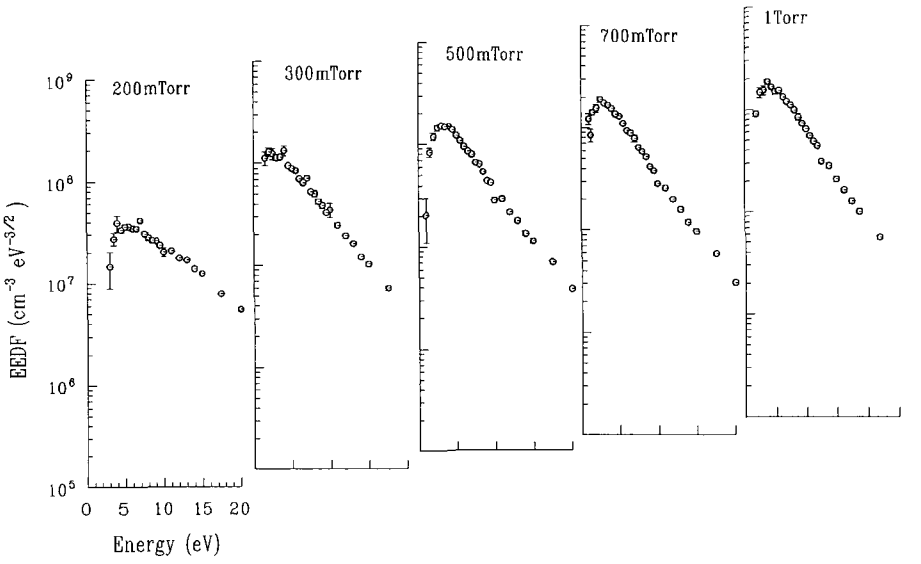

Figure 7 5 EEDFs taken in helium at 175mAmps with a 25 4mm electrode gap

over from stochastic heating to become the dominant heating mode and is accompanied by an increase in the bulk electron temperature from ~2 7 to 3 2eV and a decrease in density initially as less electrons during the transition have energies greater than the ionisation potential

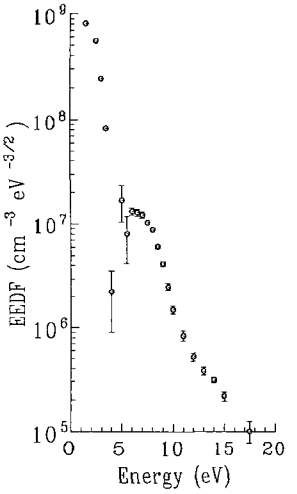

Figure 7 6 Nitrogen eedf taken at 200mTorrand175mAmps

Work has been carried out subsequently on helium, shown in Figure 7 5 and taken by J Xie [7] and also nitrogen and carbontetraflouride plasmas The results from helium compare well the results of Godyak et al [8], taken at low current density, which too show the electron temperature decrease as the pressure is increased, as opposed to argon where the opposite occurs The most distinguishing difference between this set of eedf's and that of the argon eedf's shown in Figure 7 4, is the obvious lack of a transition from one heating mode to another with helium This could possibly be used as confirmation that the abnormally low heating mode and sharp heating mode transition is intrinsic to a

Ramsauer gas Others have observed a transition from α to γ mode heating at much higher pressures and voltages in helium in both experiments and mathematical models [8-10] The eedf data obtained for nitrogen plasmas agree very well with the work of Scanlan [11,12] and of Hopkins et al [13] The depletion of the 2-4 eV region due to the large cross section for inelastic collisions involving the vibration excitation of the N_2 molecule and the superelastic collisions repopulating the 5-7 eV range are clearly visible in Figure 7 6, taken at 200 mTorr and 175 mAmps A pressure scan from 60 to 300 mTorr at constant current showed the evolution of these characteristics as the pressure was increased [7,11,14] These features have been regularly seen in dc discharges [15], and simulations [11,16] but their observation in rf plasmas have been detected by only a few [12,17] Recent work on the GEC cell using the tuned probes and the microwave interferometer includes investigation into CF_4 plasmas and radial scans across the centre of the plasma in both argon and nitrogen to check for variations in electron temperature and density which might be due to changes in the electric field

7.4 The Thomson Scattering System.

Thomson scattering is a technique generally confined to high temperature, highly ionised, plasmas, see Section 1 7 2 The research system in Bochum, Germany was designed to see if this diagnostic method could be used on low pressure plasmas In order to check the validity of the measurements obtained, a comparative analysis had to be performed A tuned probe was therefore installed to measure the plasma parameters and compare them with the Thomson scattering data A schematic diagram of the system used is shown in Figure 7 7 The plasmas were generated in an aluminium parallel plate capacitively coupled system which could be operated in either symmetric or asymmetric mode Both electrodes were 7cm in diameter with a 4cm gap between them They were composed of very pure aluminium to reduce impurities to the plasma however they were not cooled which led to contamination problems at higher powers Ultra high vacuum techniques were employed so a base pressure of 10^{-7} Torr was possible The system is generally operated by flowing the required gas into the chamber and then closing a gate valve to the pump The gas flow is continued to produce the desired pressure before being switched off The

chamber then has the gas at a specific pressure but since there is no throughput of gas, disturbances to the plasma are reduced which is essential for Thomson scattering. The main drawback of this method is that contaminants are not removed from the

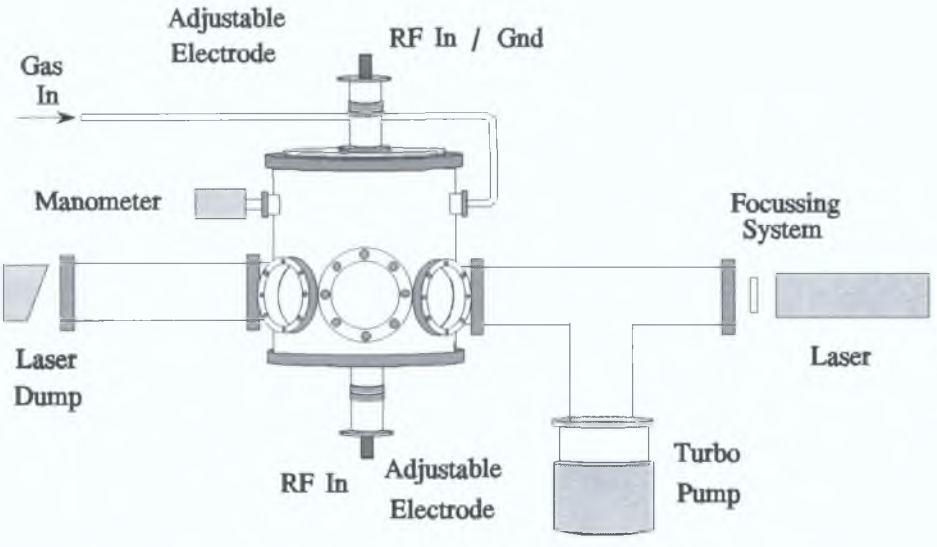

Figure 7.7: Schematic diagram of the Thomson scattering system in Bochum, Germany.

plasma since the chamber is no longer being pumped and again at high input powers to the plasma this can create many problems. For the results shown here, the valve was left open and the pressure controlled by altering the flow of gas into the chamber. The probe for the results shown was situated in approximately the centre of the discharge between the two electrodes. It was cleaned by biasing it to +100Volts in either helium or argon to allow the contaminants to burn off.

7.5 Results and Discussion.

When the probe was initially installed measurements were taken in argon to analyse its performance even though most work was to be carried out in helium. Argon was tested first as its behaviour is well characterised. The power to the plasma was measured using an rf power meter since neither current nor voltage probes were available. For argon at 20watts the results are shown. The eedfs are clearly bi-Maxwellian with a low bulk electron temperature of ~ 2 eV. The densities are in the region of 1×10^{10} cm^{-3}. The transition from stochastic to bulk heating is not shown

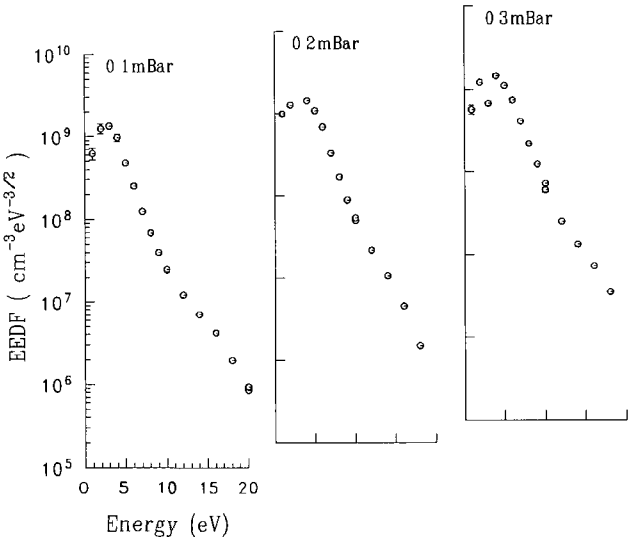

Figure 7 8 Electron energy distribution functions taken in argon at 20Watts input power

as it occurs at higher pressure A scan at ~0 4 Torr was tried but unfortunately the probe was positioned on the edge of the sheath of the lower electrode and so measurements could not be taken at higher pressures in argon A pressure scan was taken then in an asymmetric helium plasma, the results of which agreed quite well with those of Godyak et al [18], for helium with a high current density With the pressure fixed at 225 Torr the power was varied from 35 to 120 Watts Over this

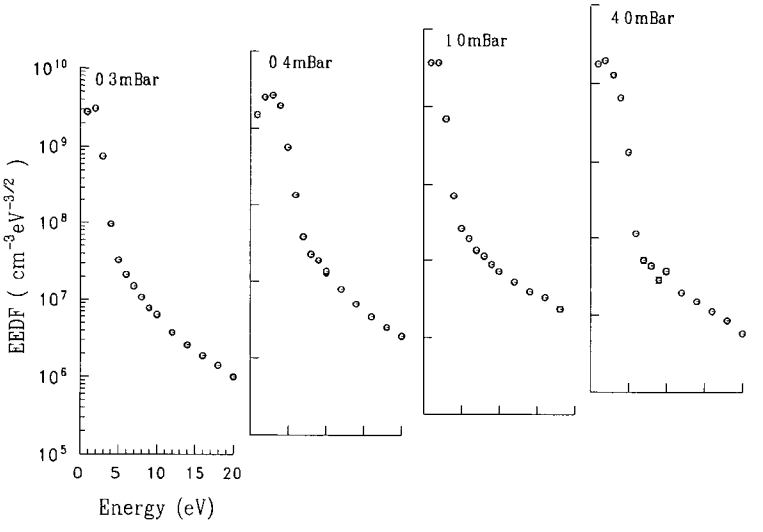

Figure 7 9 Electron energy distribution functions taken in helium with 20Watts input power

range of power the bulk electron temperature remains at ~1.0eV while the density increased by almost 50%. The low electron temperatures are the result of fast electrons generated in the sheaths providing ionisation near the plasma boundaries only. The cold electrons produced just diffuse through the main bulk of the plasma [8]. At 120Watts the eedf changes giving a slightly higher bulk electron temperature but reduced density. In this case very few fast electrons at all could make it past the sheath region to the bulk of the plasma and so the total electron density measured by the probe was reduced.

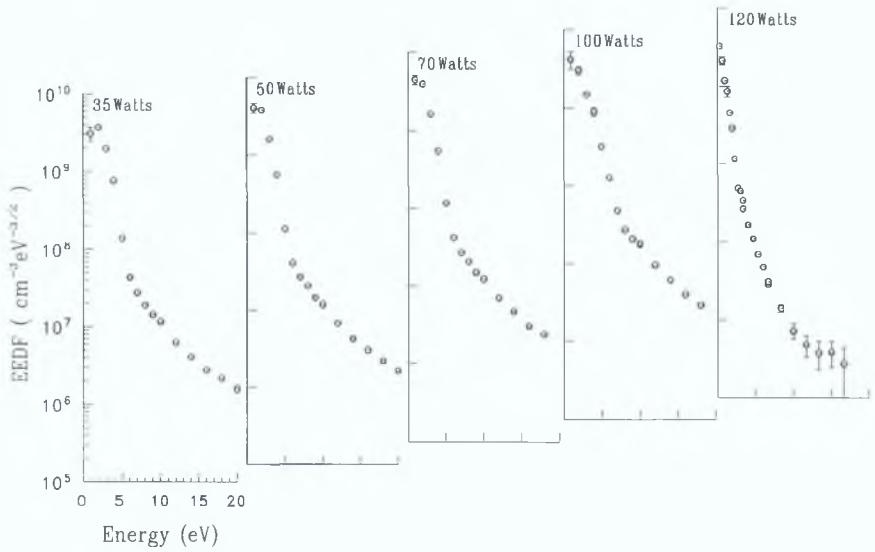

Figure 7.10: Helium eedfs taken at 300mBar with varying input power.

The system was altered to produce a symmetrical plasma. The power from the rf generator was split between the two electrodes. However a 180° phase shift was introduced to the input power to one of the electrodes and the wall was grounded as shown. The plasma was almost entirely confined to the region between the two plates. During cleaning of the probe it was observed that sputtering occurred at the chamber wall indicating that the plasma was in contact to some degree with the walls. A varying pressure scan was performed at 20Watts so direct comparison with the asymmetric case could be performed. Visually the plasma appeared quite different as both electrodes were surrounded by sheaths with a bright region in between them at low pressures. However when the pressure was increased the sheath regions became

much brighter and a dark space region formed between them leading to a much reduced electron density The electron temperature remained close to 1 0eV for the lower pressures (up to ~0 6 Torr) At the higher pressure though, where the dark space region formed, the temperature increased to ~4 0eV The large drop in density which also occurred here would indicate that this temperature value be ignored as the probe does not work at its best in very low density plasmas The formation of the dark space can be seen in the eedf taken at 4 0mBar (3 0 Torr) in Figure 7 12 The electron density decreases substantially as more electrons become confined to the sheath regions and less remain in the bulk of the plasma Finally, as was mentioned previously the electrodes were not cooled during any of the experiments for which results are shown For this reason the probe was cleaned frequently as it had been found that

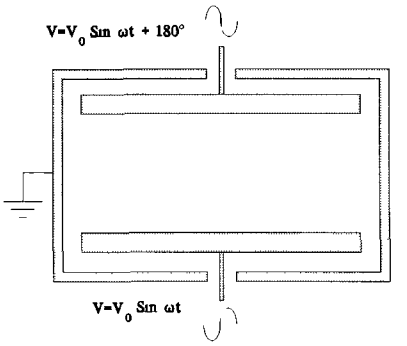

Figure 7 11 Electrical setup for the symmetric mode operation

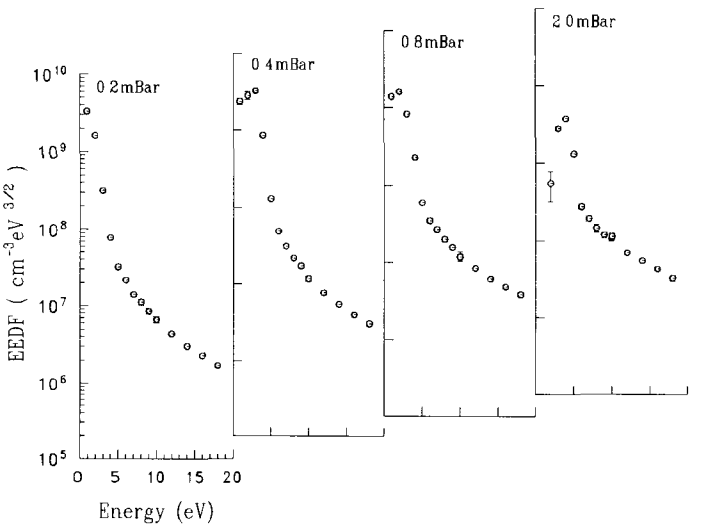

Figure 7 12 Eedfs taken in a symmetric helium plasma with 20Watts input power

contamination due to outgassing of the electrodes was a major problem

7.6 The Thin Film Evaporation System.

A tuned probe was installed on a system designed for developing diamond like thin films These films are deposited onto a particular surface to both harden it, reduce corrosion and subsequently increase the lifetime of the whole device The films are produced using acetylene (ethyne) plasmas, or acetylene/hydrogen plasmas It has been found that the physical properties of the films vary drastically from soft to ultra hard, conducting to resistive, depending on the plasma process parameters such as the rf power input, the gas pressure and flow rate, the substrate temperature and the bias potential [19-23] The purpose of the probe was to measure the plasma parameters for comparison with the film produced in an attempt to correlate both results Hydrogen was to be examined initially with work then to be mainly concentrated on acetylene However the contamination to the probe by the plasma was such that the probe was rendered unusable after only six minutes in a relatively low powered plasma since a thin film formed over the probe tip surface A method of cleaning the probe was later incorporated during the scanning routine to overcome these problems Results of this technique were presented at a GEC conference [24]

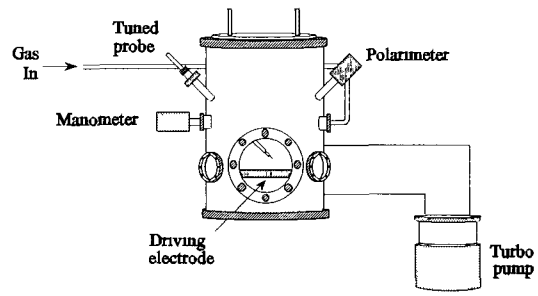

Figure 7 13 Schematic diagram of the thin film evaporation system

The hydrogen plasmas, which were examined and proved to be quite interesting, are still not fully understood A schematic diagram of the system used is shown in Figure 7 13 The chamber was extremely asymmetric, with only a small driving electrode and no ground electrode specifically, though the entire wall area was at ground potential Several diagnostic techniques were employed on the system Optical emission spectroscopy was performed in conjunction with the Langmuir probe to see if the presence of any particular elements were responsible for the observed anomalies Polarimetry was also performed This is a technique to measure the thickness of the film as it is being deposited upon the substrate Finally photo-

detachment experiments were also carried out to measure the percentage of free hydrogen in the plasma and compared with the thickness of the films produced [25]. The probe was inserted through a port in the side of the chamber, because of the design the probe was then at an angle to the driving electrode. The chamber was pumped using a turbomolecular pump and along with the gas flow, gas selection, and pressure monitoring, were all computer controlled. An automatic tuning network matched the power into the plasma.

7.7 Results and Discussion.

Hydrogen forms an interesting plasma in that a double layer is formed around the sheath region whose position varies with pressure and power. The intensely bright region is thought to be the result of sheath accelerated electrons loosing their energy consistently at a particular point in space. In effect, bremstrahlung, where the electrons are stopping suddenly and the energy lost is given out in the form of visible light. The reason why this should occur however is not understood at all since very little work has ever been carried out on capacitively coupled hydrogen discharges. Another feature of hydrogen is that the mobility of the ions is quite high since it is a light gas. The ion frequency is given as,

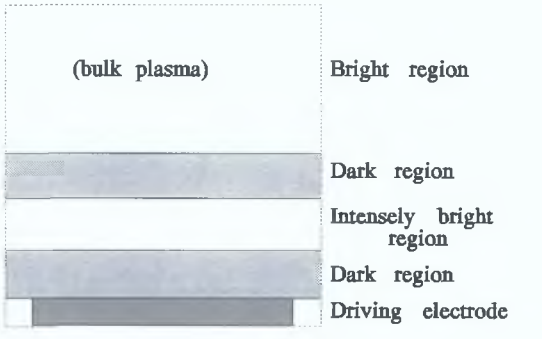

Figure 7.14: Schematic diagram of the double layer in hydrogen.

$$\omega_i = \sqrt{\frac{e^2 n_e}{\epsilon_0 m_i}} \qquad \textbf{Eqn: 7.1}$$

where all terms have their usual meaning. For argon this is $\sim$2 MHz, which is somewhat lower than the driving frequency. Therefore the ions cannot follow the oscillating plasma and so the probe theory which effectively considers the ions as mobile as the backround neutral gas is valid. However for hydrogen the ion frequency is $\sim$13 MHz, which is very close to the driving frequency of the plasma. The ions will therefore have a much greater effect on the plasma as they can almost follow the

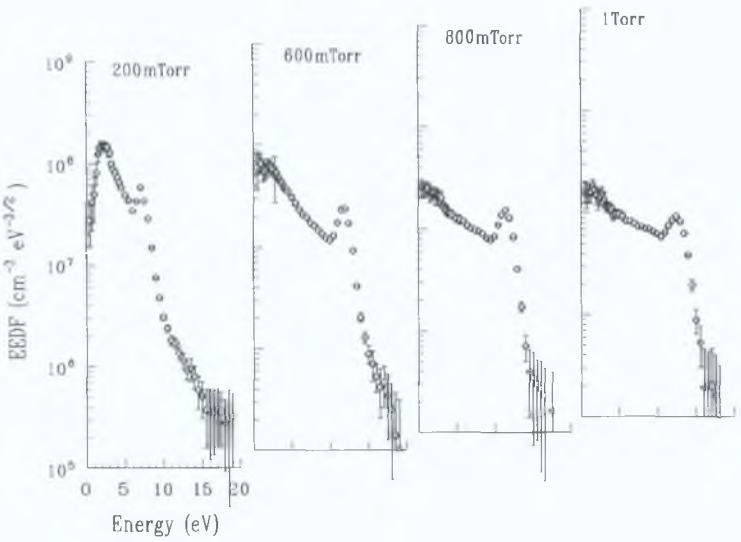

Figure 7.15: Hydrogen eedfs taken at ~30-35 Watts input power in a thin film evaporation system.

oscillations. This condition was not accounted for in the probe theory.

Initially a pressure scan at constant power was performed, the results of which are shown in Figure 7.15. A peak in the eedf varying with pressure was observed. It was thought at first that this peak was connected with the double layer mentioned earlier since power as well as pressure affected its position and magnitude. However recently it has come to light that this peak may in actual fact be a result of rf affecting the probe characteristic as hydrogen plasmas produced on the experimental system described in Section 4.2 do not exhibit the same structure. Godyak et al [8] mentions how insufficient filtering of the rf can lead to the formation of anomalous structures with the eedf. Most recently data taken suggests that this structure is not actually present in the eedf, the double layer in the plasma being due to anomalous sheath heating. An optical emission spectroscopy system is currently being installed on the system here. It should then be possible to scan through the layers for further examination.

7.8 Conclusions.

The tuned probe and its associated diagnostic unit have been tried on a variety

of different plasma systems with varying degrees of success The probe results obtained on the GEC reference cell are comparable with measurements taken by others in argon, helium and nitrogen plasmas Work is being performed there on CF_4 at present to correlate plasma parameters measured by the probe with etch profiles of substrates inserted into the plasma The results obtained in Bochum also compared quite well with the work of others in both helium and argon plasmas New mathematical algorithms have been formulated to evaluate the electron velocity distribution function from Langmuir probe and Thomson scattering measurements [26] so work is continuing there too, although initial comparison of the two techniques have not yet been published Finally the results obtained from the thin film deposition system are still under question It seems that the peak in the eedfs is due to bad filtering of the probe It is hoped that through the emission spectroscopy analysis of the layers of the plasma the source of the double layer structure will be understood

References.

[1] P.J. Hargis Jr., K.E. Greenberg, P.A. Miller, J.B. Gerardo, T.R. Torczynski, M.E. Riley, G.A. Hebner, J.R. Roberts, J.K. Olthoff, J.R. Whetstone, R.J. Van Brunt, M.A. Sobolewski, H.M. Anderson, M.P. Splichal, L.J. Mock, P. Beltzinger, A. Garscadden, R.A. Gottscho, G. Selwyn, M. Dalvie, J. Heidenreich, J.W. Butterbaugh, M.L. Brake, M.L. Passow, J. Pender, A. Lujan, M.E. Elta, D.B. Graves, H.H. Sawin, M.J. Kushner, J.T. Verdeyen, R. Horwath and T.R. Turner, Rev. Sci. Instrum., 65(1),1994, 140-154.

[2] M.A. Sobolewski, J.Vac. Sci. A, 10(6), 1992, 3550-3562.

[3] L.J. Overzet and M.B. Hopkins, Appl. Phys. Lett., 63(18), 1993, 2484-2486

[4] L.J. Overzet and M.B.Hopkins, J. Appl. Phys. 74(7), 1993, 4323-4330.

[5] V.A. Godyak and R.B. Piejak, Appl. Phys. Lett., 63(23), 1993, 3137-3139.

[6] M.M. Turner, R.A. Doyle and M.B. Hopkins, Appl. Phys. Lett., 62(25), 1993, 3247-3249.

[7] J. Xie, L.J. Overzet, R.A. Doyle and M.B. Hopkins, Conference paper at the 47th Annual Gaseous Electronics Conference, NIST, Maryland 1994.

[8] V.A. Godyak, R.B. Piejak and B.M. Alexandrovich, Plasma Sources Sci. Technol. 1, 1992, 36-58.

[9] T.J. Sommerer, W.N.G. Hitchon and J.E. Lawler, Phys. Rev. Lett., 63(21), 2361-2364.

[10] Ph. Belenguer and J.P. Boeuf, Phys. Rev. A., 41(8), 1990, 4447-4459.

[11] J.V. Scanlan, M.B. Hopkins and M.M. Turner, Conference paper at the 10th International Conference on Gas Discharges and their Applications, Swansea, U.K. 1992, 436-439.

[12] J.V. Scanlan and M.B. Hopkins, J. Vac. Sci. Technol. A 10(4), 1992, 1207-1211.

[13] M.B. Hopkins, C.A. Anderson and W.G. Graham, Europhys. Lett., 8(2), 1989, 141-145.

[14] L.Overzet, In correspondence, University of Texas at Dallas, 1994.

[15] T. Kimura, K. Akatsuka and K. Ohe, J. Phys. D. 27, 1994, 1664-1671.

[16] M.M. Turner and M.B. Hopkins, Phys. Rev. Lett., 69(24), 1992, 3511-3514

[17] M Capitelli, R Celiberto, C Gorse, R Winkler and J Wilhelm, J Phys D 21, 1998, 691-699

[18] V A Godyak, R B Piejak and B M Alexandrovich, Phys Rev Lett , 68 (1), 1992, 40-43

[19] I Ivanov, P Kazansky, L Hultman, I Petrov and J-E Sundgren, J Vac Sci A , 12(2),1994, 314-320

[20] J W Coburn, IEEE Trans Plasma Sci , 19(6), 1991, 1048-1062.

[21] J L Shohet, IEEE Trans Plasma Sci , 19 (5), 1991, 725-733

[22] A A Saada, C Michel, M Remy and J-R Cussenot, J Phys D Appl Phys 21, 1988, 1524-1530

[23] Y Catherine, A Pastol, L Athouel and C Fourrier, IEEE Trans Plasma Sci 18(6), 1990, 923-929

[24] W G Graham, R A Doyle, M B Hopkins and T O'Brien, Conference paper at the 46^{t} Annual Gaseous Electronics Conference, Boston, MA, 1993

[25] R Cheshire, PhD Thesis, Queens University Belfast, 1994

[26] M V Chegotov, J Phys D , 27, 1994, 54-62

Chapter 8: Conclusions and Further Work.

8.1 Summary of Work.

Low pressure rf plasmas have been investigated experimentally using tuned Langmuir probes and microwave interferometry Different plasma parameters were examined as a function of pressure, current, voltage and spatial position within the plasma A small transverse magnetic field was also applied to the plasma to observe how it affected the heating regimes of the plasma Finally the tuned probes were installed on other experimental systems to examine how well the probe behaved under different conditions and it compared to the results of other diagnostic techniques

Initial measurements of the sheath resistance as a function of both current and voltage were presented in Chapter 4 along with a method of measuring this parameter This resistance increases the electron temperature calculated and shifts the value of the plasma potential by several volts if neglected from the analysis of the I-V curve A criterion stating when this resistance becomes appreciable was also presented The temperature of the bulk electrons was shown to increase abruptly with increasing pressure as bulk heating takes over from stochastic heating as the primary heating mechanism of the plasma This transition was also obvious from the eedfs which showed a change from a bi-maxwellian to a Druyvesteyn shaped curve The transition which depends only on the pressure of the plasma p, and the half-width of the discharge d, occurred for a pd of 0 1 to 0 15 Torr cm The electron density was found to decrease while the pressure was increased when the current was kept constant The reason being that as the transition from one type of heating to another occurred, less electrons with energies sufficient to cause ionisation were available resulting in a general decrease in ionisation throughout the bulk plasma even though the average energy of the bulk electrons increased

Spatial variations of the plasma parameters were presented in Chapter 5 Two pressures were chosen for the spatial measurements, 10 and 150 mTorr, to examine if any spatial anomalies were heating mode dependant The results show that for both pressures the temperature stays constant within the bulk of the plasma outside of the sheath regions The plasma potential showed no great variation leading to the conclusion that the plasma is virtually field free and homogenous The electron

densities which did vary as a function of position within the plasma were compared with the theoretical expectations of the diffusion equation At 10 mTorr the agreement between the experimental and theoretical was quite good for the data as a function of position from the driving electrode However, the comparison between the two was not so good at 150 mTorr since the theory assumed ionisation at a point source in the centre of the discharge This could not be assumed in this case since the electrodes and consequently the sheath regions were of differing sizes For the radial scan however, the data taken for both pressures agreed with the theoretical expectations

A small transverse magnetic field was applied to the plasma to examine its affect on the heating regimes and electron density of the plasma At low pressure and constant current it was found that bulk heating took over from stochastic heating as the primary heating mode With a field applied the induced cyclotron motion of the electrons prevented their bouncing from opposite sheaths therefore disrupting the stochastic heating mechanism As less electrons diffused to the walls bulk heating then took over as the dominant heating process The initial drop in electron density associated with this transition was clearly visible from both the probe and microwave interferometry techniques of measuring electron density As the field strength was increased further though the density increased as the bulk ionisation rate rose and losses to the walls decreased At field strengths above 7 Gauss the simulations showed that motion of the electrons in cyclotron orbits could lead to enhanced sheath heating as electrons repeatedly bounce off the same sheath The electrons in question were however confined to the sheath regions and so were not examinable by the probe techniques employed here

The tuned probe and its associated diagnostic unit were also tried on a variety of different plasma systems with varying degrees of success The probe results obtained on the GEC reference cell were comparable with measurements taken by others in argon, helium and nitrogen plasmas so too were the results obtained in Bochum, however the results obtained from the thin film deposition system are still under question

8.2 Suggestions for Further Work.

Several questions have arisen from the work conducted for this thesis The

first of these being the double layer in the hydrogen plasma It is now thought that anomalous sheath heating is responsible for the appearance of these layers Optical analysis of the bright regions should therefore yield information of their origin Emission spectroscopy of the layers of the plasma currently underway to try and resolve this problem

The variation of plasma parameters with electrode gap is also being investigated Although the transition between heating modes is know to be dependant on this gap size, the variation of electron temperature and density is still not quite clear It is hoped that an investigation of this nature may reveal why the electron temperature measurements of workers in this field are so diverse

It is hoped to place a current monitor into the chamber, onto the driving electrode of the system to examine how the current density changes in the centre of the plasma as a function of pressure Indications are that the current is confined to the centre of the plasma at low pressure, becoming more dispersed as the pressure is increased This may in fact be another reason why the electron density appears to decrease as the pressure increases